

AD-A066 531

VERMONT UNIV BURLINGTON DEPT OF CHEMISTRY

F/6 11/9

SYNTHESIS, MAGNETIC SUSCEPTIBILITY, AND SPECTROSCOPIC PROPERTIES--ETC(U)

MAR 79 J T WROBLESKI, D B BROWN

N00014-75-C-0756

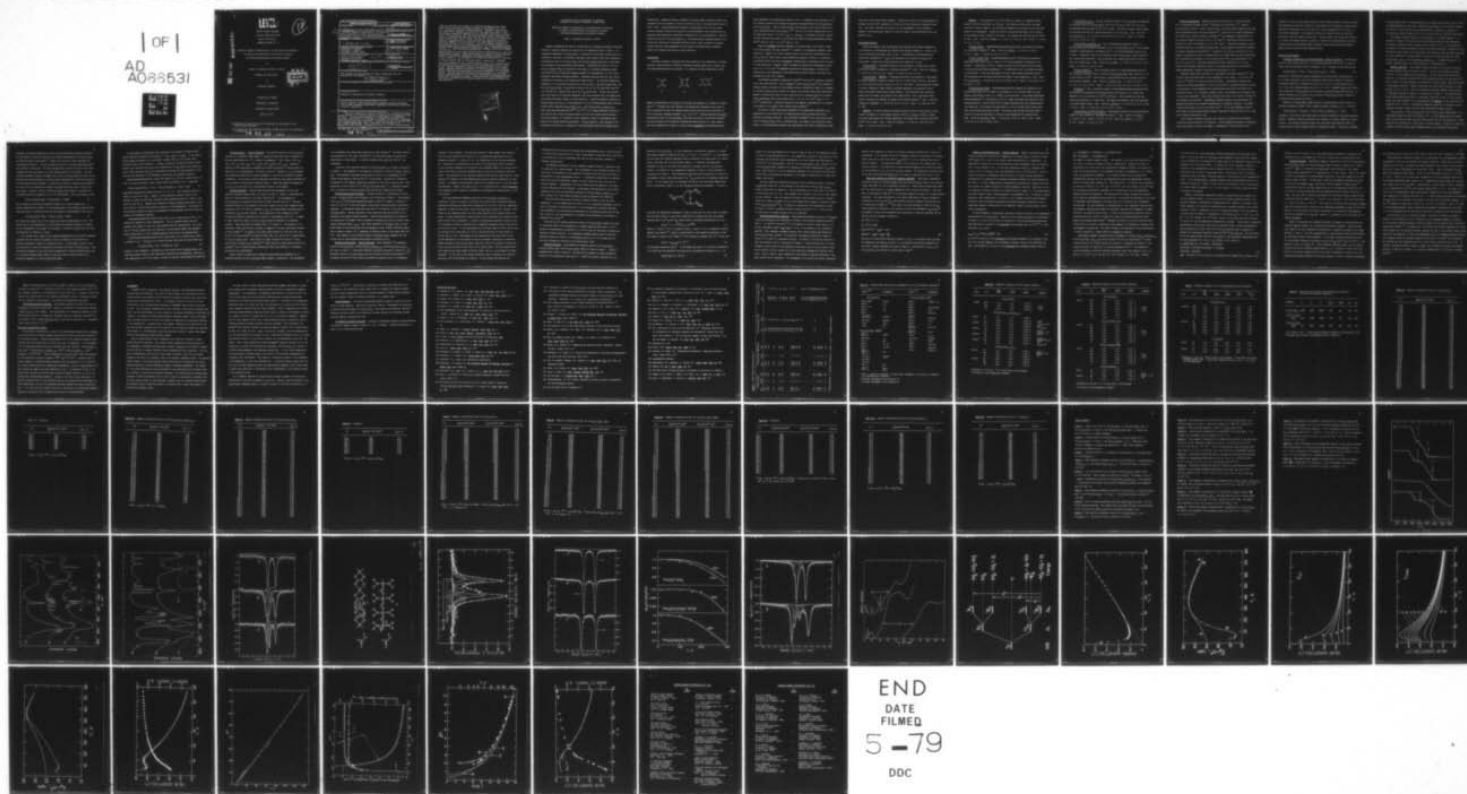
UNCLASSIFIED

TR-15

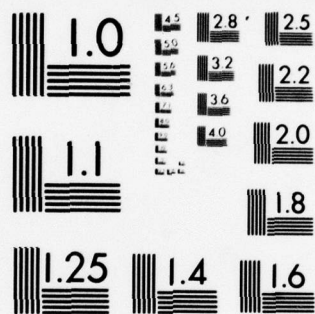
NL

1 OF 1

AD
A066531



END
DATE
FILMED
5-79
DDC



MICROCOPY RESOLUTION TEST CHART
NATIONAL BUREAU OF STANDARDS-1963-A

LEVEL II

12

OFFICE OF NAVAL RESEARCH

Contract N00014-75-C-0756

Task No. NR 356-593

TECHNICAL REPORT NO. 15

AD A0 66531

Synthesis, Magnetic Susceptibility, and Spectroscopic Properties
of Single- and Mixed-Valence Iron Oxalate, Squarate,
and Dihydroxybenzoquinone Coordination Polymers

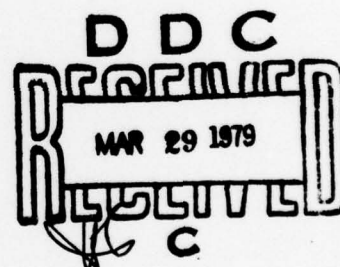
by

James T. Wroblewski and David B. Brown

Prepared for Publication

in

Inorganic Chemistry



University of Vermont

Department of Chemistry

Burlington, Vermont 05405

March 16, 1979

Reproduction in whole or in part is permitted for any purpose of the
United States Government

This document has been approved for public release and sale; its distribution
is unlimited.

9 03 27 118

DDC FILE COPY

SECURITY CLASSIFICATION OF THIS PAGE (When Data Entered)

REPORT DOCUMENTATION PAGE		READ INSTRUCTIONS BEFORE COMPLETING FORM
1. REPORT NUMBER 15	2. GOVT ACCESSION NO.	3. RECIPIENT'S CATALOG NUMBER 9
4. TITLE (and Subtitle) Synthesis, Magnetic Susceptibility, and Spectroscopic Properties of Single- and Mixed-Valence Iron Oxalate, Squarate, and Dihydroxybenzoquinone Coordination Polymers		5. TYPE OF REPORT & PERIOD COVERED Technical Report
7. AUTHOR(s) J. T. Wroblewski and D. B. Brown		6. PERFORMING ORG. REPORT NUMBER
9. PERFORMING ORGANIZATION NAME AND ADDRESS Department of Chemistry University of Vermont Burlington, Vermont 05401		8. CONTRACT OR GRANT NUMBER(s) N00014-75-C-0756
11. CONTROLLING OFFICE NAME AND ADDRESS Office of Naval Research Department of the Navy Arlington, Virginia 22217		10. PROGRAM ELEMENT, PROJECT, TASK AREA & WORK UNIT NUMBERS 11 16 Mar 79
14. MONITORING AGENCY NAME & ADDRESS (if different from Controlling Office) 14 TR-15		12. REPORT DATE March 16, 1979
		13. NUMBER OF PAGES 71
		15. SECURITY CLASS. (of this report) Unclassified
		15a. DECLASSIFICATION/DOWNGRADING SCHEDULE
16. DISTRIBUTION STATEMENT (of this Report) This document has been approved for public release and sale; its distribution is unlimited 10 James T. /Wroblewski David B. /Brown		
17. DISTRIBUTION STATEMENT (of the abstract entered in Block 20, if different from Report)		
18. SUPPLEMENTARY NOTES Prepared for publication in Inorganic Chemistry		
19. KEY WORDS (Continue on reverse side if necessary and identify by block number) Oxalate complexes, Dihydroxybenzoquinone complexes, Squarate complexes, Iron polymers, Mossbauer spectroscopy, Magnetism, Mixed-Valence, Electronic structure, Conductivity		
20. ABSTRACT (Continue on reverse side if necessary and identify by block number) Magnetic susceptibility data for several Fe(II) coordination polymers containing oxalate or squarate dianions are reported in the temperature range 4.2-300 K. Low temperature magnetism of $\text{Fe}(\text{C}_2\text{O}_4)(\text{H}_2\text{O})_2$ is dominated by intrachain ordering near 32 K followed by the onset of interchain long-range order slightly below this temperature. Susceptibility data for $\text{Fe}(\text{C}_4\text{O}_4)(\text{H}_2\text{O})_2$ and $\text{Fe}(\text{C}_4\text{O}_4)(\text{C}_5\text{H}_5\text{N})_2 \cdot 2\text{H}_2\text{O}$ show no detectable spin exchange in the temperature range studied. Susceptibility data to 1.8 K for $\text{Fe}(\text{C}_4\text{O}_4)(\text{C}_4\text{H}_4\text{N}_2)$		

DD FORM 1 JAN 73

1473

EDITION OF 1 NOV 68 IS OBSOLETE
S/N 0102-014-6601408 892
J.O.B.
SECURITY CLASSIFICATION OF THIS PAGE (When Data Entered)

$\cdot 4\frac{1}{2}\text{H}_2\text{O}$ are analyzed on the basis of a modified Heisenberg linear chain model with an intrachain exchange parameter of approximately -0.3 cm^{-1} and a negligible interchain exchange parameter. Mössbauer spectral data for these Fe(II) complexes are reported in the temperature range 17-300 K. The observed temperature dependence of the quadrupole splitting for $\text{Fe}(\text{C}_4\text{O}_4)(\text{H}_2\text{O})_2$, $\text{Fe}(\text{C}_4\text{O}_4)(\text{C}_5\text{H}_5\text{N})_2 \cdot 2\text{H}_2\text{O}$, and $\text{Fe}(\text{C}_4\text{O}_4)(\text{C}_5\text{H}_5\text{N})_2 \cdot 4\frac{1}{2}\text{H}_2\text{O}$ is described in terms of an excited $^5\text{E}_g$ term which lies 525, 425, and 850 cm^{-1} respectively, above the $^5\text{B}_{2g}$ ground term. Ground- and excited- term splittings are in essential agreement with those obtained from room-temperature solid-state electronic spectra of these materials. Controlled chemical oxidation of $\text{Fe}(\text{C}_2\text{O}_4)(\text{H}_2\text{O})_2$ with Br_2 or 1,4-benzoquinone in 1,2,4-trichlorobenzene yields discrete mixed-valence compounds $\text{Fe}(\text{C}_2\text{O}_4)(\text{H}_2\text{O})_{1.4}\text{Br}_{0.6}$ and $\text{Fe}(\text{C}_2\text{O}_4)(\text{H}_2\text{O})_{0.9}(\text{C}_6\text{H}_4\text{O}_2)_{0.05}$. These semiconducting materials ($\sigma_{300\text{K}} \approx 10^{-4}\Omega^{-1}\text{ cm}^{-1}$) display Mössbauer spectra in the range 20-400 K which are characteristic of Fe(II,III) mixed-valence polymers. Below approximately 20 K spectra of these compounds consist of superimposed paramagnetic and Zeeman hyperfine multiplets. $\text{Fe}(\text{C}_4\text{O}_4)(\text{C}_5\text{H}_5\text{N})_{1.5}$ and $\text{Fe}(\text{C}_6\text{H}_2\text{O}_4)\text{I}$ are obtained by solid-state I_2 oxidation of $\text{Fe}(\text{C}_4\text{O}_4)(\text{C}_5\text{H}_5\text{N})_2 \cdot 2\text{H}_2\text{O}$ and $\text{Fe}(\text{C}_6\text{H}_2\text{O}_4)(\text{H}_2\text{O})_2$, respectively. Mössbauer spectral parameters for these iodine oxidation products are consistent with the presence of Fe(II) and Fe(III) sites in the approximate ratio of three to one. Variable-temperature magnetic susceptibility data for the mixed-valence complexes indicate the presence of antiferromagnetic spin exchange which is described with appropriate theoretical expressions for the susceptibility. With the possible exception of $\text{Fe}(\text{C}_4\text{O}_4)(\text{C}_5\text{H}_5\text{N})_{1.5}$, the mixed-valence compounds appear to be structurally described as randomly-oxidized linear chain coordination polymers. Infrared spectral band assignments for the single- and mixed-valence complexes support the proposed structures for these materials.

EXCLUSION for	
White Section	<input checked="" type="checkbox"/>
Buff Section	<input type="checkbox"/>
UNANNOUNCED	<input type="checkbox"/>
RESTRICTION	
BY	
DISTRIBUTION/AVAILABILITY CODES	
A	

Contribution from the Department of Chemistry
University of Vermont, Burlington, Vermont 05405

Synthesis, Magnetic Susceptibility, and Spectroscopic Properties
of Single- and Mixed-Valence Iron Oxalate, Squarate,
and Dihydroxybenzoquinone Coordination Polymers

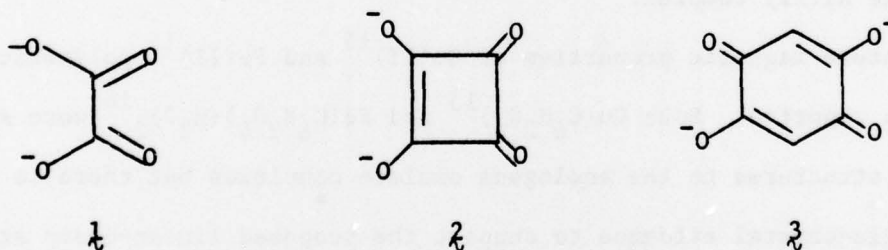
James T. Wroblewski and David B. Brown*

Magnetic susceptibility data for several Fe(II) coordination polymers containing oxalate or squarate dianions are reported in the temperature range 4.2-300 K. Low temperature magnetism of $\text{Fe}(\text{C}_2\text{O}_4)(\text{H}_2\text{O})_2$ is dominated by intrachain ordering near 32 K followed by the onset of interchain long-range order slightly below this temperature. Susceptibility data for $\text{Fe}(\text{C}_4\text{O}_4)(\text{H}_2\text{O})_2$ and $\text{Fe}(\text{C}_4\text{O}_4)(\text{C}_5\text{H}_5\text{N})_2 \cdot 2\text{H}_2\text{O}$ show no detectable spin exchange in the temperature range studied. Susceptibility data to 1.8 K for $\text{Fe}(\text{C}_4\text{O}_4)(\text{C}_4\text{H}_4\text{N}_2) \cdot 4\frac{1}{2}\text{H}_2\text{O}$ are analyzed on the basis of a modified Heisenberg linear chain model with an intrachain exchange parameter of approximately -0.3 cm^{-1} and a negligible interchain exchange parameter. Mössbauer spectral data for these Fe(II) complexes are reported in the temperature range 17-300 K. The observed temperature dependence of the quadrupole splitting for $\text{Fe}(\text{C}_4\text{O}_4)(\text{H}_2\text{O})_2$, $\text{Fe}(\text{C}_4\text{O}_4)(\text{C}_5\text{H}_5\text{N})_2 \cdot 2\text{H}_2\text{O}$, and $\text{Fe}(\text{C}_4\text{O}_4)(\text{C}_4\text{H}_4\text{N}_2) \cdot 4\frac{1}{2}\text{H}_2\text{O}$ is described in terms of an excited $^5\text{E}_g$ term which lies 525, 425, and 850 cm^{-1} , respectively, above the $^5\text{B}_{2g}$ ground term. Ground- and excited-term splittings are in essential agreement with those obtained from room-temperature solid-state electronic spectra of these materials. Controlled chemical oxidation of $\text{Fe}(\text{C}_2\text{O}_4)(\text{H}_2\text{O})_2$ with Br_2 or 1,4-benzoquinone in 1,2,4-trichlorobenzene yields discrete mixed-valence compounds $\text{Fe}(\text{C}_2\text{O}_4)(\text{H}_2\text{O})_{1.4}\text{Br}_{0.6}$ and $\text{Fe}(\text{C}_2\text{O}_4)(\text{H}_2\text{O})_{0.9}(\text{C}_6\text{H}_4\text{O}_2)_{0.05}$. These semiconducting materials ($\sigma^{300 \text{ K}} \approx 10^{-4} \Omega^{-1} \text{ cm}^{-1}$) display Mössbauer spectra in the range 20-400 K which are characteristic of Fe(II,III) mixed-valence polymers. Below approximately 20 K spectra of these compounds consist of superimposed paramagnetic and Zeeman hyperfine multiplets. $\text{Fe}(\text{C}_4\text{O}_4)(\text{C}_5\text{H}_5\text{N})_{1.5}$ and $\text{Fe}(\text{C}_6\text{H}_2\text{O}_4)\text{I}$ are obtained by solid-state I_2 oxidation of $\text{Fe}(\text{C}_4\text{O}_4)(\text{C}_5\text{H}_5\text{N})_2 \cdot 2\text{H}_2\text{O}$ and $\text{Fe}(\text{C}_6\text{H}_2\text{O}_4)(\text{H}_2\text{O})_2$.

respectively. Mössbauer spectral parameters for these iodine oxidation products are consistent with the presence of Fe(II) and Fe(III) sites in the approximate ratio of three to one. Variable-temperature magnetic susceptibility data for the mixed-valence complexes indicate the presence of antiferromagnetic spin exchange which is described with appropriate theoretical expressions for the susceptibility. With the possible exception of $\text{Fe}(\text{C}_4\text{O}_4)(\text{C}_5\text{H}_5\text{N})\text{I}_{1.5}$, the mixed-valence compounds appear to be structurally described as randomly-oxidized linear chain coordination polymers. Infrared spectral band assignments for the single- and mixed-valence complexes support the proposed structures for these materials.

Introduction

Cooperative magnetic phenomena have been observed at low temperature in several polymeric transition-metal complexes containing bridging oxalate (1), squarate (2), and dihydroxybenzoquinone (3) dianions. For example, variable-temperature powder



magnetic susceptibility of $\text{Cu}(\text{C}_2\text{O}_4) \cdot 1/3 \text{H}_2\text{O}$ has been measured by a number of investigators.¹⁻⁴ McGregor and Soos⁴ applied a one-dimensional Heisenberg chain model to their susceptibility data for hydrated copper oxalate and derived an excellent fit with an isotropic exchange parameter, $J_0 = -132 \text{ cm}^{-1}$.⁶ Variable-temperature magnetic susceptibility data for $\text{Fe}(\text{C}_2\text{O}_4)(\text{H}_2\text{O})_2$ have been collected by Barros and Friedberg⁷ who found evidence for two distinct ordering processes below 35 K. Their results were best interpreted in terms of a rather strong interchain spin-exchange process

which dominated the susceptibility below ca. 20 K. In addition, van Kralingen et al.⁸ have recently reported low-temperature magnetic susceptibilities for $\text{Ni}(\text{C}_2\text{O}_4)(\text{H}_2\text{O})_2$ and $\text{Co}(\text{C}_2\text{O}_4)(\text{H}_2\text{O})_2$. Both of these polymers were assumed to have linear chain structures isomorphous with $\text{Fe}(\text{C}_2\text{O}_4)(\text{H}_2\text{O})_2$.^{9,10} Data for the Co(II) complex were fit to an Ising model with $\underline{J} = -9.3 \text{ cm}^{-1}$, $\underline{g}_{\parallel} = 6.1$, and $\underline{g}_{\perp} = 3.3$ whereas the Ni(II) complex was best described in terms of the de Neef zero-field splitting-Heisenberg exchange model¹¹ with $\underline{D} = -|\underline{J}| = -11.5 \text{ cm}^{-1}$ and $\underline{g} = 2.22$.

Among the polymeric squarate complexes of divalent metal ions studied to date only $\text{Ni}(\text{C}_4\text{O}_4)(\text{H}_2\text{O})_2$ has been reported¹² to undergo a low-temperature magnetic phase transition. Based on the recent single-crystal x-ray structure determination for $\text{Ni}(\text{C}_4\text{O}_4)(\text{H}_2\text{O})_2$ ¹³ which shows a three-dimensional polymeric network of octahedrally-coordinated Ni(II) ions this ferromagnetic ordering must be associated with the onset of long-range order. However, Long¹⁴ was unable to observe any ferromagnetic ordering at $T \geq 1.3 \text{ K}$ in the ^{57}Fe Mössbauer spectrum of $\text{Fe}(\text{C}_4\text{O}_4)(\text{H}_2\text{O})_2$, although this complex has a room temperature x-ray powder pattern which indicates structural isomorphism with the Ni(II) complex.

Low-temperature magnetic properties of Cu(II)¹⁵ and Fe(II)¹⁶ polymeric complexes with λ have been reported. Both $\text{Cu}(\text{C}_6\text{H}_2\text{O}_4)$ ¹⁵ and $\text{Fe}(\text{C}_6\text{H}_2\text{O}_4)(\text{H}_2\text{O})_2$ ¹⁶ were assumed to possess similar structures to the analogous oxalate complexes but there is at present no complete single-crystal evidence to support the proposed linear-chain structures. Magnetic susceptibility data for the Cu(II) and Fe(II) complexes were fit to appropriate Heisenberg linear chain models with $\underline{J} = -9.7$ to -16.7 cm^{-1} ¹⁵ and $\underline{J} = -1.4 \text{ cm}^{-1}$,¹⁶ respectively. Essential features of the magnetic susceptibility vs. temperature behavior of $\text{Cu}(\text{C}_6\text{H}_2\text{O}_4)$ have recently been confirmed.¹⁷

Occurrence of these cooperative phenomena in low-dimensional complexes of λ - λ suggested to us the possibility of preparing mixed-valence analogs which would possess interesting properties. Our preliminary findings¹⁸ on the solid-state oxidation of $\text{Fe}(\text{C}_6\text{H}_2\text{O}_4)(\text{H}_2\text{O})_2$ with I_2 indicated that, for example, the electrical conductivity of the mixed-valence material was approximately six orders of magnitude larger

than that of the single-valence complex. During the course of this investigation we prepared two new Fe(II) complexes of \sim which were also subjected to chemical oxidation. This paper describes the results of our investigation of the synthetic, magnetic, and spectroscopic aspects of both the single- and mixed-valence iron complexes of \sim 1-3.

Experimental Section

Oxalic and squaric acids and pyrazine were obtained from Aldrich Chemical Co. 2,5-Dihydroxy-1,4-benzoquinone was obtained from Eastman Chemical Co. Squaric acid was recrystallized from water prior to use. 2,5-Dihydroxy-1,4-benzoquinone was purified by sublimation.¹⁹ $K_2C_4O_4$ was prepared by the reaction of $H_2C_4O_4$ with aqueous KOH. Pyridine was vacuum distilled from $CaSO_4$ prior to use.

$Fe(C_2O_4)(H_2O)_2$. Diaquooxalatoiron(II) was prepared as a bright yellow microcrystalline powder according to a published procedure.²⁰ Anal. Calcd for $C_2FeH_4O_6$: C, 13.34; Fe, 31.04; H, 2.24. Found: C, 13.30; Fe, 31.0; H, 2.14.

$Fe(C_4O_4)(H_2O)_2$. Method A. Diaquosquaratoiron(II) was prepared in this method by rapidly adding an ethanolic solution (50 mL) of $FeSO_4 \cdot 7H_2O$ (0.553 g, 1.992 mmol) to a 50°C aqueous solution of $H_2C_4O_4$ (0.227 g, 1.992 mmol). The solution was brought to reflux, whereupon a light purple coloration appeared in the solution²¹ and a yellow precipitate formed after several minutes. The precipitate was collected, washed with cold water, and dried at 50°C under vacuum. The ir spectrum of this product indicates the presence of ethanol in the dried compound.²² Anal. Calcd for $C_4FeH_4O_6 \cdot 1/3 CH_3CH_2OH$: C, 25.56; Fe, 25.47; H, 2.76. Found: C, 25.60; Fe, 25.5; H, 2.80.

Method B. In this procedure an aqueous solution (50 mL) of $FeCl_2 \cdot 4H_2O$ (0.398 g, 2 mmol) was added to a cold aqueous solution (150 mL) of $K_2C_4O_4$ (0.380 g, 2 mmol). The yellow precipitate which formed immediately was washed with cold water and dried at 60°C for 24 hours. Anal. Calcd for $C_4FeH_4O_6$: C, 23.56; H, 1.98; Fe, 27.39. Found: C, 23.51; H, 2.01; Fe, 27.4.

Method C. In this method 1.0 g of iron wire was placed in a degassed aqueous solution (500 mL) containing 2 g of $\text{H}_2\text{C}_4\text{O}_4$. The flask was fitted with a nitrogen inlet and a mercury bubbler. The solution was purged with N_2 gas for 30 min and then sealed to the atmosphere. During the course of several months small cubic crystals of yellow-green product formed in the flask. The product was collected and air dried at 50°C . Anal. Calcd for $\text{C}_4\text{FeH}_4\text{O}_6$: C, 23.56; Fe, 27.39; H, 1.98. Found: C, 23.60; Fe, 27.5; H, 2.06.

$\text{Fe}(\text{C}_6\text{H}_4\text{O}_2)(\text{H}_2\text{O})_2$. Diaquodihydroxybenzoquinonatoiron(II) was prepared according to a published procedure.¹⁶ Anal. Calcd for $\text{C}_6\text{FeH}_6\text{O}_6$: C, 31.34; Fe, 24.29; H, 2.63. Found: C, 30.99; Fe, 24.3; H, 2.63.

$\text{Fe}(\text{C}_4\text{O}_4)(\text{C}_5\text{H}_5\text{N})_2 \cdot 2\text{H}_2\text{O}$. Bispyridinesquaratoiron(II) dihydrate was prepared by dissolving $\text{FeCl}_2 \cdot 4\text{H}_2\text{O}$ (1.01 g, 5 mmol) in 70 mL cold *n*-propanol containing 0.8 mL pyridine. Solid $\text{H}_2\text{C}_4\text{O}_4$ (0.570 g, 5 mmol) was added to this solution with stirring. A white precipitate formed immediately.²³ An additional 25 mL of pyridine was added to the solution. After slow stirring for 30 min a dark yellow precipitate formed. The precipitate was collected and dried over CaSO_4 at room temperature. Anal. Calcd for $\text{C}_{14}\text{FeH}_{14}\text{N}_2\text{O}_6$: C, 46.44; Fe, 15.42; H, 3.90; N, 7.74. Found: C, 46.36; Fe, 15.4; H, 3.89; N, 7.72.

$\text{Fe}(\text{C}_4\text{O}_4)(\text{C}_4\text{H}_4\text{N}_2) \cdot 4\frac{1}{2}\text{H}_2\text{O}$. Pyrazinesquaratoiron(II) hydrate was prepared by dissolving $\text{FeCl}_2 \cdot 4\text{H}_2\text{O}$ (1.0 g, 5 mmol) in *n*-propanol at -5°C (ice-salt bath) and then adding solid pyrazine (0.411 g, 5.1 mmol) to this solution. A red-orange precipitate formed immediately.²⁴ Solid $\text{H}_2\text{C}_4\text{O}_4$ (0.570 g, 5 mmol) was added with stirring to the resulting mixture. After 15 min, 20 mL of water was added until the orange precipitate dissolved. The solution was maintained at -5°C for several hours during which time a dark orange precipitate formed. The product was filtered and dried under a stream of N_2 gas and then kept in vacuum at room temperature for several hours. Anal. Calcd for $\text{C}_8\text{FeH}_4\text{N}_2\text{O}_4 \cdot 4\frac{1}{2}\text{H}_2\text{O}$: C, 29.20; Fe, 16.97; H, 3.98; N, 8.51. Found: C, 29.44; Fe, 17.0; H, 3.73; N, 8.36.

$\text{Fe}(\text{C}_2\text{O}_4)(\text{H}_2\text{O})_{1.4}\text{Br}_{0.6}$. The Br_2 oxidation product of $\text{Fe}(\text{C}_2\text{O}_4)(\text{H}_2\text{O})_2$ was prepared by treating 0.500 g of $\text{Fe}(\text{C}_2\text{O}_4)(\text{H}_2\text{O})_2$ with 0.500 g of Br_2 in 250 mL of 1,2,4-trichlorobenzene with stirring at 90°C for 10 hours. The dark red product which formed was collected and kept in a vacuum desiccator at 3°C over P_2O_5 . Anal. Calcd for $\text{Br}_{0.6}\text{C}_2\text{FeH}_{2.8}\text{O}_{5.4}$: Br, 22.09; C, 11.07; Fe, 25.73; H, 1.30. Found: Br, 22.18; C, 11.34; Fe, 25.7; H, 1.18.

$\text{Fe}(\text{C}_2\text{O}_4)(\text{H}_2\text{O})_{0.9}(\text{C}_6\text{H}_4\text{O}_2)_{0.05}$. The 1,4-benzoquinone oxidation product of $\text{Fe}(\text{C}_2\text{O}_4)(\text{H}_2\text{O})_2$ was prepared by treating 1.0 g of $\text{Fe}(\text{C}_2\text{O}_4)(\text{H}_2\text{O})_2$ with 2.5 g of freshly sublimed 1,4-benzoquinone in refluxing (260°C) 1,2,4-trichlorobenzene under N_2 for 24 hours. During the course of the reaction yellow $\text{Fe}(\text{C}_2\text{O}_4)(\text{H}_2\text{O})_2$ slowly dissolved and a black solid deposited. This precipitate was collected and dried in vacuo at 150°C for several days. Anal. Calcd for $\text{C}_{2.3}\text{FeH}_2\text{O}_5$: C, 16.69; Fe, 33.75; H, 1.22. Found: C, 16.60; Fe, 33.8; H, 0.87.

$\text{Fe}(\text{C}_4\text{O}_4)(\text{C}_5\text{H}_5\text{N})_{1.5}\text{I}$. The I_2 oxidation product of bispyridinesquaratoiron(II) was prepared by heating 0.500 g of solid $\text{Fe}(\text{C}_4\text{O}_4)(\text{C}_5\text{H}_5\text{N})_2 \cdot 2\text{H}_2\text{O}$ with 1.000 g of I_2 in an open vessel at 120°C . After excess I_2 had sublimed from the reaction mixture a black product remained. Anal. Calcd for $\text{C}_9\text{FeH}_5\text{I}_{1.5}\text{NO}_4$: C, 24.72; Fe, 12.77; H, 1.15; I, 43.52; N, 3.20. Found: C, 24.24; Fe, 12.9; H, 1.24; I, 43.50; N, 3.15.

$\text{Fe}(\text{C}_6\text{H}_2\text{O}_4)\text{I}$. The I_2 oxidation product of diaquodihydroxybenzoquinonatoiron(II) was prepared by treating solid $\text{Fe}(\text{C}_6\text{H}_2\text{O}_4)(\text{H}_2\text{O})_2$ with excess I_2 in a sealed tube immersed in an oil bath held at 180°C for 48 hours. After reaction the tube was broken and connected to a vacuum line. The sample was heated to 100°C and unreacted I_2 sublimed under vacuum. Anal. Calcd for $\text{C}_6\text{FeH}_2\text{IO}_4$: C, 22.46; Fe, 17.41; H, 0.63; I, 39.56. Found: C, 23.06; Fe, 17.6; H, 0.62; I, 39.61.

$\text{Cu}(\text{C}_4\text{O}_4)(\text{H}_2\text{O})_2$ and $\text{Ni}(\text{C}_4\text{O}_4)(\text{H}_2\text{O})_2$. Diaquosquarato-copper(II) and diaquosquarato-nickel(II) were prepared by published procedures.²⁶ Anal. Calcd for $\text{C}_4\text{CuH}_4\text{O}_6$: C, 22.70; H, 1.91. Found: C, 22.72; H, 2.08. Calcd for $\text{C}_4\text{H}_4\text{NiO}_6$: C, 23.23; H, 1.95. Found: C, 23.11; H, 1.99.

Physical Measurements. Magnetic susceptibilities above 15 K were determined with a conventional Faraday balance²⁷ calibrated with $\text{Hg}[\text{Co}(\text{NCS})_4]$.²⁸ Magnetic susceptibilities below 15 K were obtained using a Princeton Applied Research vibrating sample magnetometer which has been described.²⁹ Corrections for ligand diamagnetism were taken from a table of Pascal's constants.³⁰ The diamagnetic susceptibility of the squarate dianion was taken as 30.6×10^{-6} cgsu.²⁶ Underlying filled-shell diamagnetism for Fe^{2+} was assumed to be 13×10^{-6} cgsu.³¹ Experimental magnetic susceptibilities were fit to theoretical models with a local computer routine which employs the Simplex minimization algorithm.³² In general, the relative uncertainty of the magnetic susceptibility data is somewhat greater at higher than at lower temperatures. This uncertainty is estimated to be no greater than $\pm 0.02 \mu_B$ at approximately 20 K and $\pm 0.04 \mu_B$ at 300 K. Replicate determinations were reproducible to $\pm 0.02 \mu_B$. Within the overlapping temperature range of the Faraday balance and the vibrating sample magnetometer, magnetic susceptibility data agreed to $\pm 1\%$.

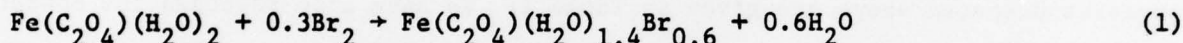
Mössbauer spectra were obtained on a spectrometer previously described.³³ The $^{57}\text{Co}(\text{Pd})$ source was maintained at room temperature in all cases. A $25 \mu\text{m}$ $\alpha\text{-Fe}$ foil ($430 \mu\text{g}$ of $^{57}\text{Fe}/\text{cm}^2$) was used as velocity calibrant. Spectrometer linearity was checked by plotting experimental Fe foil line positions vs accepted positions in mm/s. In this manner it was determined that system linearity was better than 99% of the theoretical limit. As a secondary linearity check, the positions of the Zeeman lines of Fe_3O_4 were determined. These line positions were found to be within 0.005 mm/s of the accepted line positions. Experimental Mössbauer spectra were deconvoluted by assuming Lorentzian line contours superimposed on a parabolic baseline. The mixed-valence spectra were fit with the routine FITA.³⁴ In all cases Mössbauer spectra were taken on finely ground powdered samples dispersed in Vaseline and held in a lead block between Fe-free mylar tape.

X-ray powder diffraction patterns were obtained by employing the Straumanis technique with Ni-filtered $\text{Cu K}\alpha$ radiation. Film shrinkage was checked by incorporating a small amount of KBr in the sample. Transmission of optical spectra were

recorded on a Cary 14 with samples mullied in Kel-F grease supported on quartz windows. Room-temperature electrical conductivity measurements were obtained on pressed pellet specimens by employing the van der Pauw four probe configuration³⁵ or the four in-line probe arrangement. Low-temperature electrical conductivities were obtained exclusively with the former configuration. Thermal weight loss curves were obtained on a Dupont 900 thermal analyzer coupled to a Dupont 950 thermogravimetric analyzer. Infrared spectra were obtained using a Beckman IR 20A infrared spectrophotometer. Samples were in the form of KBr pressed pellets.

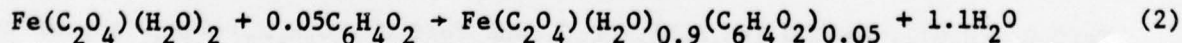
Results and Discussion

Syntheses, Stabilities, and Stoichiometries. Oxalate Complexes. Diaquooxalato-iron(II) reacts slowly with Br_2 in 1,2,4-trichlorobenzene (TCB) at 90°C to yield a single dark red oxidation product according to eq 1. Progress of this reaction was



monitored by observing the gradual disappearance of solid yellow $\text{Fe}(\text{C}_2\text{O}_4)(\text{H}_2\text{O})_2$. C, Fe, H, and Br analyses of the iron-containing product from a number of replicate experiments establish a bromine-iron ratio of 0.6 ± 0.02 , an iron-carbon ratio of 0.5 ± 0.01 , and a carbon-hydrogen ratio of 0.71 ± 0.03 . Attempted sealed-tube, solid-state oxidation of $\text{Fe}(\text{C}_2\text{O}_4)(\text{H}_2\text{O})_2$ with excess Br_2 yielded hydrated FeBr_3 and CO_2 . A similar reaction with 0.3 mole of Br_2 per mole of $\text{Fe}(\text{C}_2\text{O}_4)(\text{H}_2\text{O})_2$ gave a mixture of unreacted ferrous oxalate and FeBr_3 .

Reaction of $\text{Fe}(\text{C}_2\text{O}_4)(\text{H}_2\text{O})_2$ with purified 1,4-benzoquinone in TCB at 260°C in a nitrogen atmosphere yielded a black oxidation product according to eq 2. The stoi-



chiometry of the product was established by replicate analyses of the iron-containing product. Anaerobic reaction conditions were necessary to prevent formation of hydroquinone. The isolated oxidation product was dried under high vacuum at 150°C for several hours to insure complete removal of unreacted quinone. Solid-state treatment

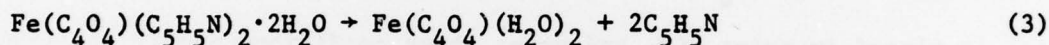
of $\text{Fe}(\text{C}_2\text{O}_4)(\text{H}_2\text{O})_2$ with 1,4-benzoquinone gave no reaction after several days at 150°C . 1,4-Naphthoquinone also apparently oxidized $\text{Fe}(\text{C}_2\text{O}_4)(\text{H}_2\text{O})_2$ in TCB at 260°C ; however, the product of this reaction was not characterized. Attempted I_2 oxidation of $\text{Fe}(\text{C}_2\text{O}_4)(\text{H}_2\text{O})_2$ either in TCB at 90°C or in the solid state at 120°C was unsuccessful.

The quinone oxidation product of $\text{Fe}(\text{C}_2\text{O}_4)(\text{H}_2\text{O})_2$ is a stable compound. We observed no change in its properties after prolonged storage at room temperature. The bromine oxidation product, however, must be stored at 0°C in a dry atmosphere. In addition the compound apparently reacts with plastic materials. Whereas the x-ray diffraction powder pattern of $\text{Fe}(\text{C}_2\text{O}_4)(\text{H}_2\text{O})_2$ was consistent with published d -spacings and line intensities,⁹ we were unable to obtain any diffraction lines for either $\text{Fe}(\text{C}_2\text{O}_4)(\text{H}_2\text{O})_{1.4}\text{Br}_{0.6}$ or $\text{Fe}(\text{C}_2\text{O}_4)(\text{H}_2\text{O})_{0.9}(\text{C}_6\text{H}_4\text{O}_2)_{0.05}$. Prolonged exposure of the bromine oxidation product to x-rays resulted in its decomposition.

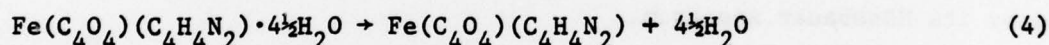
Squarate Complexes. X-ray powder diffraction data for the iron(II) squarate complexes prepared above are given in Table I. We have also recorded the powder patterns of $\text{Ni}(\text{C}_4\text{O}_4)(\text{H}_2\text{O})_2$ and $\text{Cu}(\text{C}_4\text{O}_4)(\text{H}_2\text{O})_2$. We find these powder diffraction patterns to be entirely consistent with the d -spacings tabulated by West and Niu.²⁶ Data in Table I for $\text{Fe}(\text{C}_4\text{O}_4)(\text{H}_2\text{O})_2$ are reported for $\text{Fe}(\text{C}_4\text{O}_4)(\text{H}_2\text{O})_2$ obtained by method C (Experimental Section). Based on these data the cubic lattice constant for this polymer is 8.22 ± 0.03 Å. Data for the ethanol-containing complex, $\text{Fe}(\text{C}_4\text{O}_4)(\text{H}_2\text{O})_2 \cdot \frac{1}{3} \text{CH}_3\text{CH}_2\text{OH}$, prepared by method A, are also given in Table I. This material has a powder diffraction pattern which is essentially identical to that of $\text{Fe}(\text{C}_4\text{O}_4)(\text{H}_2\text{O})_2$ except that there appears to be an approximately 5% expansion in the cubic unit cell parameter (8.63 ± 0.03 Å). The material prepared by method B is identical to that prepared by method C except that the latter method gives larger crystals.

$\text{Fe}(\text{C}_4\text{O}_4)(\text{H}_2\text{O})_2$, $\text{Fe}(\text{C}_4\text{O}_4)(\text{C}_5\text{H}_5\text{N})_2 \cdot 2\text{H}_2\text{O}$, and $\text{Fe}(\text{C}_4\text{O}_4)(\text{C}_4\text{H}_4\text{N}_2) \cdot 4\frac{1}{2}\text{H}_2\text{O}$ appear to be indefinitely stable if stored over CaSO_4 at 0°C . At room temperature the pyridine adduct turns brown and loses pyridine within several days of its preparation. These materials were insoluble in a wide range of solvents tested. In order to confirm the presence of lattice rather than coordinated water in the pyrazine and pyridine

complexes we obtained weight loss curves for the three ferrous squarate complexes. In this regard it should be noted that the thermal decomposition of $\text{Fe}(\text{C}_4\text{O}_4)(\text{H}_2\text{O})_2$ has been previously investigated.³⁶ Weight loss curves for these compounds are illustrated in Figure 1. We have included the curve for $[\text{Fe}(\text{C}_4\text{O}_4)(\text{H}_2\text{O})_2\text{OH}]_2 \cdot 2\text{H}_2\text{O}$ ³⁷ for purposes of comparison. The final decomposition product for each of the Fe(II) compounds was Fe_2O_3 as shown by an x-ray powder pattern of the residue. The most striking difference between the weight loss curve of $\text{Fe}(\text{C}_4\text{O}_4)(\text{H}_2\text{O})_2$ and those of the pyridine and pyrazine adducts is the much slower decomposition of the first relative to the second and third compound. In addition two distinct processes are apparent in the curves for the pyridine and pyrazine compounds while only one is found in the aquo analog. Process 1 (160°C) in $\text{Fe}(\text{C}_4\text{O}_4)(\text{C}_5\text{H}_5\text{N})_2 \cdot 2\text{H}_2\text{O}$ (Figure 1) accounts for a 44% weight loss and corresponds to eq 3 (44% calculated). Loss of pyridine at 160°C



was confirmed by collecting the gaseous products in a liquid nitrogen trap. A similar experiment for process 1 in the decomposition of the pyrazine compound indicates that water is initially lost from this complex at approximately 140°C (eq 4).

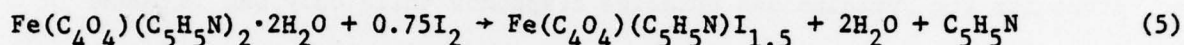


The theoretical weight loss, 24.6%, agrees well with the experimental, 24.0%. The second step in the decomposition of the pyridine and pyrazine complexes is complex but the experimental total weight loss (process 1 + process 2) agrees very well with that expected for formation of Fe_2O_3 .

It is evident that a study of the thermal decomposition of the iron(II) squarate complexes does not uniquely determine if water is present in the pyridine and pyrazine complexes as lattice or coordinated water. It does appear, however, that the structures of these two complexes are different than that of $\text{Fe}(\text{C}_4\text{O}_4)(\text{H}_2\text{O})_2$. The complicated mechanism of the solid-state decomposition of these materials may be due to a strongly hydrogen bonded network of $\text{H}_2\text{O}-\text{C}_4\text{O}_4$ units in these structures as previously suggested for $[\text{Fe}(\text{C}_4\text{O}_4)(\text{H}_2\text{O})_2\text{OH}]_2 \cdot 2\text{H}_2\text{O}$.

A large number of experiments were undertaken in an attempt to prepare mixed-valence materials derived from $\text{Fe}(\text{C}_4\text{O}_4)\text{L}_2$; $\text{L} = \text{H}_2\text{O}$, $\text{C}_5\text{H}_5\text{N}$, or $\text{C}_4\text{H}_4\text{N}_2$. In the case of $\text{Fe}(\text{C}_4\text{O}_4)(\text{H}_2\text{O})_2$ prolonged (up to one month) treatment with I_2 in the solid state resulted in very little oxidation. A number of partially oxidized and fully $\text{Fe}(\text{III})$ products were obtained from solid-state oxidations of $\text{Fe}(\text{C}_4\text{O}_4)(\text{H}_2\text{O})_2$ with excess Br_2 . None of these materials were fully characterized although the time dependence of the oxidation was monitored by ^{57}Fe Mössbauer spectroscopy and elemental analysis.

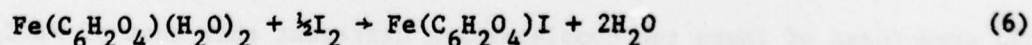
Bispyridinesquaratoiron(II) reacts with excess I_2 at 75°C in a sealed tube or at 120°C in an open container to give a black product according to eq 5. Replicate



experiments establish an iodine-iron ratio of 1.5 ± 0.1 . This oxidation product is stable if stored over CaSO_4 . However, a slow hydrolysis reaction occurs if the material is placed in moist air, and under these conditions nearly all (>90%) of the iodine is lost as I_2 . Complete Br_2 oxidation of $\text{Fe}(\text{C}_4\text{O}_4)(\text{C}_5\text{H}_5\text{N})_2 \cdot 2\text{H}_2\text{O}$ either in the solid state or in TCB occurs within two minutes at room temperature. The product of this reaction contains no carbon (as determined by microanalysis) and only $\text{Fe}(\text{III})$ as judged by its Mössbauer spectrum.

Pyrazinesquaratoiron(II) reacts slowly with I_2 in a sealed tube at 150°C . No reaction was observed at lower temperatures. The I_2 oxidation product was very unstable with respect to loss of I_2 and therefore was not characterized. As in the case of $\text{Fe}(\text{C}_4\text{O}_4)(\text{C}_5\text{H}_5\text{N})_2 \cdot 2\text{H}_2\text{O}$, Br_2 oxidation of the pyrazine complex was extremely facile giving rise to a fully oxidized material which we have not characterized.

Diaquodihydroxybenzoquinonatoiron(II) reacts with I_2 in a sealed tube at 180°C according to eq 6. $\text{Fe}(\text{C}_6\text{H}_2\text{O}_4)\text{I}$ is a stable material which does not lose iodine upon



exposure to the atmosphere. Although Br_2 reacts rapidly with $\text{Fe}(\text{C}_6\text{H}_2\text{O}_4)(\text{H}_2\text{O})_2$, the oxidation product, which we have tentatively identified as $\text{Fe}(\text{C}_6\text{H}_2\text{O}_4)\text{Br}_2$, loses Br_2 at room temperature or at 0°C in vacuum. We have not further characterized this material.

Infrared Spectra. Oxalate Compounds. The infrared spectrum of $\text{Fe}(\text{C}_2\text{O}_4)(\text{H}_2\text{O})_2$ consists of a relatively small number of absorption bands which may be assigned as follows (peak position in cm^{-1} followed by assignment): 3400, $\nu(\text{H}_2\text{O})$; 1700, ν_{CO} ; 1325, 1370, ν_{CC} ; 820, δ_{OCO} ; 700, $\rho_{\text{r}}(\text{H}_2\text{O})$; 500, $\rho_{\text{w}}(\text{H}_2\text{O})$; 490, $\nu_{\text{Fe-O}}$. Essential features of this spectrum are unchanged upon partial oxidation of $\text{Fe}(\text{C}_2\text{O}_4)(\text{H}_2\text{O})_2$ by either Br_2 or 1,4-benzoquinone. The band at 1700 cm^{-1} assigned to ν_{CO} is unchanged upon chemical oxidation and no bands assignable to free C=O are observed at higher frequencies. We are able to detect additional weak bands in the region $1100\text{--}1600 \text{ cm}^{-1}$ in the spectrum of the quinone oxidation product. These weak bands are assigned to ν_{CO} and ν_{CC} for the form of 1,4-benzoquinone present in the complex.

Squarate Compounds. Infrared band positions and assignments for the iron squarate complexes prepared above are listed in Table II. Figure 2 illustrates the spectra of these complexes in the range $1900\text{--}250 \text{ cm}^{-1}$. Our assignments for $\text{Fe}(\text{C}_4\text{O}_4)(\text{H}_2\text{O})_2$ are consistent with those of Long¹⁴ and West and Niu.²⁶ The most pronounced feature of the spectrum of the aquo complex is the broad, symmetric band centered at 1520 cm^{-1} which is assigned to ν_{CO} , the carbon-oxygen stretching mode of coordinated (D_{4h}) squarate dianion. This absorption is more asymmetric in the pyridine and pyrazine complexes and is shifted to approximately 1500 cm^{-1} . A number of sharp absorption bands in $\text{Fe}(\text{C}_4\text{O}_4)(\text{C}_5\text{H}_5\text{N})_2 \cdot 2\text{H}_2\text{O}$ are assigned to coordinated pyridine. These absorptions are marked with a + in Figure 2. The presence of coordinated, rather than lattice, pyridine is suggested by certain band shifts relative to free pyridine.³⁸ For example, the normal modes observed at 1580, 990, 601, and 405 cm^{-1} in free pyridine³⁹ are found at 1590, 1017, 630, and 420 cm^{-1} , respectively, in $\text{Fe}(\text{C}_4\text{O}_4)(\text{C}_5\text{H}_5\text{N})_2 \cdot 2\text{H}_2\text{O}$. These shifts to higher frequency are similar to those observed for $\text{Fe}(\text{C}_5\text{H}_5\text{N})_{2,4}\text{Cl}_2$ complexes.³⁸ These relatively large positive shifts are presumed³⁸ due to pyridine-ligand interactions rather than pyridine σ/π framework distortions upon coordination.

Similar shifts are observed in absorption bands which are assignable to coordinated pyrazine in $\text{Fe}(\text{C}_4\text{O}_4)(\text{C}_4\text{H}_4\text{N}_2) \cdot 4\text{H}_2\text{O}$ (Figure 2, spectrum C). Our assignments

are in agreement with those made previously for neat pyrazine.⁴⁰ We observe several weak absorptions in the range 1650-1800 cm^{-1} but have been unable to ascribe any significance to these bands. In addition several broad bands near 600 cm^{-1} are unassigned.

A portion of the infrared spectrum of $\text{Fe}(\text{C}_4\text{O}_4)(\text{C}_5\text{H}_5\text{N})\text{I}_{1.5}$ is shown as spectrum D in Figure 2. The remainder of the spectrum is identical to that of $\text{Fe}(\text{C}_4\text{O}_4)(\text{C}_5\text{H}_5\text{N})_2 \cdot 2\text{H}_2\text{O}$. The essential difference between spectra D and B is the appearance of two rather strong bands at 1810 and 870 cm^{-1} in the former. The 1810 cm^{-1} absorption corresponds to the carbonyl stretching frequency for free C=O in squaric acid. This absorption occurs at 1815 cm^{-1} in $[\text{Fe}(\text{C}_4\text{O}_4)(\text{H}_2\text{O})_2\text{OH}]_2 \cdot 2\text{H}_2\text{O}$.³⁷ It therefore appears that I_2 oxidation of $\text{Fe}(\text{C}_4\text{O}_4)(\text{C}_5\text{H}_5\text{N})_2 \cdot 2\text{H}_2\text{O}$ has partially degraded the polymer.

Dihydroxybenzoquinone Compounds. Infrared spectra of 2,5-dihydroxy-1,4-benzoquinone, $\text{Fe}(\text{C}_6\text{H}_2\text{O}_4)(\text{H}_2\text{O})_2$ and $\text{Fe}(\text{C}_6\text{H}_2\text{O}_4)\text{I}$ are illustrated in Figure 3. Upon complexation ν_{CO} of the dihydroxybenzoquinone ligand at 1630 cm^{-1} (Figure 3, spectrum A) shifts to 1510 cm^{-1} in both the single- (spectrum B) and mixed-valence (spectrum C) complexes. An additional strong band near 500 cm^{-1} is observed in the spectrum of $\text{Fe}(\text{C}_6\text{H}_2\text{O}_4)(\text{H}_2\text{O})_2$. Several shoulders on this absorption band are resolved in the spectrum of the iodine oxidation product. Because these absorptions are absent in the spectrum of the ligand it may be possible to assign one or more of them to iron-oxygen stretching modes, $\nu_{\text{Fe-O}}$. Upon iodine oxidation of $\text{Fe}(\text{C}_6\text{H}_2\text{O}_4)(\text{H}_2\text{O})_2$ no additional bands are introduced which may be assigned to free carbonyl stretching modes. This is shown in Figure 3 by a comparison of spectra B and C in the region 1800-1550 cm^{-1} . This absence of free carbonyl groups in $\text{Fe}(\text{C}_6\text{H}_2\text{O}_4)(\text{H}_2\text{O})_2$ suggests that the polymer has not been degraded during chemical oxidation with I_2 .

Mössbauer Spectroscopy. Oxalate Compounds. Room temperature ⁵⁷Fe Mössbauer spectra of $\text{Fe}(\text{C}_2\text{O}_4)(\text{H}_2\text{O})_2$, $\text{Fe}(\text{C}_2\text{O}_4)(\text{H}_2\text{O})_{0.9}(\text{C}_6\text{H}_4\text{O}_2)_{0.05}$, and $\text{Fe}(\text{C}_2\text{O}_4)(\text{H}_2\text{O})_{1.4}\text{Br}_{0.6}$ are shown in Figure 4. Appropriate Mössbauer parameters are given in Table III. The Mössbauer spectrum of $\text{Fe}(\text{C}_2\text{O}_4)(\text{H}_2\text{O})_2$ has been studied by several investigators.⁴¹⁻⁴⁵ De Menezes and Barros⁴⁵ have recently published an analysis of the 4.2 K Mössbauer

spectrum of this compound. The spectrum consists of eight Zeeman lines (seven of which are well resolved) which were fit to an appropriate hamiltonian with the asymmetry parameter, η , equal to 0.76. The significance of the fitting parameters was understood by considering the structure of $\text{Fe}(\text{C}_2\text{O}_4)(\text{H}_2\text{O})_2$ ⁹ shown in Figure 5. If the principal component of the electric field gradient tensor lies along the Fe-O (water) bond then the internal hyperfine field is found in the $\text{Fe}(\text{C}_2\text{O}_4)$ molecular plane. The orientation of the internal hyperfine field and the large value of η were assumed to⁴⁵ support a two-step magnetization process previously observed⁷ for this complex. Our magnetic susceptibility results do not indicate such a two-step ordering mechanism. However, the large value of η is consistent with a strong intrachain spin exchange process leading to substantial one-dimensional ordering below ca. 30 K (vide infra).

The room-temperature Mössbauer spectrum of $\text{Fe}(\text{C}_2\text{O}_4)(\text{H}_2\text{O})_{0.9}(\text{C}_6\text{H}_4\text{O}_2)_{0.05}$ (spectrum B, Figure 4) consists of discrete Fe(II) and Fe(III) quadrupole doublets. Quadrupole splitting and isomer shift parameters for the Fe(II) site are essentially identical to those for the Fe(II) site in $\text{Fe}(\text{C}_2\text{O}_4)(\text{H}_2\text{O})_2$ (Table III); however, line widths in the oxidation product are very large compared to the single-valence compound. At lower temperatures a second Fe(II) site is discerned as a shoulder on the high velocity Fe(II) absorption. A typical low-temperature spectrum, taken at 50 K, is illustrated in Figure 6 together with a suggested assignment based on one Fe(III) and two Fe(II) sites. In this particular fit the fitted areas of Fe(II) sites A and B are found to be in the ratio of 1.56 to 1.00 and the ratio of total Fe(II) to Fe(III) area is 3.18. The presence of the second Fe(II) site may be due to the partial dehydration of the polymer or may be a necessary consequence of oxidation. Random oxidation of the $\text{Fe}(\text{C}_2\text{O}_4)(\text{H}_2\text{O})_2$ chain will result in a polymer in which each Fe(II) ion may be bound to zero, one, or two Fe(III) sites. The site distribution will depend on the total number of Fe(III) sites, that is, on the degree of polymer oxidation. In the case of the quinone oxidation product, assuming a two electron reduction, 10% of the polymer is oxidized. On the average both hydrated and

dehydrated Fe(II) sites will be oxidized and the approximate ratio of Fe(II)-Fe(III) to Fe(II)-Fe(II) pairs will be 0.1; thus a large number of distinct Fe(II) and Fe(III) sites exist and it is not surprising that they are only partially resolved by Mössbauer spectroscopy.

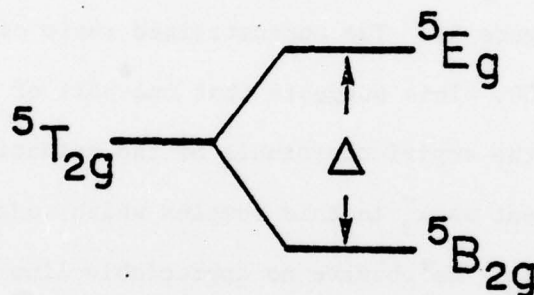
The Mössbauer spectrum of the Br_2 oxidation complex (Figure 4, spectrum C) may be understood in a similar manner. The stoichiometry of the oxidation product indicates that no dehydration of the polymer has occurred other than that which may be accounted for by H_2O displacement with Br^- . A statistical distribution of oxidized sites would provide significant numbers of Fe(II) sites with zero, one, and two Fe(III) neighbors. Consequently, even more breadth would be expected in the high-velocity absorption of this compound. Surprisingly this absorption is quite sharp suggesting that the broad absorption observed for $\text{Fe}(\text{C}_2\text{O}_4)(\text{H}_2\text{O})_{0.9}(\text{C}_6\text{H}_4\text{O}_2)_{0.05}$ is most probably due to the partial dehydration which accompanies its formation.

Fe(III)-Fe(II) area ratios for the Br_2 oxidation product do not vary with temperature. At room temperature this ratio is 1.10 in reasonable agreement with the ratio of oxidized to unoxidized sites of 1.50 as determined by chemical analysis. This agreement is acceptable given uncertainties in the analytical data and the fact that it may be a poor approximation to determine site populations on the basis of Mössbauer area ratios.⁴⁶

Both the Br_2 and quinone oxidation products of $\text{Fe}(\text{C}_2\text{O}_4)(\text{H}_2\text{O})_2$ display the onset of long-range order by the appearance of a complex Zeeman pattern below ca. 20 K. Because our measurements are limited to $T \geq 15$ K we have not been able to observe the completely ordered spectrum. Our preliminary findings indicate that at least two hyperfine fields are present in the Mössbauer spectra at ca. 20 K along with the four-line paramagnetic spectrum of the mixed-valence chain.

Squarate Complexes. Room-temperature Mössbauer spectra of $\text{Fe}(\text{C}_4\text{O}_4)(\text{H}_2\text{O})_2$, $\text{Fe}(\text{C}_4\text{O}_4)(\text{C}_5\text{H}_5\text{N})_2 \cdot 2\text{H}_2\text{O}$, and $\text{Fe}(\text{C}_4\text{O}_4)(\text{C}_4\text{H}_4\text{N}_2) \cdot 4\frac{1}{2}\text{H}_2\text{O}$ are shown in Figure 7. Spectral parameters are listed in Table IV. The spectra are composed of simple quadrupole doublets in the temperature range 300-17 K. Long¹⁴ has recently obtained the 1.3 K

spectrum of $\text{Fe}(\text{C}_4\text{O}_4)(\text{H}_2\text{O})_2$. At this temperature the spectrum consists of a single unbroadened quadrupole doublet with $\Delta E_Q = 2.76$ and $\delta = 1.41$ mm/s.¹⁴ At room temperature the aquo and pyridine complexes display quadrupole splittings which are considerably lower than that of the pyrazine complex. In addition the temperature dependence of ΔE_Q for the first two complexes is greater than for the pyrazine complex. An analysis of the temperature dependence of ΔE_Q for these compounds is illustrated in Figure 8. This temperature dependence may be explained in terms of a low-symmetry crystal field splitting of the $^5T_{2g}$ ground term of octahedral high-spin Fe(II). If the ligand field is tetragonal the ground term splitting diagram shown below is applicable, where $|\Delta|$ is the tetragonal distortion parameter. In order to



calculate the temperature dependence of ΔE_Q by using this two level model we assume that the small effect of spin orbit coupling may be ignored and that the thermal distribution of the 5E_g and $^5B_{2g}$ terms follows a Boltzmann distribution as in eq 7

$$F(\Delta, T) = (1 - e^{-\Delta/kT}) / (a + b e^{-\Delta/kT}) \quad (7)$$

where $a = 1$ and $b = 2$ if Δ is positive and $a = 2$ and $b = 1$ if Δ is negative (orbital doublet lies lowest).⁴⁶ $F(\Delta, T)$ is proportional to the valence contribution to the EFG tensor as given in eq 8 where α^2 is the covalency parameter and r_o^{-3} is the free

$$F(\Delta, T) = q_{\text{valence}} / 4/7 r_o^{-3} \alpha^2 \quad (8)$$

ion 3d radial expectation value.⁴⁷ If we assume that there is no lattice contribution to the EFG then the quadrupole splitting may be determined according to eq 9. In

$$\Delta E_Q(T) / \Delta E_Q(0 \text{ K}) = F(\Delta, T) \quad (9)$$

Figure 8 we have approximated the 0 K value of ΔE_Q for each of the complexes by using our value of ΔE_Q determined at 17 K. The temperature variation of ΔE_Q for each of the complexes was reproduced within experimental error with ground term splittings of $475\text{--}550\text{ cm}^{-1}$ for $\text{Fe}(\text{C}_4\text{O}_4)(\text{H}_2\text{O})_2$, 425 cm^{-1} for $\text{Fe}(\text{C}_4\text{O}_4)(\text{C}_5\text{H}_5\text{N})_2 \cdot 2\text{H}_2\text{O}$, and 850 cm^{-1} for $\text{Fe}(\text{C}_4\text{O}_4)(\text{C}_4\text{H}_4\text{N}_2) \cdot 4\frac{1}{2}\text{H}_2\text{O}$ (Figure 8) by assuming an orbitally nondegenerate $^5\text{B}_{2g}$ ground term. These values of Δ are in substantial agreement with the ground term splitting derived from the temperature dependence of the magnetic susceptibility of these complexes (vide infra).

The room temperature Mössbauer spectrum of the I_2 oxidation product of $\text{Fe}(\text{C}_4\text{O}_4)(\text{C}_5\text{H}_5\text{N})_2 \cdot 2\text{H}_2\text{O}$ (Table IV) is very similar to the spectrum of $\text{Fe}(\text{C}_2\text{O}_4)(\text{H}_2\text{O})_{1.4}\text{Br}_{0.6}$ (shown as spectrum C in Figure 4). The unconstrained ratio of the area of the Fe(II) to the Fe(III) sites is 1.00. This suggests that one-half of the iron in this complex has been oxidized. Given the empirical formula of the oxidation product it appears likely that iodine is present as I_3^- in this complex which suggests a molecular formula $[\text{Fe}^{\text{II}}(\text{C}_4\text{O}_4)_2(\text{C}_5\text{H}_5\text{N})_2\text{Fe}^{\text{III}}]\text{I}_3$. We observe no appreciable line broadening of either the Fe(II) or Fe(III) quadrupole doublets in going from 300 to 17 K. There is also no indication of a Zeeman pattern in the 17 K spectrum.

Dihydroxybenzoquinone Compounds. Room-temperature Mössbauer spectra of $\text{Fe}(\text{C}_6\text{H}_2\text{O}_4)(\text{H}_2\text{O})_2$ and $\text{Fe}(\text{C}_6\text{H}_2\text{O}_4)\text{I}$ are illustrated in Figure 9 and spectral parameters given in Table V. As reported previously,¹⁶ it is necessary to include a small amount of an Fe(III) quadrupole doublet ($A_{\text{Fe}^{3+}}/A_{\text{Fe}^{2+}} = 0.14$) in the analysis of the unoxidized material. This component presumably results from a chain-terminating oxidation of the $\text{Fe}(\text{C}_6\text{H}_2\text{O}_4)(\text{H}_2\text{O})_2$ polymer. The spectrum of $\text{Fe}(\text{C}_6\text{H}_2\text{O}_4)\text{I}$ (spectrum B, Figure 9) consists of at least two quadrupole doublets. The result of fitting the spectrum to four unconstrained lines is illustrated in Figure 9. This particular fit is of questionable utility because of the unrealistic line width ratio of the two Fe(II) lines. We were unable to find a unique fit to this spectrum by assuming two distinct Fe(II) sites. Spectra taken at lower temperatures also showed no improved resolution of the high velocity Fe(II) absorption. Our assignments of the Fe(II) and Fe(III) quadrupole

doublets were suggested by results of numerous attempted fittings with a variety of constraints. If we consider the Fe(II) quadrupole doublet as referring to an average Fe(II) site then an area ratio $\text{Fe(II)}_{\text{total}}/\text{Fe(III)} = 2.44$ is obtained from the fit shown in Figure 9. If iodine were present as the iodide ion, the complex would contain only Fe(III). The large Fe(II) content observed suggests that iodine is present as the triiodide ion, I_3^- , as in the squarate complex. The appropriate molecular formula is then $[\text{Fe(II)}_2\text{Fe(III)}(\text{C}_6\text{H}_2\text{O}_4)_3]\text{I}_3$, for which the expected area ratio is 2.00.

~~Electronic Spectra of the Fe(II) Squarate Complexes.~~ Solid-state transmission electronic spectra of $\text{Fe}(\text{C}_4\text{O}_4)(\text{C}_5\text{H}_5\text{N})_2 \cdot 2\text{H}_2\text{O}$ and $\text{Fe}(\text{C}_4\text{O}_4)(\text{C}_4\text{H}_4\text{N}_2) \cdot 4\frac{1}{2}\text{H}_2\text{O}$ in the spectral region $4000\text{--}24000\text{ cm}^{-1}$ are illustrated in Figure 10. Sharp spectral bands below 8000 cm^{-1} are characteristic of ligand combination and/or overtone absorption. The broad band at approximately 20000 cm^{-1} in the pyrazine complex is typical of a charge-transfer transition. The broad absorptions in the region $9000\text{--}13000\text{ cm}^{-1}$ may be assigned as transitions to the $^5\text{B}_{1g}$ and $^5\text{A}_{1g}$ terms derived from the octahedral $^5\text{E}_g$ excited term as illustrated in Figure 11.⁴⁸ This figure also gives energies of each of the D_{4h} terms expressed as functions of the quadrate crystal-field parameters, D_s and D_t .⁴⁹ Low-symmetry crystal-field parameters were calculated by using the relations (eq 10) derived from the energies in Figure 11.

$$\text{D}_s = \frac{1}{7}(\nu_3 - \nu_2 + \nu_1)$$

$$\text{D}_t = \frac{1}{5}(\nu_3 - \nu_2 - 4\text{D}_s)$$

$$\text{D}_q(\text{equatorial}) \equiv \text{D}_q(\underline{e}) = \nu_2/10$$

$$\text{D}_q(\text{axial}) \equiv \text{D}_q(\underline{a}) = \text{D}_q(\underline{e}) - \frac{7}{4}\text{D}_t \quad (10)$$

Positions of crystal-field absorption maxima, ν_2 and ν_3 , the ground state splitting (see Mössbauer spectroscopy section), ν_1 , and derived crystal-field parameters for the Fe(II) squarate complexes are given in Table VI. Our values of ν_2 and ν_3 for $\text{Fe}(\text{C}_4\text{O}_4)(\text{H}_2\text{O})_2$ are identical to those given by Long.¹⁴

Magnetic Susceptibility Data. Oxalate Compounds. Magnetic susceptibilities and effective moments as a function of temperature for $\text{Fe}(\text{C}_2\text{O}_4)(\text{H}_2\text{O})_2$ are given in Table VII.⁵⁰ Figure 12 is a plot of the inverse molar susceptibility vs temperature. At temperature in excess of 90 K the susceptibility shows approximate Curie law behavior with a Curie constant of 3.0. In this high temperature range $\bar{\mu}_{\text{eff}}$ increases from $4.82\mu_B$ at 90 K to $5.00\mu_B$ at 200 K and thereafter falls to $4.91\mu_B$ at 286 K. This behavior is typical of tetragonally distorted Fe(II) in which the high temperature susceptibility is dominated by a Boltzman distribution between two terms separated by $kT \approx 200$ K. At lower temperature the susceptibility deviates very strongly from Curie law behavior in a manner indicative of antiferromagnetic ordering. These data in the low temperature region are shown on an expanded scale in Figure 13. The susceptibility data pass through a smooth rounded maximum at approximately 32 K. We observe no second maximum at lower temperatures, in contrast to the findings of Barros and Friedberg.⁷ We believe that the addition susceptibility maximum previously reported⁷ is due to significant amounts of impurities in the commercial sample of $\text{Fe}(\text{C}_2\text{O}_4)(\text{H}_2\text{O})_2$ used by these investigators.

We have attempted to theoretically reproduce essential features of the experimental susceptibility of $\text{Fe}(\text{C}_2\text{O}_4)(\text{H}_2\text{O})_2$. Results for two fitting procedures are illustrated in Figure 13. Curve A is the best fit obtained by using the Heisenberg linear-chain model modified by inclusion of an interchain spin-exchange term, eq 11.^{51,52} In this expression χ_{LC} is given

$$\chi_{\text{inter}} = \chi_{\text{LC}} / (1 - 2ZJ'\chi_{\text{LC}} / N\beta^2 S^2) + N\alpha \quad (11)$$

by eq 12⁵² in which J is the intrachain spin-exchange parameter, N is Avogadro's number, β is the Bohr magneton, k is Boltzmann's constant, and S is the individual ion spin. The parameter J' in eq 11 is the interchain spin-exchange parameter and Z is

$$\chi_{LC} = N\beta^2 g^2 S(S+1) \{1 - T/2JS(S+1) + \coth[2JS(S+1)/T]\} / 3kT \{1 + T/2JS(S+1) - \coth[2JS(S+1)/T]\} \quad (12)$$

the number of nearest neighbor chains. The behavior of the functions described by eq 12 and 11 is shown in Figures 14 and 15, respectively. Whereas the effect of decreasing J is to both shift the susceptibility maximum to higher T and reduce the value of the susceptibility at the maximum, the effect of decreasing J' is to simply lower the susceptibility maximum. In no instance however does the theoretical susceptibility approach zero at low temperatures as does the experimental susceptibility of $\text{Fe}(\text{C}_2\text{O}_4)(\text{H}_2\text{O})_2$ (Figure 13). The upper curve, A, in Figure 13 was calculated by using eq 11 with $J = -4.4 \text{ cm}^{-1}$, $ZJ' = 10.7 \text{ cm}^{-1}$, $g = 2.02$, and $N\alpha = 60 \times 10^{-6} \text{ cgsu}$. The calculated susceptibility maximum, 32.3 K, agrees well with the experimental maximum obtained by inspection. The theoretical fit however diverges very substantially from the experimental points below 25 K. We ascribe this deviation to the onset of long-range three-dimensional ordering below 25 K as observed also by Mössbauer spectroscopy. The rapid decrease in susceptibility at low temperature requires antiferromagnetic ordering even though the interchain coupling is ferromagnetic as demonstrated by the positive value of ZJ' . In fact the susceptibility below 80 K can be reproduced very well (curve B in Figure 13) using the Heisenberg-Dirac-Van Vleck $S_1=S_2=2$ spin-coupled dimer model.³⁵ Although this model has no direct physical significance here its success at modeling the data suggests the dominance of pairwise antiferromagnetic interactions. The slight increase in susceptibility below approximately 7 K may be ascribed to a small amount of paramagnetic impurity.

Experimental magnetic susceptibilities and moments for $\text{Fe}(\text{C}_2\text{O}_4)(\text{H}_2\text{O})_{0.9}(\text{C}_6\text{H}_4\text{O}_2)_{0.05}$ and $\text{Fe}(\text{C}_2\text{O}_4)(\text{H}_2\text{O})_{1.4}\text{Br}_{0.6}$ are given in Tables VIII and IX, respectively.⁵⁰ Susceptibility data for the former material are plotted vs temperature in Figure 16. The principal feature of these data is the broad maximum near 54 K. This maximum is nicely reproduced by using the modified Heisenberg linear chain equation, eq 11, in which $J = -6.8 \text{ cm}^{-1}$, $g = 1.96$, $ZJ' = 16.7 \text{ cm}^{-1}$, and $N\alpha = 60 \times 10^{-6} \text{ cgsu}$. However,

at $T < 50$ K there is a large discrepancy between experimental and calculated points which is due to the onset of long-range antiferromagnetic order below this temperature as evidenced by the appearance of Zeeman lines in the Mössbauer spectrum of this compound at ca. 20 K (vide supra). In addition to the 50 K maximum a smaller inflection in the susceptibility data is observed near 20 K. This feature may be associated with the onset of long-range order. Unfortunately lack of a suitable theoretical model precludes a detailed analysis of this portion of the susceptibility curve. As for $\text{Fe}(\text{C}_2\text{O}_4)(\text{H}_2\text{O})_2$ a gradual increase in the susceptibility below 8 K is observed in Figure 16. Again it is not clear if this feature is due to the presence of a small amount of impurity or if it is the result of a distinct physical process occurring in the polymer.

Figure 17 illustrates experimental magnetic susceptibilities and moments for the Br_2 oxidation product. As in the case of the quinone oxidation product, this material possesses a susceptibility maximum near 50 K. However, in contrast to the former compound, this material is characterized by a gradual increase in its susceptibility at $T < 25$ K. Application of eq 11 to these data results in the fit shown as the solid curve in Figure 17. Parameters of the fitting are $\underline{J} = -5.3 \text{ cm}^{-1}$, $\underline{g} = 2.43$, $\underline{ZJ}' = 3.5 \text{ cm}^{-1}$, and $\underline{N}\alpha = 60 \times 10^{-6}$ cgsu. The fit is very good above 40 K but fails to account for the low-temperature susceptibility increase. On the basis of analytical and Mössbauer results given above the Br_2 oxidation product contains approximately equal proportions of Fe(II) and Fe(III) sites and therefore may be regarded as a polymer with approximate molecular formula $\text{Fe}^{\text{II}}\text{Fe}^{\text{III}}(\text{C}_2\text{O}_4)_2(\text{H}_2\text{O})_3\text{Br}$. For this reason we fit the susceptibility data for this complex to the appropriate Heisenberg-Dirac-van Vleck expression for an $\underline{S}_1 = 2$, $\underline{S}_2 = \frac{5}{2}$ dimer, eq 13, where $\underline{X} = \underline{J}/kT$. The result of this fitting is illustrated as the dashed line in Figure 17 for

$$\chi_M = \frac{N\beta^2 g^2}{4kT} [165 + 84 \exp(9\underline{X}) + 35 \exp(16\underline{X}) + 10 \exp(21\underline{X}) + \exp(24\underline{X})] / [5 + 4 \exp(9\underline{X}) + 3 \exp(16\underline{X}) + 2 \exp(21\underline{X}) + \exp(24\underline{X})] \quad (13)$$

which $\underline{J} = -18.2 \text{ cm}^{-1}$ and $\underline{g} = 2.00$. This dimer equation predicts an increase in the susceptibility at low temperatures ($T < 25 \text{ K}$) as observed for the experimental data.

Squarate Compounds. Experimental magnetic susceptibility data for $\text{Fe}(\text{C}_4\text{O}_4)(\text{H}_2\text{O})_2$, $\text{Fe}(\text{C}_4\text{O}_4)(\text{C}_5\text{H}_5\text{N})_2 \cdot 2\text{H}_2\text{O}$, and $\text{Fe}(\text{C}_4\text{O}_4)(\text{C}_4\text{H}_4\text{N}_2) \cdot 4\frac{1}{2}\text{H}_2\text{O}$ are given in Tables X-XII, respectively.⁵⁰ Figure 18 illustrates the approximate linear behavior of the inverse corrected molar susceptibility vs temperature for the aquo complex. Thus we are unable to detect the presence of a spin-exchange interaction in the aquo complex in the temperature range 4.2-300 K. We were able to describe the magnetic susceptibility data by using the low-symmetry (\underline{D}_{4h}) electrostatic matrix elements of Figgis *et al.*⁵⁴ Susceptibility data for the aquo complex were fit to the appropriate partition function after the crystal-field matrices were diagonalized with suitable values of λ , ν , and k . The line shown in Figure 18 represents the theoretical inverse susceptibility calculated from this model with $\lambda = -80 \text{ cm}^{-1}$, $\nu = -4$, and $k = 0.8$. From the fitted value of ν ($=\nu_1/\lambda$) we find $\nu_1 = 320 \text{ cm}^{-1}$. This value for the ground term splitting is smaller than that obtained from an analysis of the temperature dependence of ΔE_Q ($475\text{--}550 \text{ cm}^{-1}$). However, if one considers the relative uncertainty in the data and the assumptions made in the analysis of the ΔE_Q data, values of ν_1 obtained by the two methods are in adequate agreement.

Figure 19 illustrates the temperature behavior of magnetic susceptibilities and effective magnetic moments for the pyrazine and pyridine complexes. Effective magnetic moments for these compounds are insensitive to temperature changes in the range 100-300 K. Above ca. 30 K the susceptibility of these materials obeys the Curie-Weiss law with small negative Weiss constants. In the range 10-300 K susceptibility data for the pyridine complex are described by using the \underline{D}_{4h} model⁵⁴ with $\lambda = -80 \text{ cm}^{-1}$, $\nu = -10$, and $k = 0.5$ (curve A in Figure 19). These parameters describe equally well the susceptibility data for the pyrazine complex above ca. 40 K. However, in order to fit the data for the pyrazine complex below 40 K we found it necessary to utilize eq 11, the Heisenberg chain model modified for interchain coupling. Curve B in Figure 19 represents

the solution to eq 11 with $\underline{J} = -0.26 \text{ cm}^{-1}$, $\underline{g} = 2.20$, $\underline{zJ}' = -0.02 \text{ cm}^{-1}$, and $\underline{N\alpha} = 53 \times 10^{-6} \text{ cgsu}$.

These models are compared in Figure 20 by illustrating the low-temperature inverse susceptibility data for the pyridine and pyrazine complexes. These data are plotted against $\log T$ in order to separate the lowest-temperature data points from one another and also to clearly distinguish the theoretical curves. Curve A represents the \underline{D}_{4h} model with parameters given above. Curve C is the Curie-Weiss law with $C = 3.54$ and $\theta = 3.0 \text{ K}$. Curve B, on the other hand, represents eq 11 with parameters given above. The modified Heisenberg model appears to be a significantly better model for the pyrazine complex than is the \underline{D}_{4h} model. Unfortunately, we were unable to detect a maximum in the susceptibility curve for the pyrazine complex down to 1.8 K. The shape of the curve in the low-temperature region does, however, suggest that the antiferromagnetic Neel temperature is slightly less than 1.8 K. A clear distinction between the Heisenberg and \underline{D}_{4h} models is not possible on the basis of our data for the pyridine complex. If eq 11 is applied to these data a value of $\underline{J} > -0.05 \text{ cm}^{-1}$ is obtained. Such a low value of the exchange parameter cannot be detected with magnetic susceptibility data above 4.2 K and low-temperature esr data will be required to determine \underline{J} for this material.

The observation that a linear-chain model is required to explain the magnetic behavior of the pyrazine but not the pyridine or aquo complexes suggests a structure for the pyrazine complex analogous to those postulated for the similar Fe(II) dihydroxybenzoquinone polymers.¹⁶ We suggest that the pyrazine and pyridine complexes are linear-chain polymers with bis-chelated squarate dianions and that in the pyrazine complex these chains are interconnected to form a two-dimensional array by bridging bidentate pyrazine. Spin exchange through the squarate bridge has been shown to be weak¹⁴ and consequently the pyridine and aquo complexes behave as if they contain isolated iron(II) ions. By contrast, bridging pyrazine is known to support spin exchange and linear-chain magnetic behavior is expected to prevail in a direction perpendicular to the squarate bridging direction.

Magnetic susceptibilities and effective magnetic moments for $\text{Fe}(\text{C}_4\text{O}_4)(\text{C}_5\text{H}_5\text{N})\text{I}_{1.5}$ are given in Table XIII.⁵⁰ Susceptibility data for this compound maximize near 70 K and a gradual increase in the susceptibility occurs below 30 K. Attempts to model this behavior were unsuccessful in that chemically-meaningful values of exchange constants were not obtained by applying any of the theoretical expressions used above.

Dihydroxybenzoquinone Compounds. Experimental magnetic susceptibility data for $\text{Fe}(\text{C}_6\text{H}_2\text{O}_4)\text{I}$ are given in Table XIV.⁵⁰ Figure 21 illustrates the temperature behavior of $\bar{\chi}'_M$ and $\bar{\mu}_{\text{eff}}$ for this complex. The susceptibility vs temperature behavior of this mixed-valence material is dramatically different from that previously observed¹⁶ for the polymeric Fe(II) complex $\text{Fe}(\text{C}_6\text{H}_2\text{O}_4)(\text{H}_2\text{O})_2$, which may be described as a Heisenberg linear chain with $J = -1.4 \text{ cm}^{-1}$.¹⁶

Electrical Conductivity Studies

Dc electrical conductivities of each of the mixed-valence materials were measured on pressed pellets of powdered samples using the van der Pauw four-probe technique³⁵ with pressure contacts. Replicate measurements for all the complexes produced conductivities which were reproducible to within one order of magnitude. At room temperature the following average electrical conductivities were obtained: $\text{Fe}(\text{C}_2\text{O}_4)(\text{H}_2\text{O})_{1.4}\text{Br}_{0.6}$, 6×10^{-4} ; $\text{Fe}(\text{C}_2\text{O}_4)(\text{H}_2\text{O})_{0.9}(\text{C}_6\text{H}_4\text{O}_2)_{0.05}$, 2×10^{-4} ; $\text{Fe}(\text{C}_4\text{O}_4)(\text{C}_5\text{H}_5\text{N})\text{I}_{1.5}$, 1×10^{-6} ; $\text{Fe}(\text{C}_6\text{H}_2\text{O}_4)\text{I}$, $5 \times 10^{-5} \Omega^{-1} \text{cm}^{-1}$. These conductivities are much larger than those measured for the respective unoxidized polymers ($\sigma^{300\text{K}} < 1 \times 10^{-10} \Omega^{-1} \text{cm}^{-1}$). Conductivities of several samples of the mixed-valence materials were also measured at ca. 20 and 80 K. For a given pressed pellet the conductivity decreased by a factor of approximately ten upon cooling the sample from room temperature to 80 K. An additional factor of ten conductivity decrease was observed upon cooling the sample from 80 to ca. 20 K, confirming their semiconducting behavior. Because of the rather large uncertainty in measured conductivities of these materials we have not extended these measurements to other temperatures, nor have we determined band gap energies from these conductivity data. It is clear that the enhanced electrical conductivity of the partially-oxidized polymers is associated with the mixed-valence nature of these materials.

Conclusions

Polymeric Fe(II) complexes of the oxalate, squarate, and dihydroxybenzoquinone dianions have been prepared. The fifth and sixth (axial) iron coordination sites in these materials are occupied by water molecules although in certain cases other basic ligands can be substituted for water. A tetragonal structure of this sort is substantiated by both the temperature dependence of Mössbauer spectra and by electronic spectra. For the squarate complexes with water, pyridine, and pyrazine occupying axial sites, the data are adequate to allow extraction of detailed information concerning term energies. The oxalate and dihydroxybenzoquinone complexes exhibit linear chain magnetism, although analysis of the data for oxalate is complicated by long-range ordering at low temperatures. Although linear chain magnetic behavior is not observed for the aquo and pyridine complexes with iron squarate, the iron squarate chains are apparently cross-linked to a two-dimensional array with pyrazine, leading to linear chain magnetism via spin exchange through pyrazine bridges.

Most of these polymeric Fe(II) complexes can be partially oxidized to mixed-valence Fe(II,III) materials. The course of these oxidations is quite sensitive to the experimental variables—oxidizing agent, solvent, temperature— and behavior ranging from no reaction to complete oxidation and/or decomposition can be observed. The ultimate stoichiometries observed span a wide range of behavior, from 10- to 60-percent oxidation, and there is no apparent trend to the specific compounds formed. The materials formed, however, are distinct species rather than mixtures of unoxidized and totally oxidized materials or non-stoichiometric phases of variable composition. The absence of X-ray powder diffraction lines attributable to the unoxidized Fe(II) polymers rules out a mixture of oxidized and unoxidized complexes. The observation that mixed-valence complexes of fixed stoichiometry result from a variety of experimental conditions, particularly large excesses of oxidizing agent, suggests that the complexes formed represent distinct energy minima with respect to oxidation level, rather than stages in a continuum of oxidation levels.

The dark colors of these mixed-valence materials suggest some degree of interaction among ions in different oxidation states, and this is supported by magnetic measurements. The observation, via Mössbauer spectroscopy, of distinct Fe(II) and Fe(III) sites rules out total electronic delocalization, thereby placing these materials in the Robin and Day mixed-valence Class II. The breadth of the Mössbauer absorptions and, in at least one case, the resolution of at least two Fe(II) absorptions, suggests multiple sites for these complexes. This is compatible with a model involving random oxidation along the chains, hence a variety of environments in which, for example, an Fe(II) ion might have zero, one, or two Fe(III) neighbors. Magnetic data are also compatible with such a random oxidation process, although the lack of suitable theoretical models precludes detailed treatment. Kudo, Matsubara, and Katsura⁵⁵ have recently discussed the expected magnetic behavior for a random mixture of $S=\frac{1}{2}$, $S=0$ or $S=\frac{1}{2}$, $S=1$ ions. Using a statistical treatment, they have demonstrated that the susceptibility is expected to have a temperature dependence which is at least qualitatively similar to that which we observe for the mixed-valence Fe(II,III) complexes. Thus at high temperatures normal paramagnetic behavior prevails, but as the temperature is lowered the susceptibility maximizes, then decreases, as a result of pairwise antiferromagnetic spin exchange interactions. At still lower temperatures the susceptibility increases again as the result of the residual paramagnetism of incomplete spin cancellation. This behavior, conceptually similar to the phenomenon of ferrimagnetism, is just that observed here. It receives further support from the fact that the high temperature data, and susceptibility maximum, can be fitted using a linear chain model with an intermediate spin corresponding to the weighted average of the oxidation states.

As is commonly observed for single-valence inorganic polymers, the electrical conductivity of the Fe(II) complexes is quite low. However, partial oxidation to the mixed-valence compounds leads to a dramatic increase in electrical conductivity, to

values of $10^{-4} \Omega^{-1} \text{cm}^{-1}$. This serves to reinforce the concept that mixed-valence is fundamental to the existence of high conductivity in inorganic and organic polymers. This work clearly demonstrates that the rational synthesis of mixed-valence polymers, and the resultant control of physical properties, is a feasible goal.

Acknowledgements. The authors acknowledge financial support of this work by the Office of Naval Research. They wish to thank Mr. Chester T. Dziobkowski for providing an analytically-pure sample of $\text{Fe}(\text{C}_2\text{O}_4)(\text{H}_2\text{O})_2$. The authors also thank Drs. William E. Hatfield and Peter Corvan of the University of North Carolina for obtaining low-temperature magnetic susceptibility data.

Supplementary Material Available: Listings of experimental magnetic susceptibilities and effective magnetic moments, Tables VII - XIV (11 pages). Ordering information is given on any current masthead page.

References and Notes

- (1) Zelenstov, V.V.; Aminov, T.G. Dokl. Akad. Nauk SSSR 1964, 158, 1393.
- (2) Dubicki, L.; Harris, C.M.; Kokot, E.; Martin, R.L. Inorg. Chem. 1966, 5, 93.
- (3) Figgis, B.N.; Martin, D.J. Inorg. Chem. 1966, 5, 100.
- (4) McGregor, K.T.; Soos, Z.G. Inorg. Chem. 1976, 15, 2159.
- (5) Bonner, J.C.; Fisher, M.E. Phys. Rev. A 1964, 135, 640.
- (6) The inadequacies of the Ising assumption in $\text{Cu}(\text{C}_2\text{O}_4) \cdot 1/3 \text{H}_2\text{O}$ were noted by Jotham. Jotham, R.W. J. Chem. Soc., Chem. Commun. 1973, 178.
- (7) Barros, S. de S.; Friedberg, S.A. Phys. Rev., 1966, 141, 637.
- (8) Van Kralingen, C.G.; van Ooijen, A.C.; Reedijk, J. Trans. Met. Chem. 1978, 3, 90.
- (9) Mazzi, C.; Caravelli, F. Period. Mineral. (Rome) 1957, 26, 2.
- (10) Cavid, S. Bull. Soc. Franc. Mineral. Cristallogr. 1959, 82, 50.
- (11) De Neef, T. Ph.D. Thesis, Eindhoven University of Technology, 1975.
- (12) Gerstein, B.C.; Habenschuss, M. J. Appl. Phys. 1972, 43, 5155.
- (13) Habenschuss, M.; Gerstein, B.C. J. Chem. Phys. 1974, 61, 852.
- (14) Long, G.J. Inorg. Chem. 1978, 17, 2702.
- (15) Kobayashi, H.; Haseda, T.; Kanda, E.; Kanda, S. J. Phys. Soc. Jpn. 1963, 18, 349.
- (16) Wroblewski, J.T.; Brown, D.B., Inorg. Chem. 1979, 18, 498.
- (17) Wroblewski, J.T.; Brown, D.B. unpublished observations.
- (18) Wroblewski, J.T.; Brown, D.B. 8th Northeast Regional ACS Meeting, Abstracts of Papers 1978, paper #INOR 16.
- (19) Cabbiness, D.K.; Amis, E.S.; Jackson, K.C. J. Chem. Eng. Data 1967, 12 90.
- (20) Pass, G.; Sutcliffe, H. "Practical Inorganic Chemistry"; Chapman and Hall; London, 1968; p 57.
- (21) The purple color in the solution is due to a small amount of dissolved $[\text{Fe}(\text{C}_4\text{O}_4)(\text{H}_2\text{O})_2\text{OH}]_2 \cdot 2\text{H}_2\text{O}$: Wroblewski, J.T.; Brown, D.B. Inorg. Chem. 1978, 17, 2959.

- (22) Inclusion of alcohols in $\text{Ni}(\text{C}_4\text{O}_4)(\text{H}_2\text{O})_2$ has been observed: reference 12.
- (23) The nature of this white precipitate is currently under investigation. Our preliminary findings indicate a molecular formula of $\text{Fe}(\text{C}_4\text{O}_4)(\text{H}_2\text{O})_2$ for this material. Wroblewski, J.T.; Brown, D.B. unpublished observations.
- (24) This orange precipitate is most likely dichloro(1,4-pyrazine)iron(II).²⁵
 Anal. Calcd for $\text{C}_4\text{Cl}_2\text{FeH}_4\text{N}_2$: C, 23.23; Cl, 34.28; H, 1.95. Found: C, 23.24; Cl, 34.58; H, 2.06.
- (25) Torardi, C.; Witten, E.; Reiff, W.M. 8th Northeast Regional ACS Meeting, Abstracts of Papers 1978, paper #INOR 10.
- (26) West, R.; Niu, H.Y. J. Am. Chem. Soc., 1963, 85, 2589.
- (27) See reference 16 for a note describing a feature of this particular balance.
- (28) Brown, D.B.; Crawford, V.H.; Hall, J.W.; Hatfield, W.E. J. Phys. Chem. 1977, 81, 1303.
- (29) See, for example, Estes, W.E.; Wasson, J.R.; Hall, J.W.; Hatfield, W.E. Inorg. Chem. 1978, 17, 3657.
- (30) Mabbs, F.E.; Machin, D.J. "Magnetism and Transition Metal Complexes"; Chapman and Hall: London, 1973, p 5.
- (31) Boudreaux, E.A.; Mulay, L.N. "Theory and Applications of Molecular Paramagnetism"; John Wiley and Sons: New York, 1976 p 494.
- (32) See, for example, Deming, S.N.; Morgan, S.L. Anal. Chem. 1973, 45, 278A, and reference therein.
- (33) Allen, C.W.; Brown, D.B. Inorg. Chem. 1974, 13, 2020.
- (34) Lang, G.; Dale, B.W. Nucl. Instrum. Methods 1974, 116, 567.
- (35) Van der Pauw, L.J. Phillips Res. Rpts. 1958, 13, 1.
- (36) Lewchalermwong, C.C. M.S. Thesis, University of North Carolina at Greensboro, 1977 and references therein.
- (37) See the paper cited in reference 21.

- (38) An excellent discussion of the effect of coordination upon the band positions in iron-pyridine complexes may be found in Little, B.F.; Long, G.J. Inorg. Chem., 1978, 17, 3401.
- (39) Corrsin, L.; Fax, B.J.; Lord, R.C. J. Chem. Phys. 1953, 21, 1170.
- (40) Ito, M.; Shimada, R.; Kuraishi, T.; Mizushima, W. J. Chem. Phys. 1956, 25, 597.
- (41) Barros, F. de S.; Zory, P.S.; Campbell, L.E. Phys. Letters 1963, 7, 135.
- (42) Ono, K.; Ito, A. J. Phys. Soc. Jpn. 1964, 19, 899.
- (43) Ingalls, R. Phys. Rev. A 1964, 133, 787.
- (44) Brady, P.R.; Duncan, J.F. J. Chem. Soc. 1964, 653.
- (45) De Menezes, J.V.; Barros, F. de S. Phys. Stat. Sol. A 1978, 45, K139.
- (46) For a discussion of this point see Bancroft, G.M. "Mössbauer Spectroscopy: An Introduction for Inorganic Chemists and Geochemists"; McGraw Hill: New York, 1973; Chapter 8. For the specific example of Fe_3O_4 see Sawatzky, G.A.; van der Woude, F.; Morrish, A.H. Phys. Rev. 1969, 183, 383.
- (47) Reference 46 p 147.
- (48) Lever, A.B.P. Coord. Chem. Rev. 1968, 3, 119.
- (49) Gerloch, M.; Slade, R.C. "Ligand-Field Parameters"; Cambridge University Press: London 1973; p 88.
- (50) Supplementary material.
- (51) McElearney, J.N.; Merchant, S.; Carlin, R.L. Inorg. Chem. 1973, 12, 906.
- (52) Fisher, M.E. Am. J. Phys. 1964, 32, 343.
- (53) The HDVV vector coupling approach is discussed in reference 30, Chapter 7.
- (54) Figgis, B.N.; Lewis, J.; Mabbs, F.E.; Webb, G.A. J. Chem. Soc. A 1967, 442.
- (55) Kudo, T.; Matsubara, F.; Katsura, S. Physica, 1978, 93A, 255.

Table I. X-Ray Powder Diffraction Data.^a

$\text{Fe}(\text{C}_4\text{O}_4)(\text{H}_2\text{O})_2$			$\text{Fe}(\text{C}_4\text{O}_4)(\text{H}_2\text{O})_2 \cdot \frac{1}{3}\text{CH}_3\text{CH}_2\text{OH}$			$\text{Fe}(\text{C}_4\text{O}_4)(\text{C}_5\text{H}_5\text{N})_2 \cdot 2\text{H}_2\text{O}$			$\text{Fe}(\text{C}_4\text{O}_4)(\text{C}_4\text{H}_4\text{N}_2) \cdot \frac{1}{2}\text{H}_2\text{O}$		
d, Å	I _{app} ^b	hkl	d, Å	I _{app}	hkl	d, Å	I _{app}		d, Å	I _{app}	
8.22	m	100	8.63	m	100	8.40	m		6.08	m	
5.80	s	110	6.10	s	110	6.14	m		5.68	s	
						5.78	m		5.11	m	
4.73	m	111	4.98	m	111	5.18	v		4.71	w	
						4.75	m		4.47	v	
4.10	s	200	4.33	s	200	4.51	m				
						4.20	w				
3.68	v	210	3.87	v	210	4.10	w		4.12	v	
						3.92	m		3.86	m	
2.89	w	220	3.05	w	220	3.71	v		3.74	v	
2.73	w	300	2.88	w	300	3.63	w		3.61	s	
						3.47	v				
2.59	w	310	2.73	w	310	3.39	w		3.35	w	
						3.22	v		3.22	w	
2.47	m	311	2.60	m	311	2.71	v		2.84	w	
						2.68	v				
						2.59	w				
						2.50	w				
									2.51	v	
									2.48	v	
									2.43	w	
									2.39	w	
									2.34	v	
2.05	w	400	2.16	w	400				2.29	w	
									2.23	w	
1.88	w	331	1.98	w	331				2.17	v	
1.83	w	420	1.93	w	420	2.13	v		2.13	v	
1.79	v	421	1.88	v	421				2.09	v	
									2.03	v	
									1.93	w	
									1.88	v	
1.67	w	422	1.80	w	422				1.84	v	
									1.80	w	

^a Abbreviations: s, strong; m, moderate; w, weak; v, very. ^b Apparent intensity.

Table II. Infrared Band Positions and Assignments for the Iron Squarate Complexes.^a

$\nu_{\text{obsd}}, \text{cm}^{-1}$	assignment	$\nu_{\text{obsd}}, \text{cm}^{-1}$	assignment
$\text{Fe}(\text{C}_4\text{O}_4)(\text{H}_2\text{O})_2$		$\text{Fe}(\text{C}_4\text{O}_4)(\text{C}_5\text{H}_5\text{N})_2 \cdot 2\text{H}_2\text{O}^{\text{b}}$	
3350 s, asym	$\nu(\text{H}_2\text{O})$	3100 s	$\nu(\text{H}_2\text{O}), \nu_{\text{CH}}$
2230 w	$2\nu_{\text{cc}}$	1618 m	
1520 s, br	ν_{co}	1590 w	$\nu_{\text{CN}}(\text{A}_1, \text{B}_1 \text{ py})$
1115 m	ν_{cc}	1500 s	ν_{CO}
1050 w		1458 w	$\text{A}_1, \text{B}_1 \text{ py}$
730 m, br	$\rho_{\text{r}}(\text{H}_2\text{O})$	1370 vw	
650 m, br		1226 m	$\text{A}_1, \text{B}_1 \text{ py}$
530 m, br	$\rho_{\text{w}}(\text{H}_2\text{O})$	1160 m	$\text{B}_1 \text{ py}$
410 m	$\nu_{\text{Fe-O}}$	1108 m	ν_{cc}
375 m	δ_{co}	1098 m	$\text{A}_1, \text{B}_1 \text{ py}$
		1075 m	
$\text{Fe}(\text{C}_4\text{O}_4)(\text{C}_4\text{H}_4\text{N}_2) \cdot 4\frac{1}{2}\text{H}_2\text{O}^{\text{c}}$		1046 m	$\text{A}_1 \text{ py}$
3300 s	$\nu(\text{H}_2\text{O})$	1017 m	
3100 s		760 m	$\text{A}_2 \text{ py}$
1500 s, br	ν_{co}	750 s, br	$\rho_{\text{w}}(\text{H}_2\text{O})$
1155 w	pyz	704 s	$\text{B}_2 \text{ py}$
1095 m	$\nu_{\text{cc}} \text{ sq}$	630 m	$\text{A}_1, \text{B}_1 \text{ py}$
1062 s	$\nu_{\text{cc}} \text{ pyz}$	420 w	$\nu_{\text{Fe-O}}, \text{py}$
1005 w	pyz	375 m	$\text{A}_2, \text{B}_2 \text{ py}$
860 m			
820 m			
745 m, br	$\rho_{\text{w}}(\text{H}_2\text{O})$		
630 m, br			
570 m, br			
455 s	pyz		
340 w	$\nu_{\text{Fe-O}}$		
320 w			
	δ_{CO}		

^a Key: s, strong; m, moderate; w, weak; asym, asymmetric; br, broad; sq, squarate; py, pyridine; pyz, pyrazine.

^b Pyridine assignments from reference 39.

^c Pyrazine assignments from reference 40.

Table III. Mössbauer Parameters for the Oxalate Complexes.

site	T,K	$\frac{\Delta E_Q}{\text{mm/s}}$	$\frac{\delta, a}{\text{mm/s}}$	$\frac{\Gamma, b}{\text{mm/s}}$	comments
$\text{Fe}(\text{C}_2\text{O}_4)(\text{H}_2\text{O})_2$					
Fe(II)	RT ^c	1.75	1.21	0.402	} $\frac{A_1}{A_2} = \frac{A_1}{A_2}$ $\Gamma_1 = \Gamma_2$
	100	1.98	1.23	0.396	
	50	2.06	1.26	0.395	
$\text{Fe}(\text{C}_2\text{O}_4)(\text{H}_2\text{O})_{0.9}(\text{C}_6\text{H}_4\text{O}_2)_{0.05}$					
Fe(II)	RT	1.71	1.17	0.608	}
	373	1.69	1.17	0.625	
Fe(III)	RT	0.97	0.32	0.528	} $\frac{A_{\text{Fe}^{2+}}}{A_{\text{Fe}^{3+}}} = 2.39$ 4-line fit
	373	0.96	0.33	0.600	
Fe(II)A	170	1.79	1.32	0.422	} $\frac{A_{\text{Fe}^{2+A}}}{A_{\text{Fe}^{2+B}}} = 1.56$
	50	1.91	1.32	0.471	
Fe(II)B	170	2.25	1.31	0.518	}
	50	2.46	1.35	0.704	
Fe(III)	170	1.04	0.42	0.570	} $\frac{A_{\text{Fe}^{2+_{\text{total}}}}}{A_{\text{Fe}^{3+}}} = 3.18$ 6-line fit
	50	1.14	0.44	0.614	
$\text{Fe}(\text{C}_2\text{O}_4)(\text{H}_2\text{O})_{1.4}\text{Br}_{0.6}$					
Fe(II)	RT	1.72	1.20	0.326	} $\frac{A_{\text{Fe}^{2+}}}{A_{\text{Fe}^{3+}}} = 0.91$
	100	1.76	1.21	0.330	
	50	1.86	1.24	0.360	
Fe(III)	RT	0.63	0.42	0.328	}
	100	0.64	0.42	0.325	
	50	0.64	0.42	0.371	

^a Relative to α -Fe foil. ^b Γ is full width at half maximum.

^c RT refers to room temperature (298±2K).

Table IV. Mössbauer Parameters for the Squarate Complexes.

site	T, K	ΔE_Q , mm/s	δ , ^a mm/s	Γ , ^b mm/s	comments
$\text{Fe}(\text{C}_4\text{O}_4)(\text{H}_2\text{O})_2$					
Fe(II)	RT ^c	2.29	1.22	0.33	} $\frac{A_1}{A_2} = \frac{A_2}{A_1}$ $\Gamma_1 = \Gamma_2$
	250	2.36	1.26	0.32	
	200	2.54	1.27	0.33	
	150	2.67	1.29	0.30	
	100	2.73	1.31	0.29	
	50	2.79	1.31	0.29	
	17	2.81	1.32	0.30	
$\text{Fe}(\text{C}_4\text{O}_4)(\text{C}_5\text{H}_5\text{N})_2 \cdot 2\text{H}_2\text{O}$					
Fe(II)	RT	2.12	1.16	0.31	} $\frac{A_1}{A_2} = \frac{A_2}{A_1}$ $\Gamma_1 = \Gamma_2$
	250	2.36	1.16	0.30	
	200	2.62	1.20	0.30	
	150	2.87	1.21	0.29	
	100	3.00	1.23	0.31	
	50	3.00	1.24	0.32	
	17	3.02	1.24	0.30	
$\text{Fe}(\text{C}_4\text{O}_4)(\text{C}_4\text{H}_4\text{N}_2) \cdot \frac{1}{2}\text{H}_2\text{O}$					
Fe(II)	RT	3.01	1.14	0.33	} $\frac{A_1}{A_2} = \frac{A_2}{A_1}$ $\Gamma_1 = \Gamma_2$
	200	3.14	1.16	0.33	
	160	3.14	1.15	0.32	
	100	3.16	1.18	0.31	
	50	3.15	1.20	0.31	
	17	3.16	1.22	0.34	
$\text{Fe}(\text{C}_4\text{O}_4)(\text{C}_5\text{H}_5\text{N})\text{I}_{1.5}$					
Fe(II)	RT	3.12	1.19	0.32	} $\frac{A_{\text{Fe}^{2+}}}{A_{\text{Fe}^{3+}}} = 1.00$
	17	3.21	1.20	0.31	
Fe(III)	RT	0.59	0.50	0.36	
	17	0.62	0.51	0.36	

^a Relative to α -Fe foil. ^b Γ is full width at half maximum.

^c RT refers to room temperature (298±2K).

Table V. Mössbauer Parameters for the Dihydroxybenzoquinone Complexes.

site	T, K	ΔE_Q , mm/s	δ , mm/s ^a	Γ_1 , mm/s ^b	Γ_2 , mm/s ^b	A_1/A_2 ^c
$\text{Fe}(\text{C}_6\text{H}_2\text{O}_4)(\text{H}_2\text{O})_2$						
Fe(II) ^d	RT ^e	1.47	1.16	0.35	0.35	1.00
	200	1.46	1.17	0.32	0.32	1.00
	130	1.47	1.17	0.31	0.31	1.00
	80	1.47	1.17	0.32	0.32	1.00
	15	1.49	1.21	0.32	0.32	1.00
Fe(III)	RT	0.83	0.38	0.39	0.28	1.62
	200	0.83	0.38	0.38	0.31	1.59
	130	0.81	0.40	0.39	0.32	1.58
	80	0.81	0.41	0.39	0.33	1.55
	15	0.84	0.41	0.36	0.30	1.58
$\text{Fe}(\text{C}_6\text{H}_2\text{O}_4)\text{I}$						
Fe(II)	RT	2.71	1.04	0.36	0.51	0.73
	23	2.76	1.14	0.35	0.55	0.72
Fe(III)	RT	0.78	0.56	0.47	0.48	1.32
	23	0.78	0.59	0.46	0.46	1.34

^a Relative to α -Fe foil. ^b Full width at half maximum. ^c Area ratio (low energy line/high energy line). ^d Area ratio constrained equal to 1.00. ^e RT refers to room temperature.

Table VI. Electronic Spectral Data and Crystal-Field Parameters for the Fe(II) Squarate Complexes.^a

compound	ν_1	ν_2	ν_3	$\frac{D}{q}(e)$	$\frac{D}{q}(a)$	$\frac{D}{s}$	$\frac{D}{t}$
$\text{Fe}(\text{C}_4\text{O}_4)(\text{H}_2\text{O})_2$	500 ^b	8500	10750	850	610	390	140
$\text{Fe}(\text{C}_4\text{O}_4)(\text{C}_5\text{H}_5\text{N})_2 \cdot 2\text{H}_2\text{O}$	425	9300	12000	930	610	450	180
$\text{Fe}(\text{C}_4\text{O}_4)(\text{C}_4\text{H}_4\text{N}_2) \cdot 4\frac{1}{2}\text{H}_2\text{O}$	850	10200	12500	1020	830	450	100

^a All values in cm^{-1} . Crystal-field parameters expressed to the nearest 10 cm^{-1} .

^b Average value obtained from Mössbauer spectra (Figure 8).

Table VII. Magnetic Susceptibility Data for $\text{Fe}(\text{C}_2\text{O}_4)(\text{H}_2\text{O})_2$.

T, K	$\bar{\chi}_M'(\text{obsd}) \times 10^5, \text{cgsu}^a$	$\bar{\mu}_{\text{eff}}, \mu_B$
4.24	1511	0.72
4.90	1468	0.76
6.05	1434	0.84
6.83	1435	0.88
7.80	1489	0.96
9.81	1783	1.18
11.93	2501	1.54
15.67	3335	2.04
18.26	3796	2.36
21.54	4160	2.68
24.09	4364	2.90
27.10	4515	3.13
29.92	4604	3.32
32.23	4649	3.46
34.43	4675	3.59
36.53	4676	3.70
38.36	4667	3.78
40.09	4658	3.86
41.59	4641	3.93
43.02	4623	3.99
44.40	4605	4.04
45.99	4570	4.10
47.91	4535	4.17
49.77	4491	4.23
51.46	4447	4.28
53.33	4394	4.32
55.59	4341	4.39
57.94	4279	4.45
62.30	4137	4.54
64.68	4067	4.59
69.9	3810	4.62
74.8	3658	4.68
80.8	3460	4.73
85.5	3326	4.77
90.2	3218	4.82
95.0	3084	4.84
100.0	2967	4.87
104.6	2860	4.89
110.2	2707	4.88
119.6	2528	4.92
129.0	2393	4.97
139.3	2214	4.97
150.5	2070	4.99
164.5	1900	5.00
178.8	1739	4.99

Table VII. Continued.

T, K	$\bar{\chi}'_M(\text{obsd}) \times 10^5, \text{ cgsu}^a$	$\bar{\mu}_{\text{eff}}, \mu_B$
193.6	1613	5.00
207.5	1506	5.00
221.7	1371	4.94
235.8	1290	4.93
250.1	1201	4.90
259.4	1164	4.91
272.0	1120	4.94
286.0	1057	4.91

^a M.Wt. = 179.9, $\chi^{\text{dia}} = -64.0 \times 10^{-6} \text{ cgsu}$.

Table VIII. Magnetic Susceptibility Data for $\text{Fe}(\text{C}_2\text{O}_4)(\text{H}_2\text{O})_{0.9}(\text{C}_6\text{H}_4\text{O}_2)_{0.05}$.

T, K	$\bar{\chi}'_{\text{M}}(\text{obsd}) \times 10^5, \text{cgsu}^{\text{a}}$	$\bar{\mu}_{\text{eff}}, \mu_{\text{B}}$
4.24	1894	0.80
5.30	1857	0.89
6.18	1820	0.95
7.11	1806	1.02
8.28	1792	1.10
9.55	1793	1.18
11.39	1824	1.30
13.67	1879	1.45
15.80	1933	1.59
18.86	1996	1.75
21.43	2050	1.89
24.45	2111	2.05
27.23	2173	2.20
29.85	2235	2.33
32.17	2296	2.45
34.75	2373	2.59
36.66	2426	2.68
38.65	2495	2.80
40.53	2557	2.90
42.44	2618	3.00
44.25	2679	3.10
45.72	2725	3.17
47.40	2786	3.23
49.03	2840	3.36
50.62	2878	3.42
52.18	2901	3.50
53.23	2924	3.55
54.49	2924	3.59
55.83	2925	3.64
57.23	2909	3.66
59.29	2894	3.73
60.94	2860	3.75
62.70	2833	3.78
64.21	2810	3.83
67.03	2780	3.88
68.37	2757	3.90
70.71	2719	3.93

^aM.Wt. = 165.49; $\chi^{\text{dia}} = -47 \times 10^{-6} \text{cgsu}$.

Table IX. Magnetic Susceptibility Data for $\text{Fe}(\text{C}_2\text{O}_4)(\text{H}_2\text{O})_{1.4}\text{Br}_{0.6}$

T, K	$\bar{\chi}_M'(\text{obsd}) \times 10^5, \text{cgsu}^a$	$\bar{\mu}_{\text{eff}}, \mu_B$
20.0	3188	2.26
21.0	3098	2.28
22.0	3068	2.32
23.0	3050	2.37
24.0	3032	2.41
25.0	3014	2.46
26.0	3014	2.50
27.0	3026	2.56
28.0	3032	2.61
29.0	3020	2.65
32.0	3032	2.79
34.0	3038	2.87
36.0	3068	2.97
38.0	3092	3.06
40.0	3128	3.16
42.0	3152	3.25
44.0	3188	3.35
46.0	3176	3.42
48.0	3194	3.50
50.0	3182	3.57
52.0	3176	3.63
54.0	3164	3.70
56.0	3170	3.77
58.0	3170	3.84
60.0	3152	3.89
62.0	3122	3.94
64.0	3086	3.97
66.0	3062	4.02
68.0	3038	4.06
70.0	3014	4.11
74.7	2935	4.19
80.1	2858	4.28
85.0	2798	4.36
89.4	2726	4.42
94.9	2666	4.50
99.5	2576	4.53
105.1	2503	4.59
109.7	2455	4.64
115.2	2395	4.70
121.7	2329	4.76
128.2	2257	4.81
137.6	2143	4.86
146.6	2077	4.94
159.1	1969	5.00
168.3	1873	5.02
178.9	1813	5.09

Table IX. Continued.

T, K	$\bar{\chi}_M^{\text{I}}(\text{obsd}) \times 10^5, \text{cgsu}^{\text{a}}$	$\bar{\mu}_{\text{eff}}, \mu_{\text{B}}$
192.7	1722	5.15
202.9	1650	5.18
213.1	1590	5.21
225.1	1518	5.23
236.3	1452	5.24
246.4	1404	5.26
257.6	1356	5.29
269.4	1320	5.33
285.0	1260	5.36

^a M.Wt. = 217.03, $\chi^{\text{dia}} = -80.0 \times 10^{-6} \text{cgsu}$.

Table X. Magnetic Susceptibility Data for $\text{Fe}(\text{C}_4\text{O}_4)(\text{H}_2\text{O})_2$.

T, K	$\bar{\chi}_M'(\text{obsd}) \times 10^5, \text{cgsu}^a$	$\bar{\chi}_M'(\text{calcd}) \times 10^5, \text{cgsu}^b$	$\bar{\mu}_{\text{eff}}, \mu_B$
4.24	49880	49780	4.11
5.88	38530	40790	4.26
6.80	34090	37040	4.30
8.45	29150	31790	4.44
10.54	23940	26960	4.49
13.44	20020	22260	4.64
16.75	16840	18560	4.75
19.56	14660	16270	4.79
21.87	13300	14770	4.82
22.55	12640	14380	4.77
22.61	13010	14350	4.85
23.60	12320	13820	4.82
24.83	11810	13210	4.84
25.55	11750	12880	4.90
28.07	10420	11840	4.84
28.25	10790	11780	4.94
31.02	10000	10820	4.98
31.14	9729	10780	4.92
34.2	8744	9372	5.04
44.1	7487	7828	5.14
52.2	6904	6683	5.40
63.6	5737	5548	5.40
76.6	4807	4639	5.43
89.7	4130	3986	5.44
107.2	3477	3354	5.46
124.1	3124	2909	5.57
131.1	2967	2759	5.58
136.1	2770	2659	5.49
156.3	2531	2323	5.62
184.6	2041	1973	5.49
196.8	1869	1852	5.42
208.8	1737	1747	5.39
220.8	1637	1675	5.38
237.1	1510	1541	5.35
247.6	1443	1477	5.34
257.9	1372	1418	5.32
265.3	1339	1379	5.33
269.6	1301	1358	5.30

^a M.Wt. = 203.92, $\chi^{\text{dia}} = -50.6 \times 10^{-6} \text{cgsu}$. ^b Calcd from the D_{4h} model with $\lambda = -80 \text{ cm}^{-1}$, $u = -4$, and $k = 0.8$

Table XI. Magnetic Susceptibility Data for $\text{Fe}(\text{C}_4\text{O}_4)(\text{C}_5\text{H}_5\text{N})_2 \cdot 2\text{H}_2\text{O}$.

T, K	$\bar{\chi}_M^i(\text{obsd}) \times 10^{-5}, \text{cgsu}^a$	$\bar{\chi}_M^i(\text{calcd}) \times 10^5, \text{cgsu}^b$	$\bar{\mu}_{\text{eff}}, \mu_B$
4.21	54050	76600	4.27
5.22	47140	61940	4.44
5.67	43240	57020	4.43
6.01	41340	53800	4.46
6.34	39790	51000	4.49
7.59	33960	42600	4.54
9.65	27740	33500	4.63
11.36	24110	28460	4.68
14.25	19960	22690	4.77
14.76	19400	21900	4.79
16.87	17330	19160	4.84
19.73	15170	16390	4.89
22.43	13620	14440	4.92
22.69	13430	14250	4.95
24.52	12630	13180	4.98
27.06	11550	11950	5.00
28.41	11030	11380	5.01
29.96	10550	10790	5.03
34.15	9345	9467	5.05
35.15	9086	9198	5.05
36.25	8670	8919	5.01
44.2	7310	7313	5.08
53.8	6015	6013	5.09
61.8	5160	5232	5.05
74.1	4403	4362	5.11
85.9	3731	3764	5.06
99.7	3234	3243	5.08
114.0	2801	2835	5.05
118.0	2771	2740	5.11
131.6	2433	2456	5.06
144.0	2243	2245	5.08
161.0	2008	2009	5.08
178.9	1802	1807	5.08
206.1	1572	1570	5.09
213.7	1516	1514	5.09
224.8	1440	1439	5.09
244.2	1323	1324	5.08
283.0	1143	1142	5.09
296.0	1090	1092	5.08

^a M.Wt. = 362.13, $\chi^{\text{dia}} = -110.0 \times 10^{-6} \text{cgsu}$. ^b Calcd from the D_{4h} model with $\lambda = -80 \text{ cm}^{-1}$, $v = -10$, and $k = 0.5$.

Table XII. Magnetic Susceptibility Data for $\text{Fe}(\text{C}_4\text{O}_4)(\text{C}_4\text{H}_4\text{N}_2) \cdot 4\frac{1}{2}\text{H}_2\text{O}$.

T, K	$\bar{\chi}'_{\text{M}}(\text{obsd}) \times 10^5, \text{cgsu}^{\text{a}}$	$\bar{\chi}'_{\text{M}}(\text{calcd}) \times 10^5, \text{cgsu}^{\text{b}}$	$\bar{\mu}_{\text{eff}}, \mu_{\text{B}}$
1.81	48500	48100	2.65
2.04	48500	48310	2.81
2.06	48500	48320	2.82
2.19	48050	48310	2.90
2.80	47160	47450	3.25
3.25	45820	46220	3.45
3.46	45370	45550	3.54
3.72	44470	44670	3.64
3.95	43580	43860	3.71
4.21	43000	42920	3.81
4.24	42770	42820	3.81
5.78	38060	37420	4.20
7.59	32630	32100	4.45
9.91	27200	26930	4.64
15.15	19710	19550	4.89
19.87	15680	15630	4.99
20.21	15220	15410	4.96
24.00	13230	13290	5.04
24.78	12850	12920	5.05
28.16	11410	11540	5.07
30.02	10790	10900	5.09
31.57	10290	10410	5.10
34.1	9615	9709	5.12
36.6	9091	9101	5.16
41.7	8013	8069	5.17
46.6	7231	7276	5.19
50.9	6575	6698	5.17
56.5	6013	6070	5.21
59.5	5718	5779	5.22
63.6	5330	5424	5.21
74.0	4593	4693	5.21
80.7	4263	4318	5.24
85.3	4018	4093	5.24
90.9	3779	3849	5.24
96.1	3569	3647	5.24
102.7	3374	3420	5.26
108.3	3177	3248	5.24
115.2	2996	3058	5.25
120.5	2872	2927	5.26
127.0	2719	2780	5.26
133.0	2603	2658	5.26
135.0	2564	2619	5.27
142.4	2438	2486	5.27
145.2	2388	2438	5.27
152.3	2281	2327	5.27
160.6	2163	2209	5.27
170.0	2050	2088	5.28

Table XII. Continued.

T, K	$\bar{\chi}'_M(\text{obsd}) \times 10^5, \text{cgsu}^a$	$\bar{\chi}'_M(\text{calcd}) \times 10^5, \text{cgsu}^b$	$\bar{\mu}_{\text{eff}}, \mu_B$
177.4	1950	2003	5.26
186.8	1855	1903	5.26
192.2	1809	1850	5.27
200.8	1735	1772	5.28
204.2	1706	1743	5.28
208.3	1667	1709	5.27
214.8	1628	1658	5.29
219.9	1583	1620	5.28
226.6	1542	1573	5.29
232.2	1502	1535	5.28
241.5	1443	1476	5.28
249.0	1402	1432	5.28
256.1	1361	1393	5.28
261.2	1333	1366	5.28
266.6	1313	1339	5.29
271.4	1285	1315	5.28
277.0	1260	1289	5.28
282.3	1235	1265	5.28
286.7	1217	1245	5.28
291.2	1197	1226	5.28
296.0	1179	1206	5.28

^a M.Wt. = 329.05, $\chi^{\text{dia}} = -126.7 \times 10^{-6} \text{cgsu}$. ^b Calcd for $\underline{J} = -0.26 \text{ cm}^{-1}$, $\underline{ZJ}' = -0.02 \text{ cm}^{-1}$, $\underline{g} = 2.20$, and $\underline{Na} = 53 \times 10^{-6} \text{cgsu}$.

Table XIII. Magnetic Susceptibility Data for $\text{Fe}(\text{C}_4\text{O}_4)(\text{C}_5\text{H}_5\text{N})\text{I}_{1.5}$.

T, K	$\bar{\chi}'_M(\text{obsd}) \times 10^5, \text{cgsu}$	$\bar{\mu}_{\text{eff}}, \mu_B$
18.0	3021	2.09
20.0	2984	2.18
23.0	2946	2.33
25.0	2910	2.41
28.0	2898	2.55
30.0	2860	2.62
33.0	2810	2.72
36.0	2790	2.83
40.0	2755	2.97
42.0	2766	3.05
45.0	2801	3.17
50.0	2888	3.40
51.0	2902	3.44
55.0	3000	3.63
60.0	3029	3.81
70.2	3146	4.20
80.3	2947	4.35
90.0	2821	4.51
101.0	2736	4.70
125.0	2521	5.02
138.0	2095	4.81
152.0	1996	4.93
181.0	1799	5.10
199.6	1717	5.24
221.0	1524	5.19
246.1	1392	5.23
286.3	1386	5.63

$\bar{\chi}^{\text{dia}} = -75 \times 10^{-6} \text{cgsu}$, M.Wt. = 437.49.

Table XIV. Magnetic Susceptibility Data for $\text{Fe}(\text{C}_6\text{H}_5\text{O}_4)\text{I}$.

T, K	$\bar{\chi}_M'(\text{obsd}) \times 10^5, \text{cgsu}^a$	$\bar{\mu}_{\text{eff}}, \mu_B$
23.8	2891	2.34
24.0	2868	2.34
26.4	2833	2.44
27.4	2817	2.48
32.0	2762	2.66
36.1	2823	2.86
43.9	2827	3.15
44.9	2846	3.20
52.6	2904	3.50
62.0	3049	3.89
65.5	3126	4.05
69.7	3155	4.19
71.1	3171	4.25
75.1	3119	4.33
80.0	3049	4.42
97.5	2769	4.65
109.8	2611	4.79
135.8	2280	4.98
167.0	1980	5.14
195.0	1765	5.24
217.8	1633	5.33
271.3	1350	5.41
277.0	1330	5.43
291.6	1289	5.48
295.2	1285	5.51

^a M.Wt. = 320.83, $\chi^{\text{dia}} = -115.6 \times 10^{-6} \text{cgsu}$.

Figure Captions

Figure 1. Weight loss curves for $\text{Fe}(\text{C}_4\text{O}_4)(\text{H}_2\text{O})_2$, A, $\text{Fe}(\text{C}_4\text{O}_4)(\text{C}_5\text{H}_5\text{N})_2 \cdot 2\text{H}_2\text{O}$, B, $\text{Fe}(\text{C}_4\text{O}_4)(\text{C}_4\text{H}_4\text{N}_2) \cdot 4 \frac{1}{2} \text{H}_2\text{O}$, C, and $[\text{Fe}(\text{C}_4\text{O}_4)(\text{H}_2\text{O})_2\text{OH}]_2 \cdot 2\text{H}_2\text{O}$, D. Heating rate was $0.5^\circ\text{C}/\text{min}$ in a nitrogen atmosphere.

Figure 2. Infrared spectra of $\text{Fe}(\text{C}_4\text{O}_4)(\text{H}_2\text{O})_2$, A, $\text{Fe}(\text{C}_4\text{O}_4)(\text{C}_5\text{H}_5\text{N})_2 \cdot 2\text{H}_2\text{O}$, B, $\text{Fe}(\text{C}_4\text{O}_4)(\text{C}_4\text{H}_4\text{N}_2) \cdot 4 \frac{1}{2} \text{H}_2\text{O}$, C, and $\text{Fe}(\text{C}_4\text{O}_4)(\text{C}_5\text{H}_5\text{N}) \text{I}_{1.5}$, D. Absorption bands which are assigned to pyridine are marked with a + while those assigned to pyrazine are marked with an x.

Figure 3. Infrared spectra of 2,5-dihydroxy-1,4-benzoquinone, A, $\text{Fe}(\text{C}_6\text{H}_2\text{O}_4)(\text{H}_2\text{O})_2$, B, and $\text{Fe}(\text{C}_6\text{H}_2\text{O}_4)\text{I}$, C.

Figure 4. Room temperature Mössbauer spectra of $\text{Fe}(\text{C}_2\text{O}_4)(\text{H}_2\text{O})_2$, A, $\text{Fe}(\text{C}_2\text{O}_4)(\text{H}_2\text{O})_{0.9}(\text{C}_6\text{H}_4\text{O}_2)_{0.05}$, B, and $\text{Fe}(\text{C}_2\text{O}_4)(\text{H}_2\text{O})_{1.4}\text{Br}_{0.6}$, C. The velocity scale is relative to α -Fe foil.

Figure 5. (a) A projection of the structure of $\text{Fe}(\text{C}_2\text{O}_4)(\text{H}_2\text{O})_2$ normal to the [1,0,0] direction. Water ligands are omitted for clarity. (b) Normal to [0,0,1].

Figure 6. 50K Mössbauer spectrum of $\text{Fe}(\text{C}_2\text{O}_4)(\text{H}_2\text{O})_{0.9}(\text{C}_6\text{H}_4\text{O}_2)_{0.05}$. This spectrum has been fitted to one Fe(III) and two Fe(II) quadrupole doublets with parameters given in Table III.

Figure 7. Room temperature Mössbauer spectra of $\text{Fe}(\text{C}_4\text{O}_4)(\text{H}_2\text{O})_2$, A, $\text{Fe}(\text{C}_4\text{O}_4)(\text{C}_5\text{H}_5\text{N})_2 \cdot 2\text{H}_2\text{O}$, B, and $\text{Fe}(\text{C}_4\text{O}_4)(\text{C}_4\text{H}_4\text{N}_2) \cdot 4 \frac{1}{2} \text{H}_2\text{O}$, C. The velocity scale is relative to α -Fe foil.

Figure 8. Plots of reduced quadrupole splitting, $\frac{\Delta E_q(T)}{\Delta E_q(17\text{K})}$ versus T for the Fe(II) squarate complexes. The numbers within the graph are ground state splittings in cm^{-1} for which the smooth curves were calculated according to eq 9.

Figure 9. Room temperature Mössbauer spectra for $\text{Fe}(\text{C}_6\text{H}_2\text{O}_4)(\text{H}_2\text{O})_2$, A and $\text{Fe}(\text{C}_6\text{H}_2\text{O}_4)\text{I}$, B. The velocity scale is relative to α -Fe foil.

Figure 10. Room-temperature electronic spectra of $\text{Fe}(\text{C}_4\text{O}_4)(\text{C}_5\text{H}_5\text{N})_2 \cdot 2\text{H}_2\text{O}$, A and $\text{Fe}(\text{C}_4\text{O}_4)(\text{C}_4\text{H}_4\text{N}_2) \cdot 4 \frac{1}{2} \text{H}_2\text{O}$, B. Note scale change at ca. 8000 cm^{-1} in spectrum A.

Figure 11. Term splitting diagram for $\text{Fe}(\text{II})$ in a D_{4h} crystal field.

Figure 12. Inverse molar susceptibility vs temperature for $\text{Fe}(\text{C}_4\text{O}_4)(\text{H}_2\text{O})_2$. The straight line represents Curie law behavior for $\underline{C} = 3.0$

Figure 13. Molar magnetic susceptibility vs temperature below 80K for $\text{Fe}(\text{C}_2\text{O}_4)(\text{H}_2\text{O})_2$. Curve A is the fit obtained by using eq 11 with $\underline{J} = -4.4 \text{ cm}^{-1}$, $\underline{g} = 2.02$, $\underline{N}\alpha = 60 \times 10^{-6} \text{ cgsu}$ and $\underline{ZJ}' = 10.7 \text{ cm}^{-1}$. Curve B is obtained by using the $\underline{S}_1 = \underline{S}_2 = 2$ HDVV model with $\underline{J} = 21.2$, $\underline{g} = 2.64$ and $\underline{N}\alpha = 120 \times 10^{-6} \text{ cgsu}$ with a 3% monomeric impurity.

Figure 14. Illustration showing the effect of varying the intrachain spin-exchange parameter in the Heisenberg chain model (eq 12; $\underline{S} = 2$, $\underline{g} = 2$.) Curves are shown for $\underline{J} = -1.0$ (a), -2.0 (b), -3.0 (c), -5.0 (d) and -10.0 cm^{-1} (e).

Figure 15. Illustration showing the effect of varying the interchain spin-exchange parameter in the modified Heisenberg chain model (eq 11; $\underline{S}=2$, $\underline{g}=2$, $\underline{J}=3.0 \text{ cm}^{-1}$). Curves are shown for $\underline{ZJ}' = 4$ (a), 3 (b), 2 (c), 1 (d), 0 (e), -1 (f), -5 (g), and -10 cm^{-1} (h).

Figure 16. Molar magnetic susceptibility vs temperature for $\text{Fe}(\text{C}_2\text{O}_4)(\text{H}_2\text{O})_{0.9}(\text{C}_6\text{H}_4\text{O}_2)_{0.05}$. The smooth curve is obtained from eq 11 with $\underline{J} = 6.8 \text{ cm}^{-1}$, $\underline{g} = 1.96$, $\underline{ZJ}' = 16.7 \text{ cm}^{-1}$, and $\underline{N}\alpha = 60 \times 10^{-6} \text{ cgsu}$.

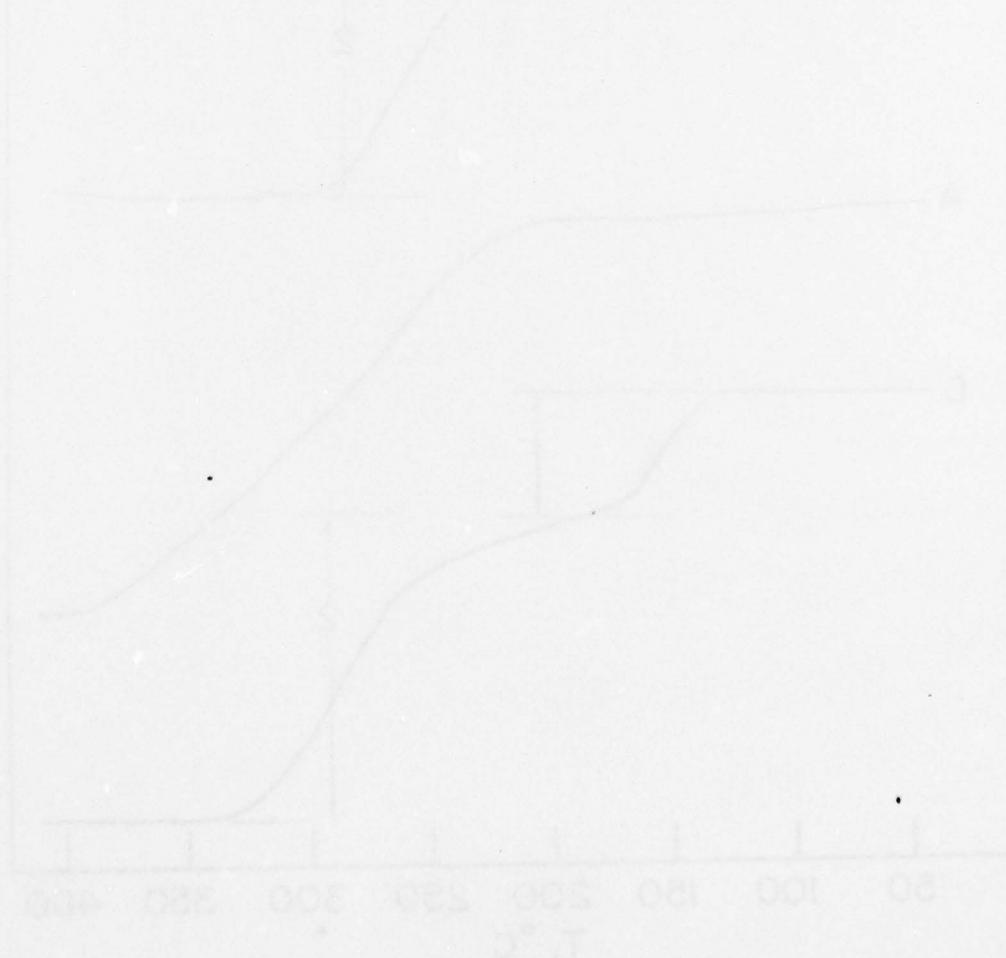
Figure 17. Molar magnetic susceptibility (+) and effective magnetic moments (■) vs temperature for $\text{Fe}(\text{C}_2\text{O}_4)(\text{H}_2\text{O})_{1.4}\text{Br}_{0.6}$. The data were fit to eq 11 (solid curve) with $\underline{J} = 5.3 \text{ cm}^{-1}$, $\underline{g} = 2.43$, $\underline{ZJ}' = 3.5 \text{ cm}^{-1}$, and $\underline{N}\alpha = 60 \times 10^{-6} \text{ cgsu}$. The dashed curve represents a fit to eq 13 with $\underline{J} = -18.2 \text{ cm}^{-1}$ and $\underline{g} = 2.00$.

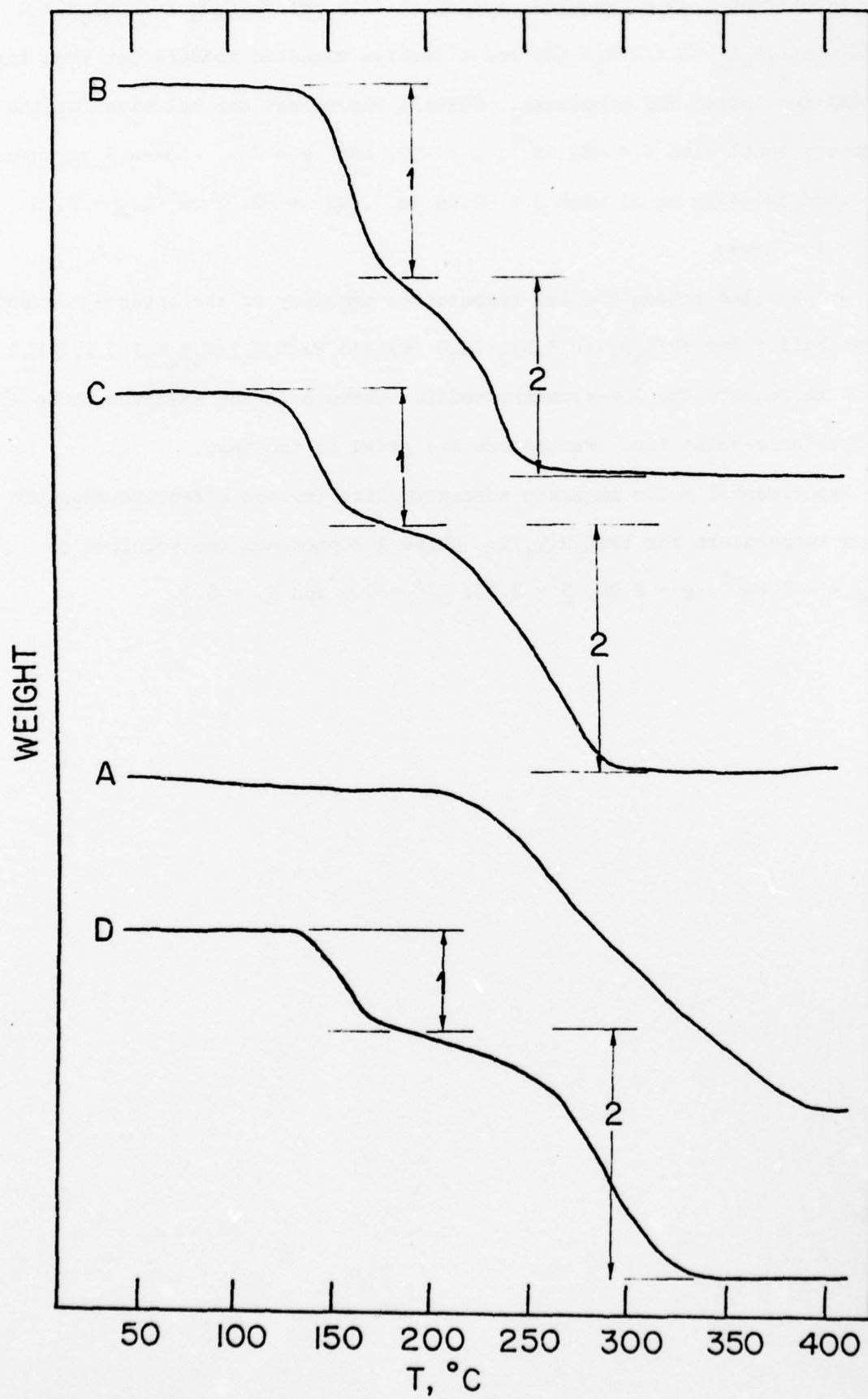
Figure 18. Inverse molar magnetic susceptibility vs temperature for $\text{Fe}(\text{C}_4\text{O}_4)(\text{H}_2\text{O})_2$. The smooth curve represents the low-symmetry model (see text) with $\lambda = 80 \text{ cm}^{-1}$, $\underline{v} = 4$, and $\underline{k} = 0.8$.

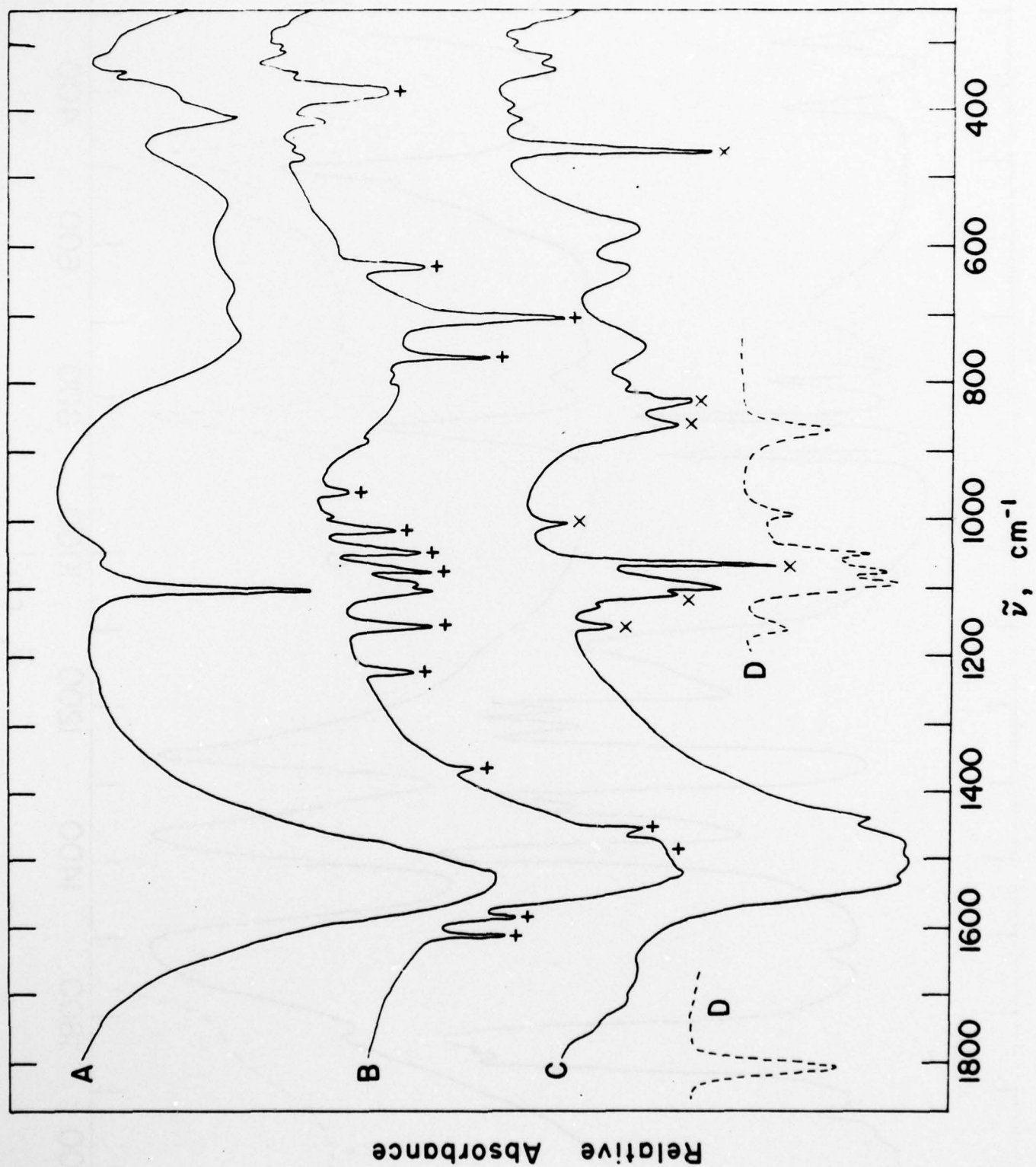
Figure 19. Experimental molar magnetic susceptibility for $\text{Fe}(\text{C}_4\text{O}_4)(\text{C}_5\text{H}_5\text{N})_2 \cdot 2\text{H}_2\text{O}$ (●) and $\text{Fe}(\text{C}_4\text{O}_4)(\text{C}_4\text{H}_4\text{N}_2) \cdot 4 \frac{1}{2} \text{H}_2\text{O}$ (○) and effective magnetic moments per iron for the former (▲) and latter (△) complexes. Curve A represents the solution for the D_{4h} low-symmetry model with $\lambda = -80 \text{ cm}^{-1}$; $\nu = -10$, and $k_{\nu} = 0.5$. Curve B represents the fit obtained by using eq 11 with $\underline{J} = -0.26 \text{ cm}^{-1}$, $\underline{ZJ}' = -0.02 \text{ cm}^{-1}$, $\underline{g} = 2.20$ and $\underline{N\alpha} = 53 \times 10^{-6} \text{ cgsu}$.

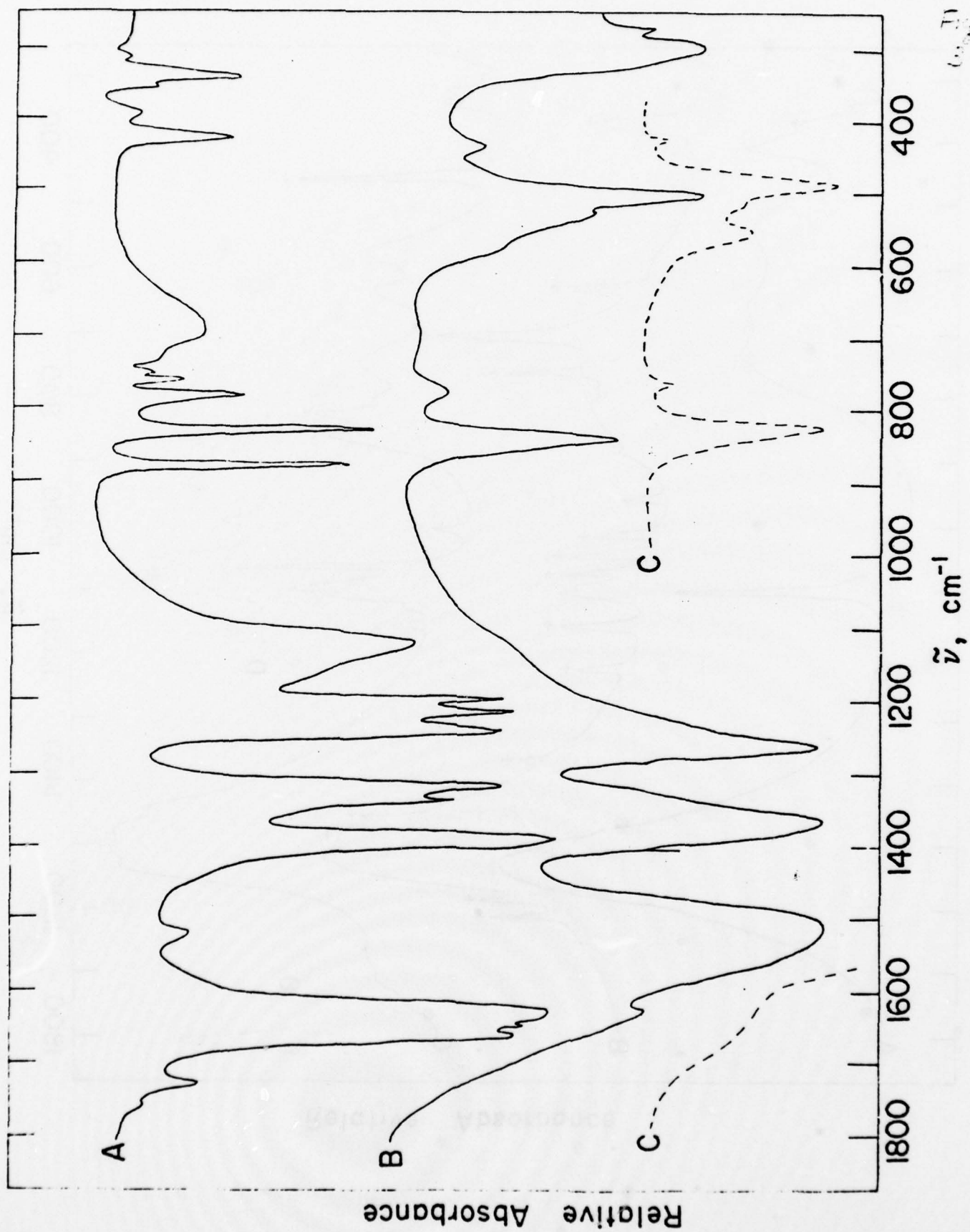
Figure 20. Graph illustrating the low-temperature behavior of the inverse corrected molar susceptibility for $\text{Fe}(\text{C}_4\text{O}_4)(\text{C}_5\text{H}_5\text{N})_2 \cdot 2\text{H}_2\text{O}$ (●) and $\text{Fe}(\text{C}_4\text{O}_4)(\text{C}_4\text{H}_4\text{N}_2) \cdot 4 \frac{1}{2} \text{H}_2\text{O}$ (○). Curve A represents the low-symmetry model. Curve B is the solution to eq 11. Curve C is the Curie-Weiss law. Parameters are given in the text.

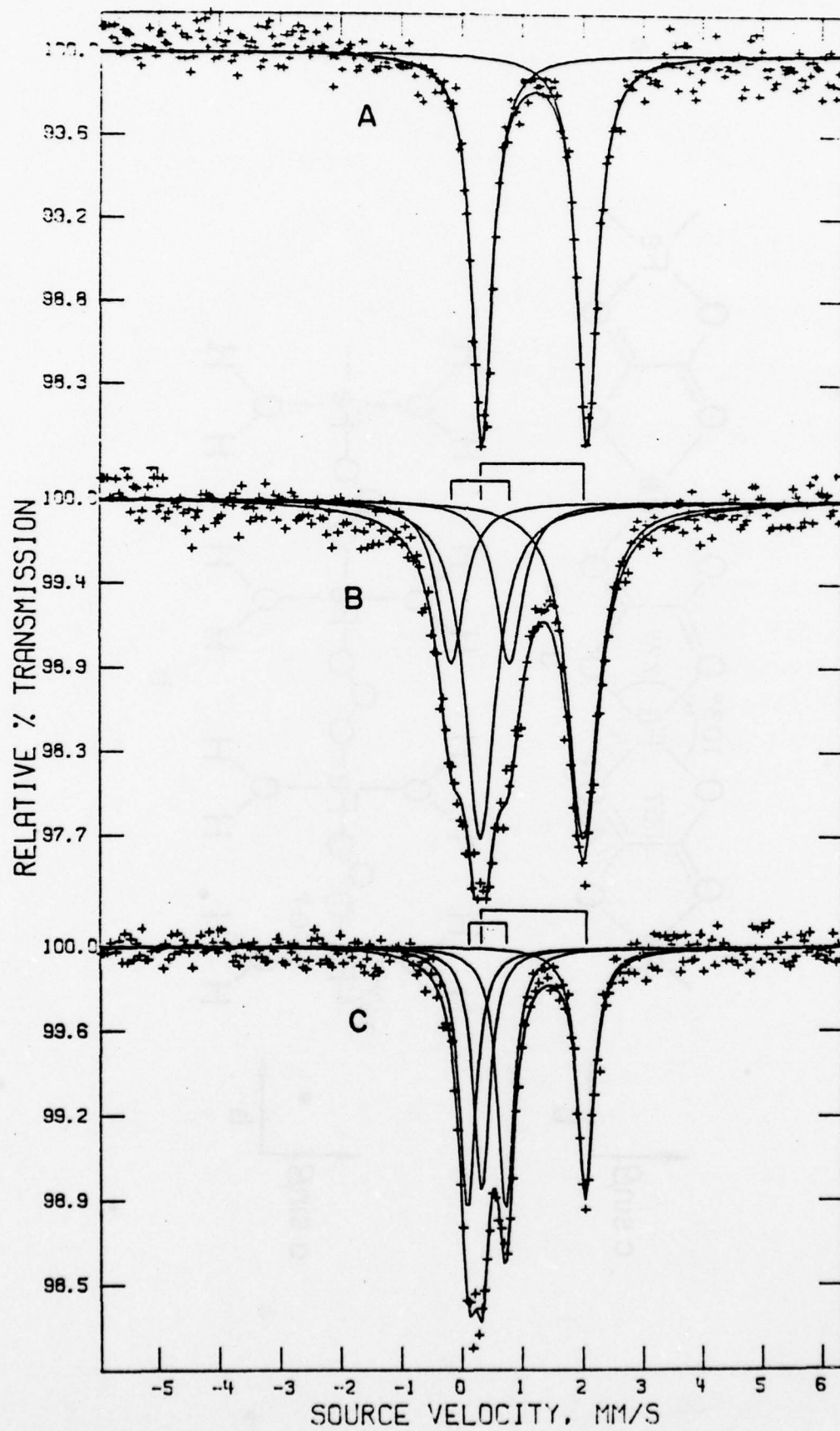
Figure 21. Experimental molar magnetic susceptibility (+) and effective magnetic moment (●) vs temperature for $\text{Fe}(\text{C}_6\text{H}_2\text{O}_4)\text{I}$. Curve A represents the solution to eq 11 with $\underline{J} = 4.1 \text{ cm}^{-1}$, $\underline{g} = 2.00$, $\underline{S} = 2.33$, $\underline{ZJ}' = 0.0$ and $\underline{N\alpha} = 0.0$.











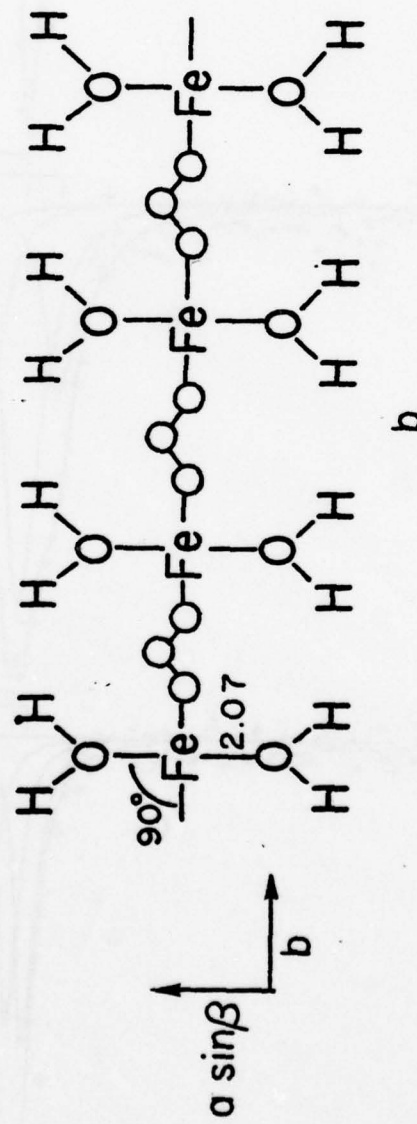
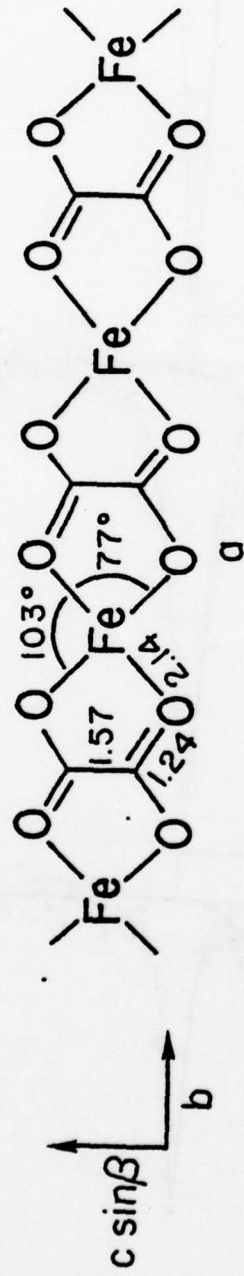
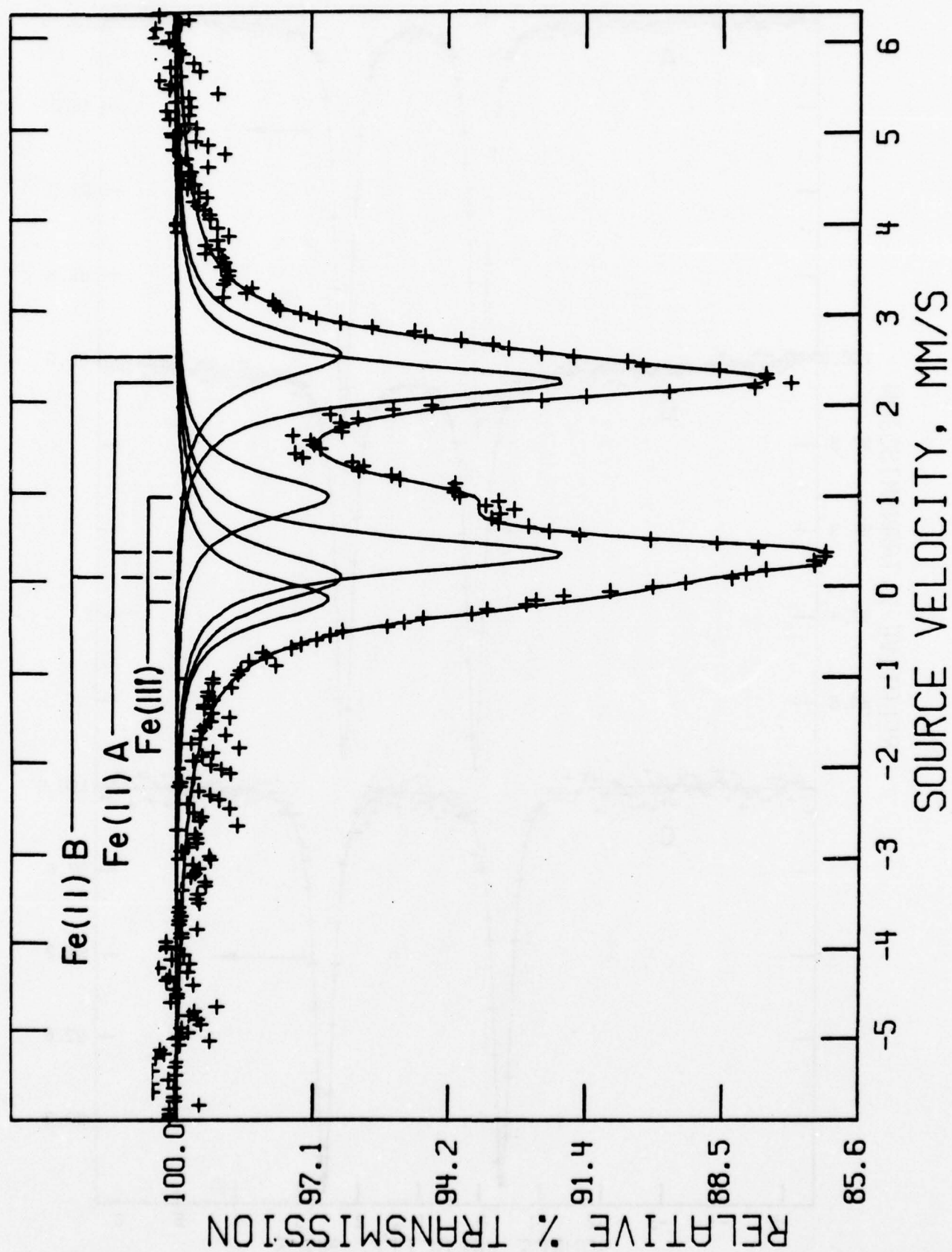
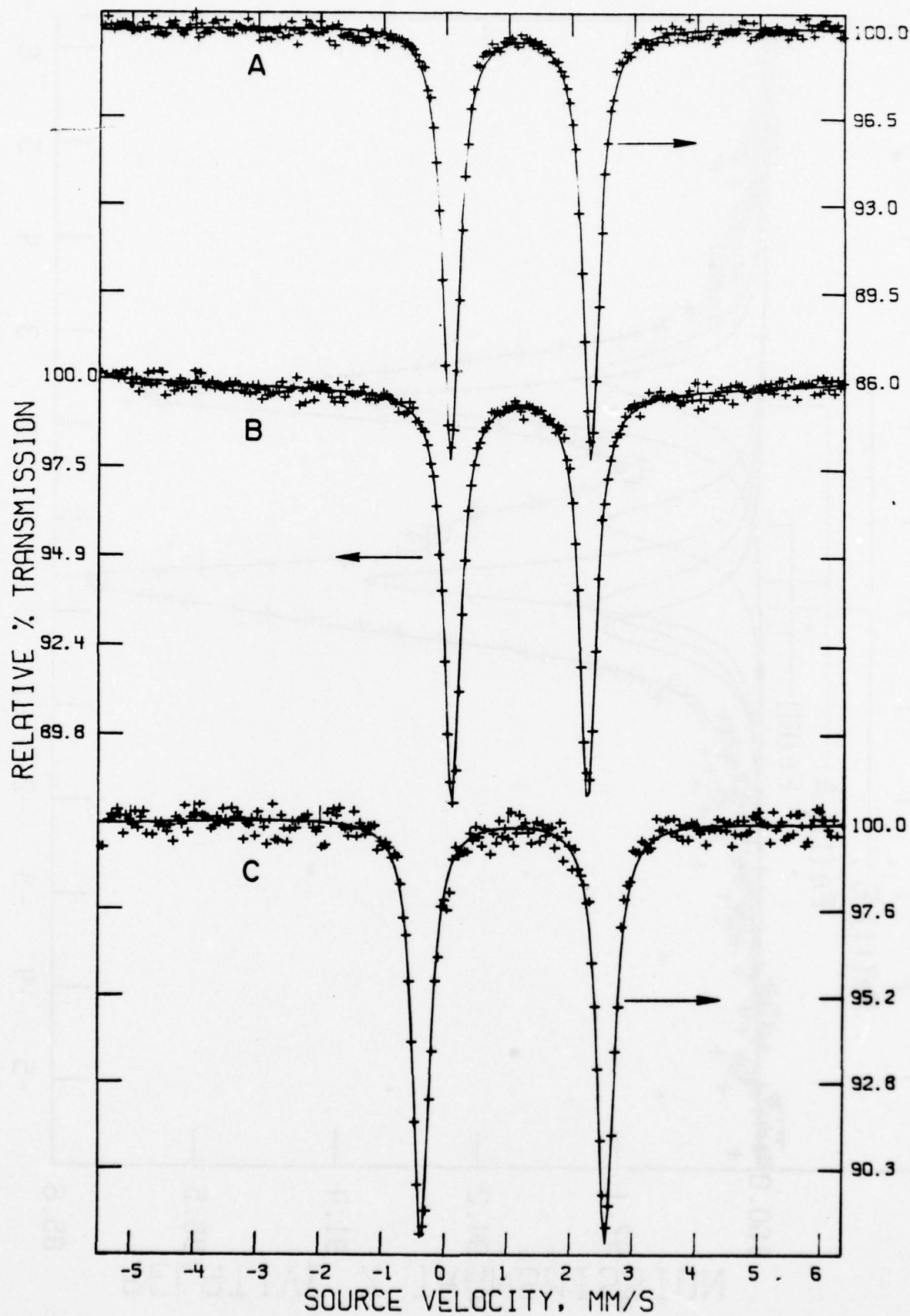


Figure 5. Wohlschlag and Rao





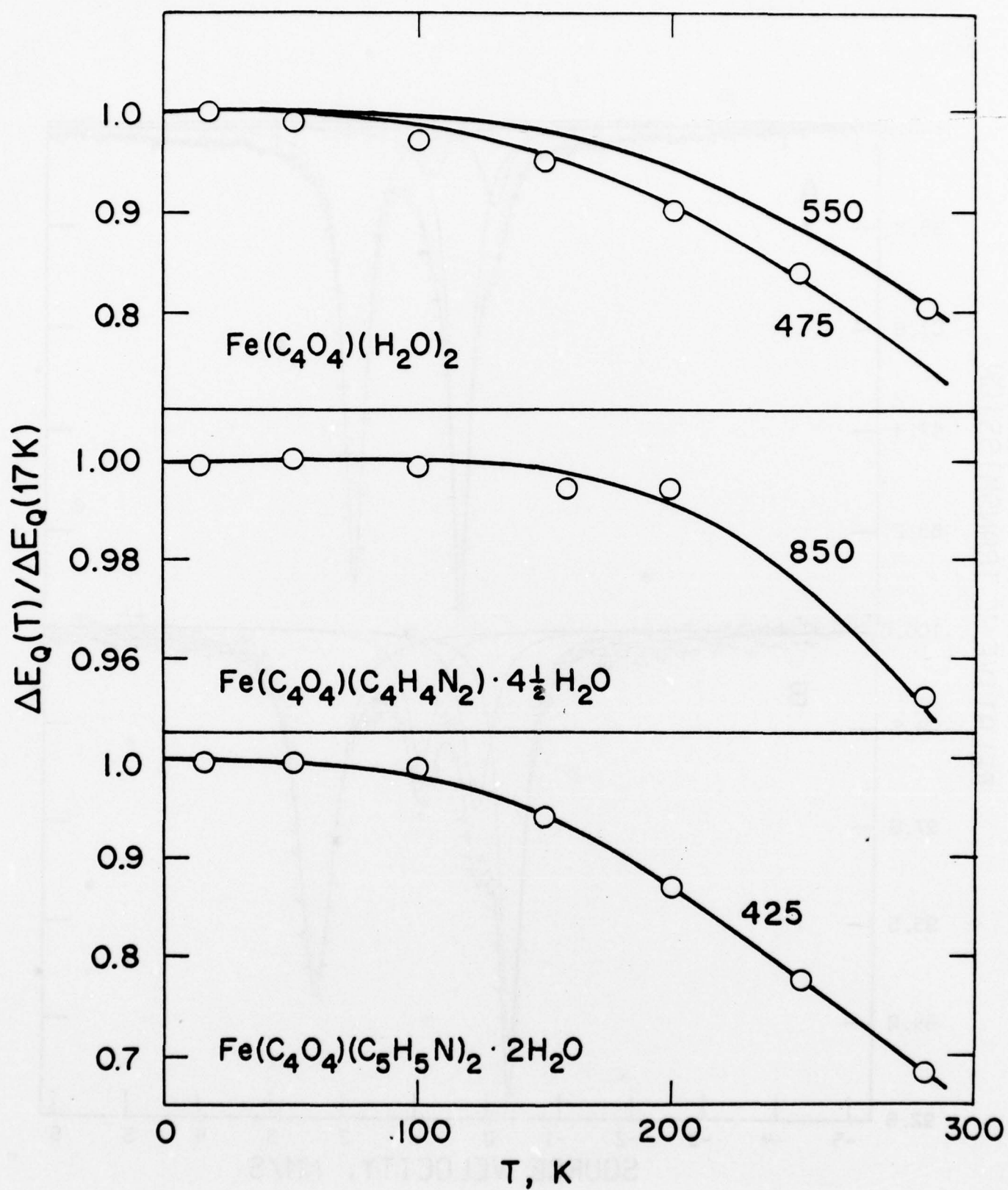
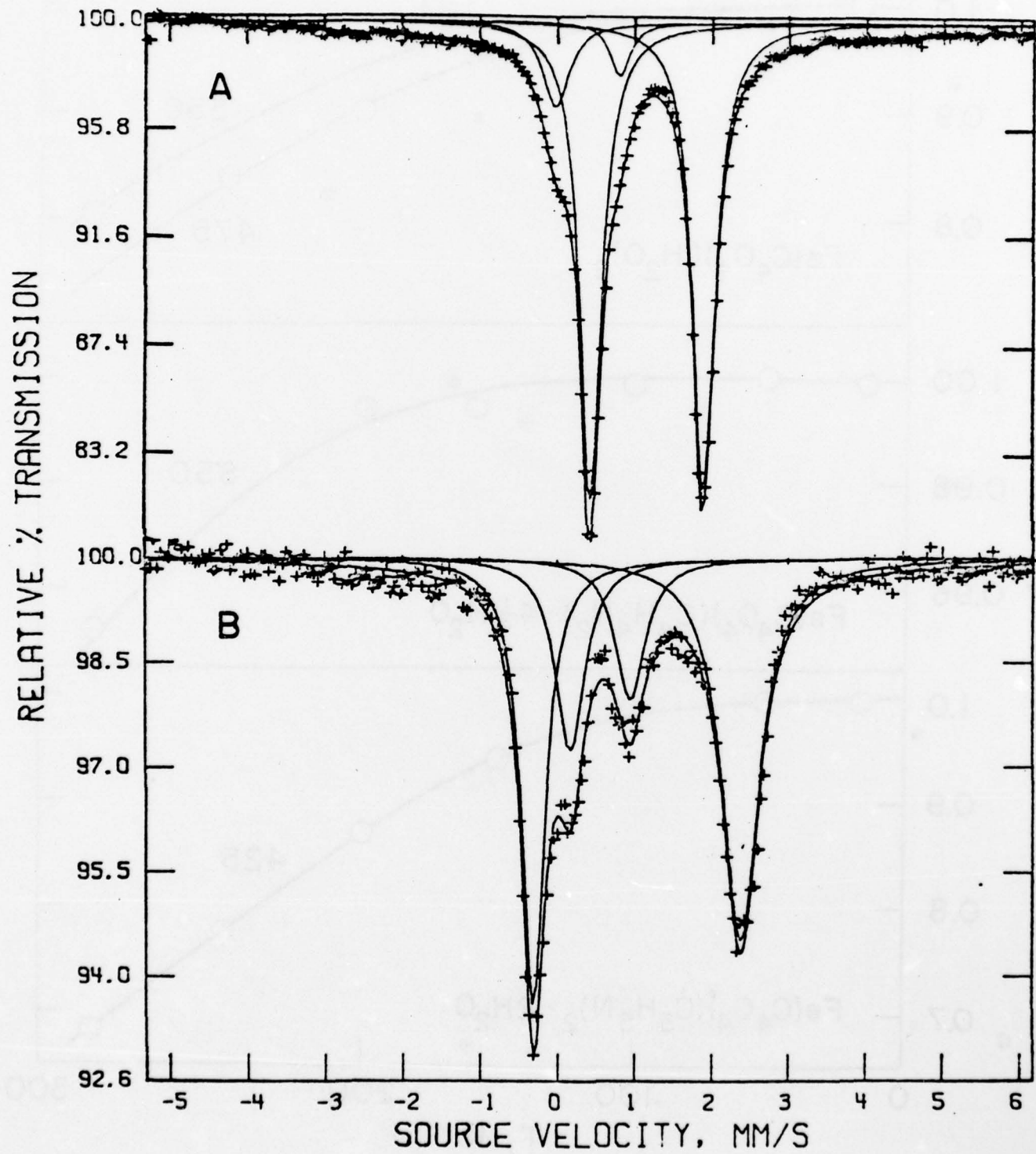
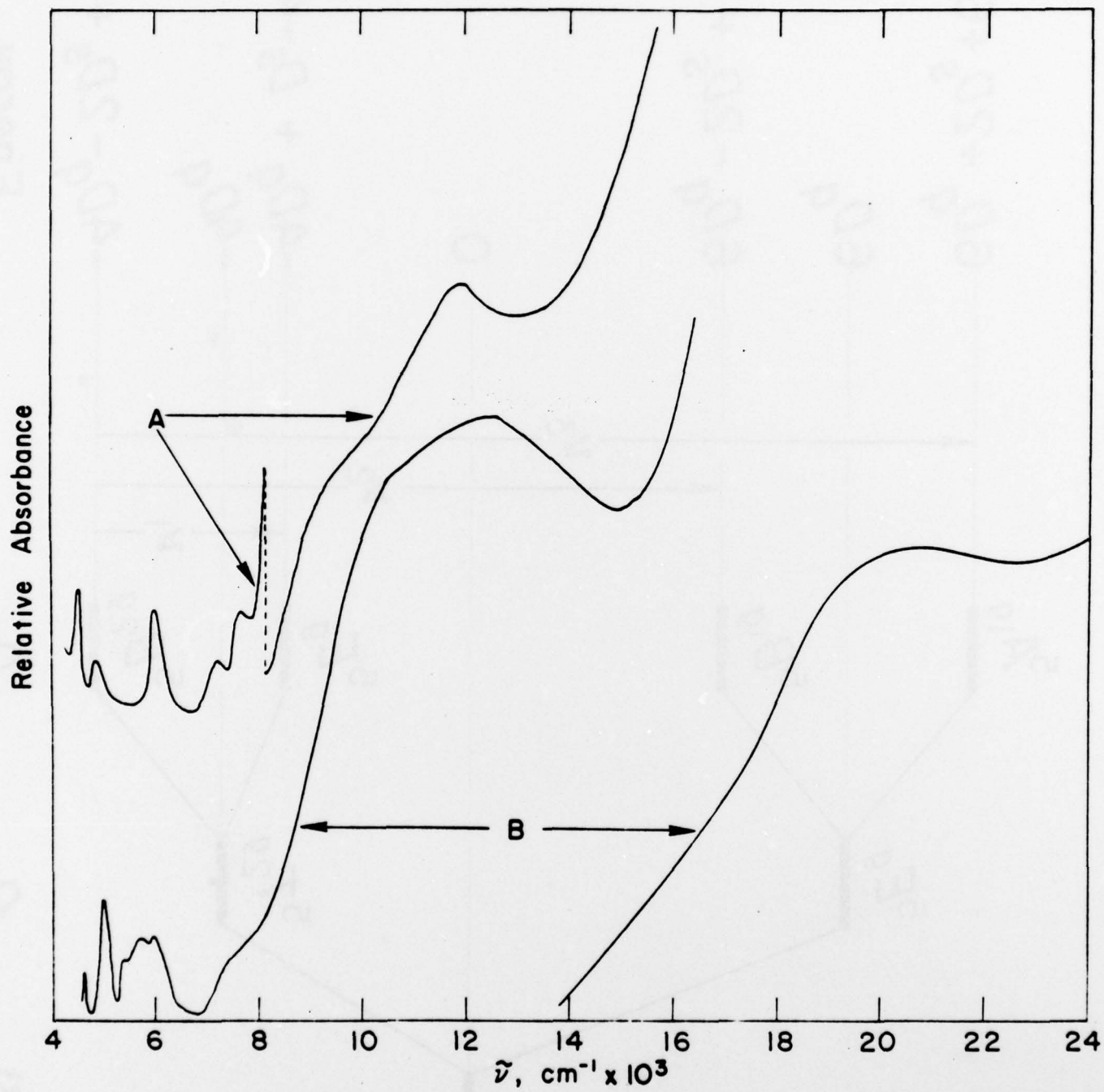
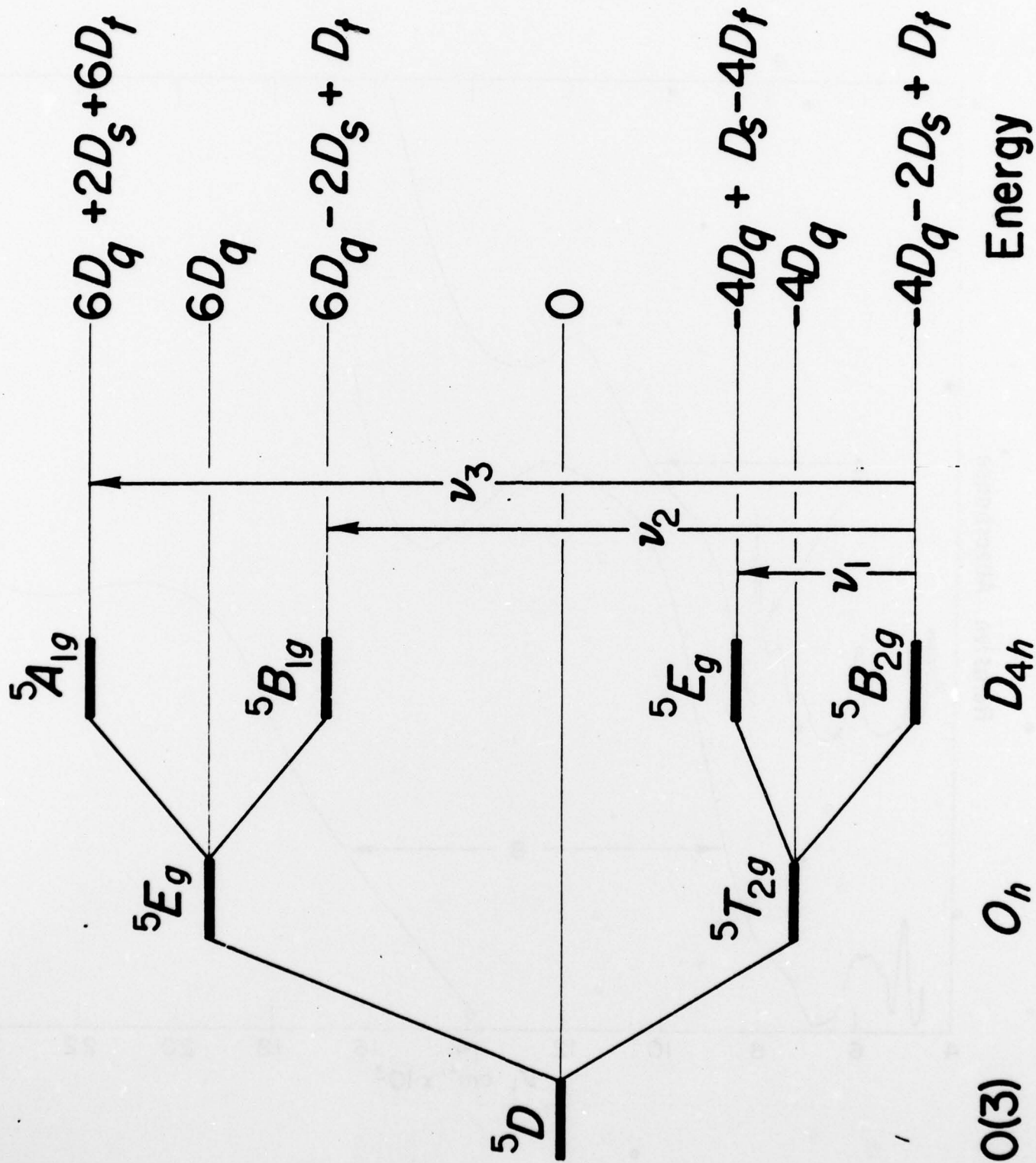
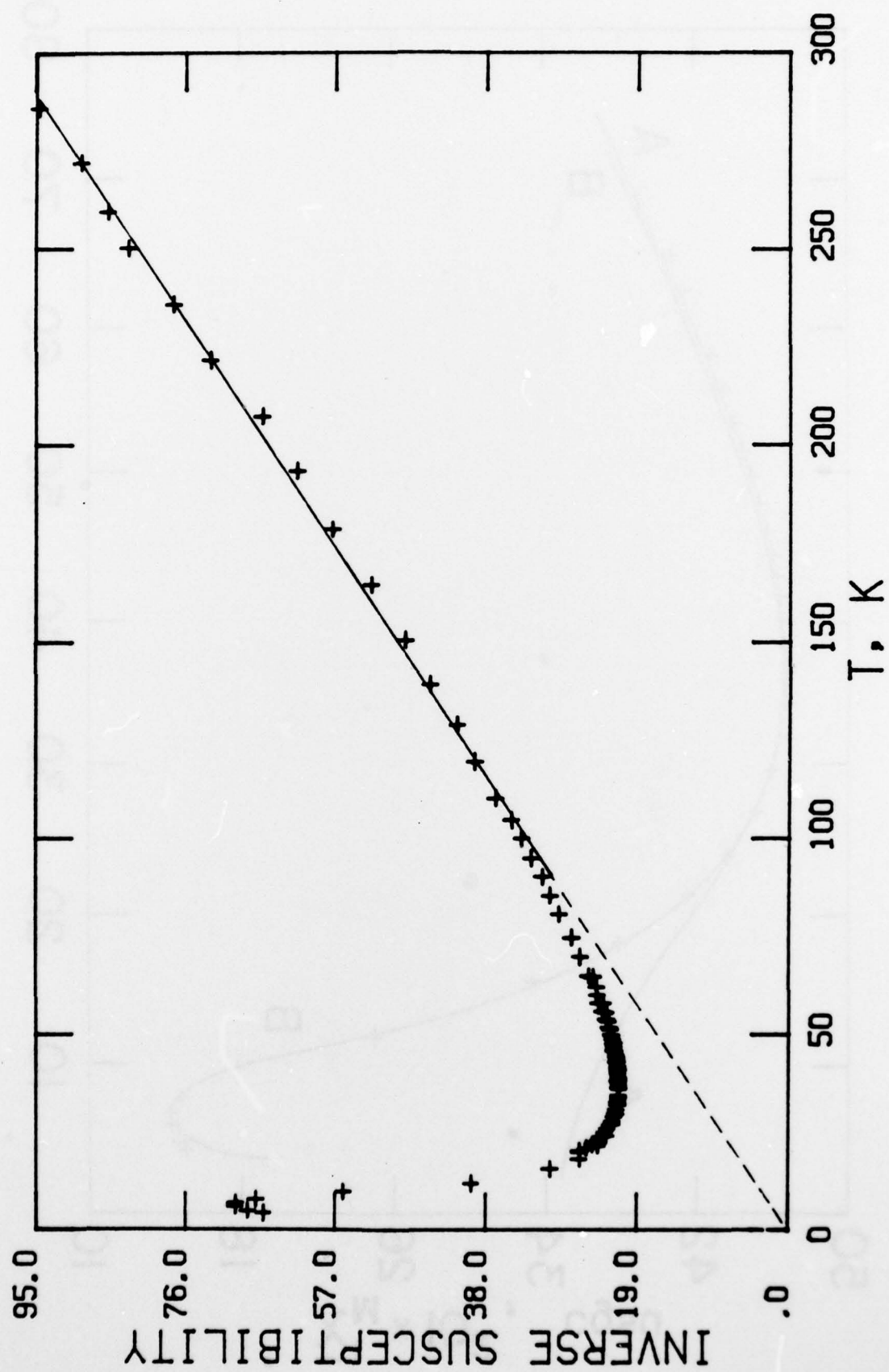


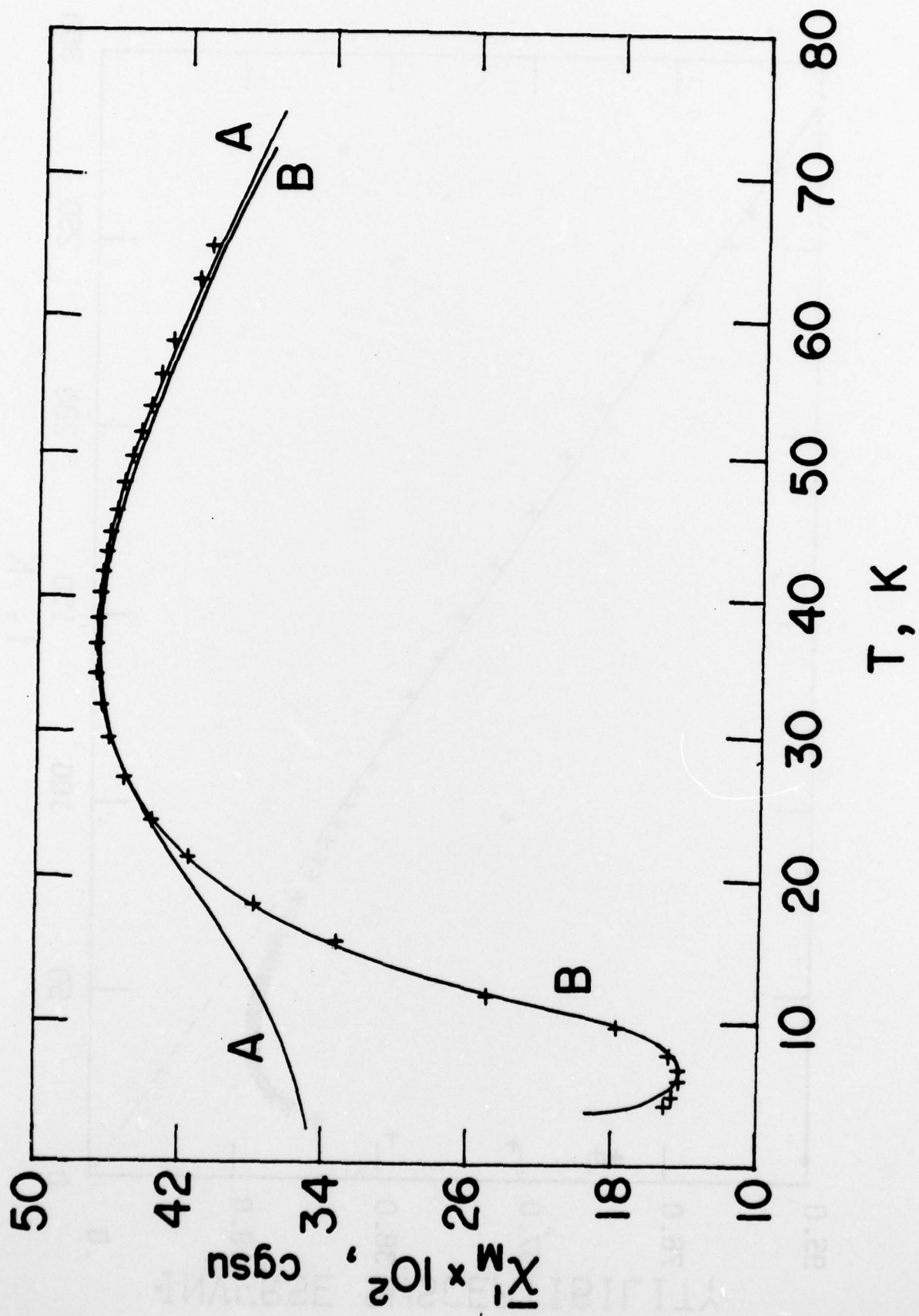
Fig.
9

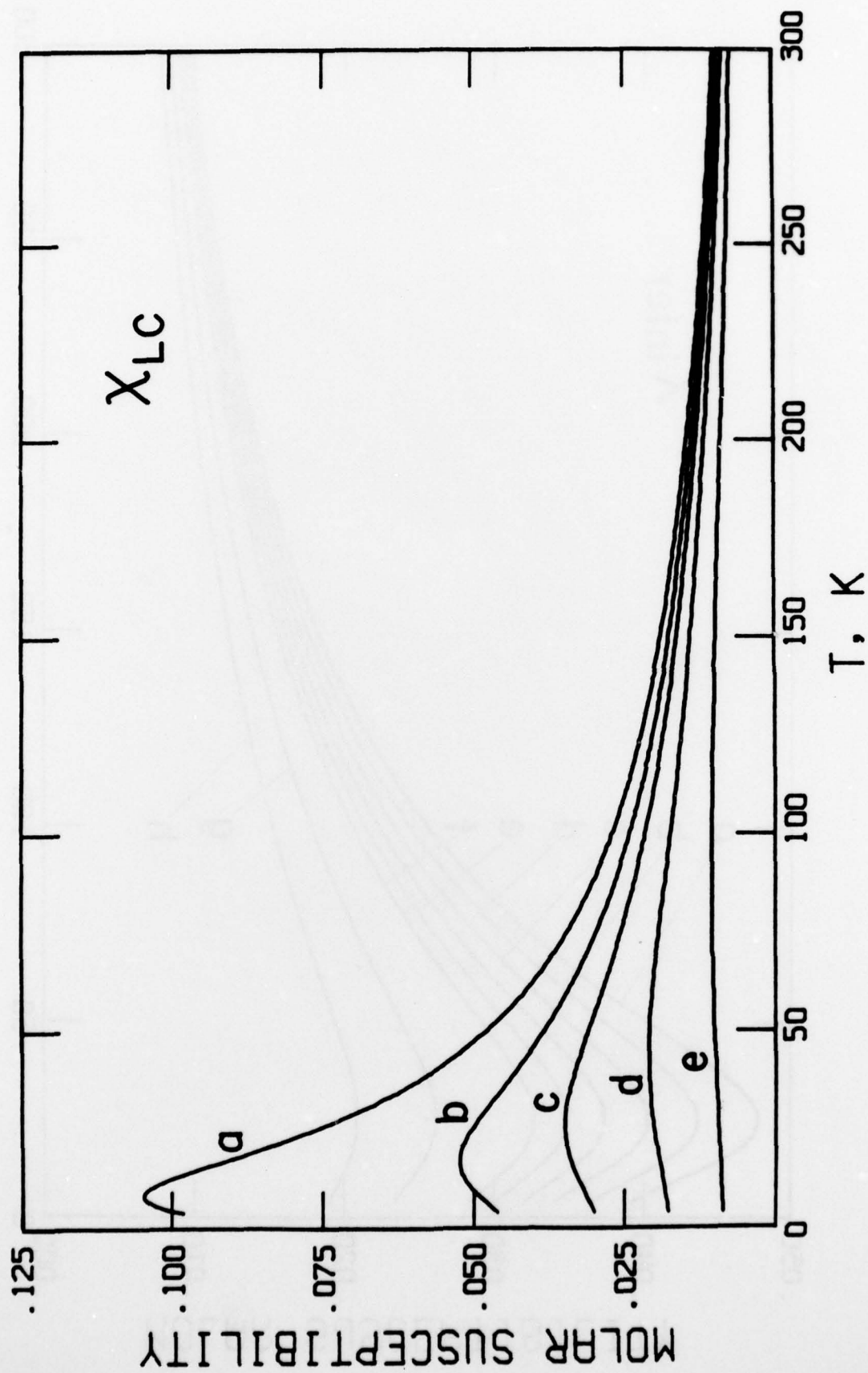


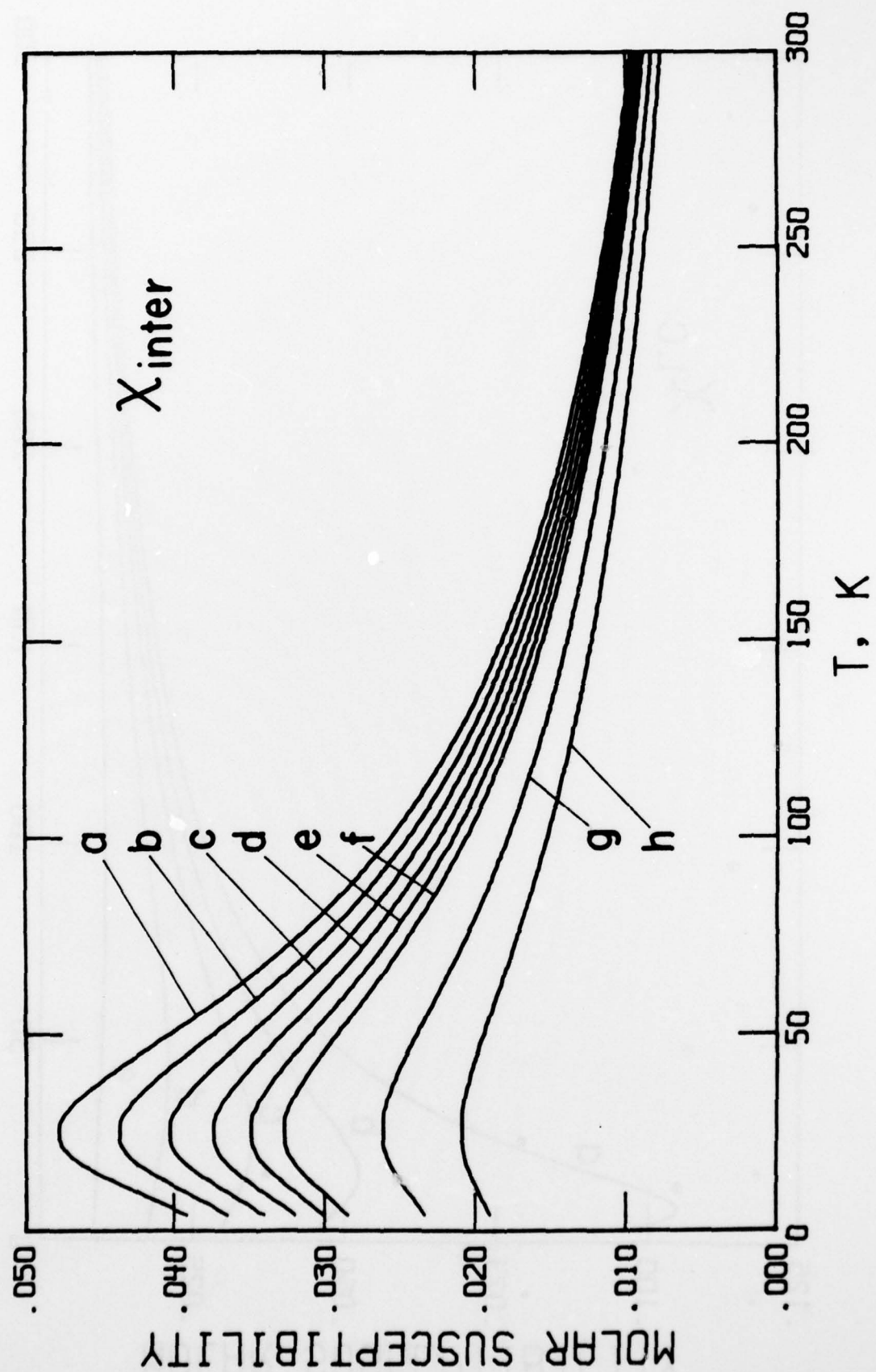


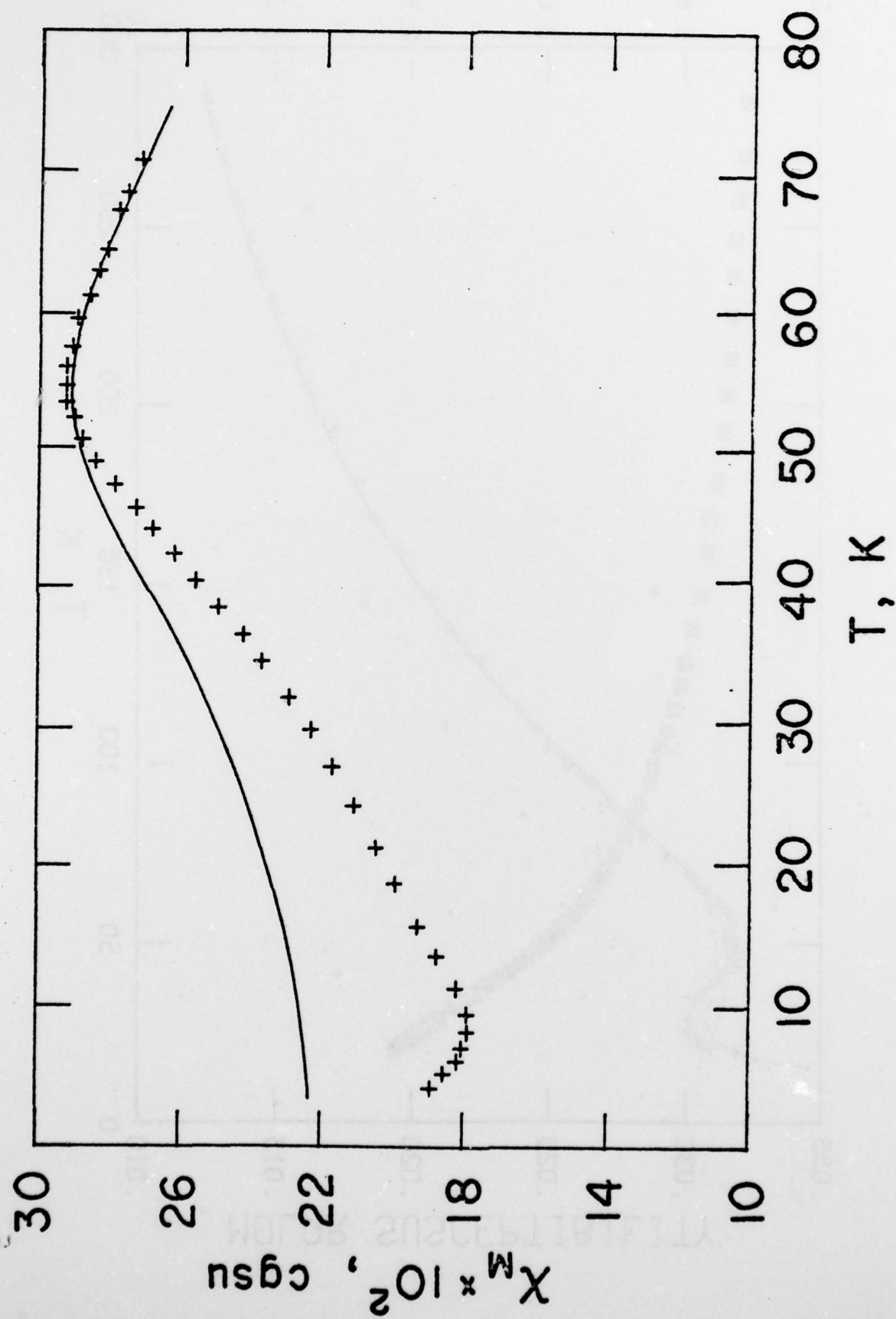












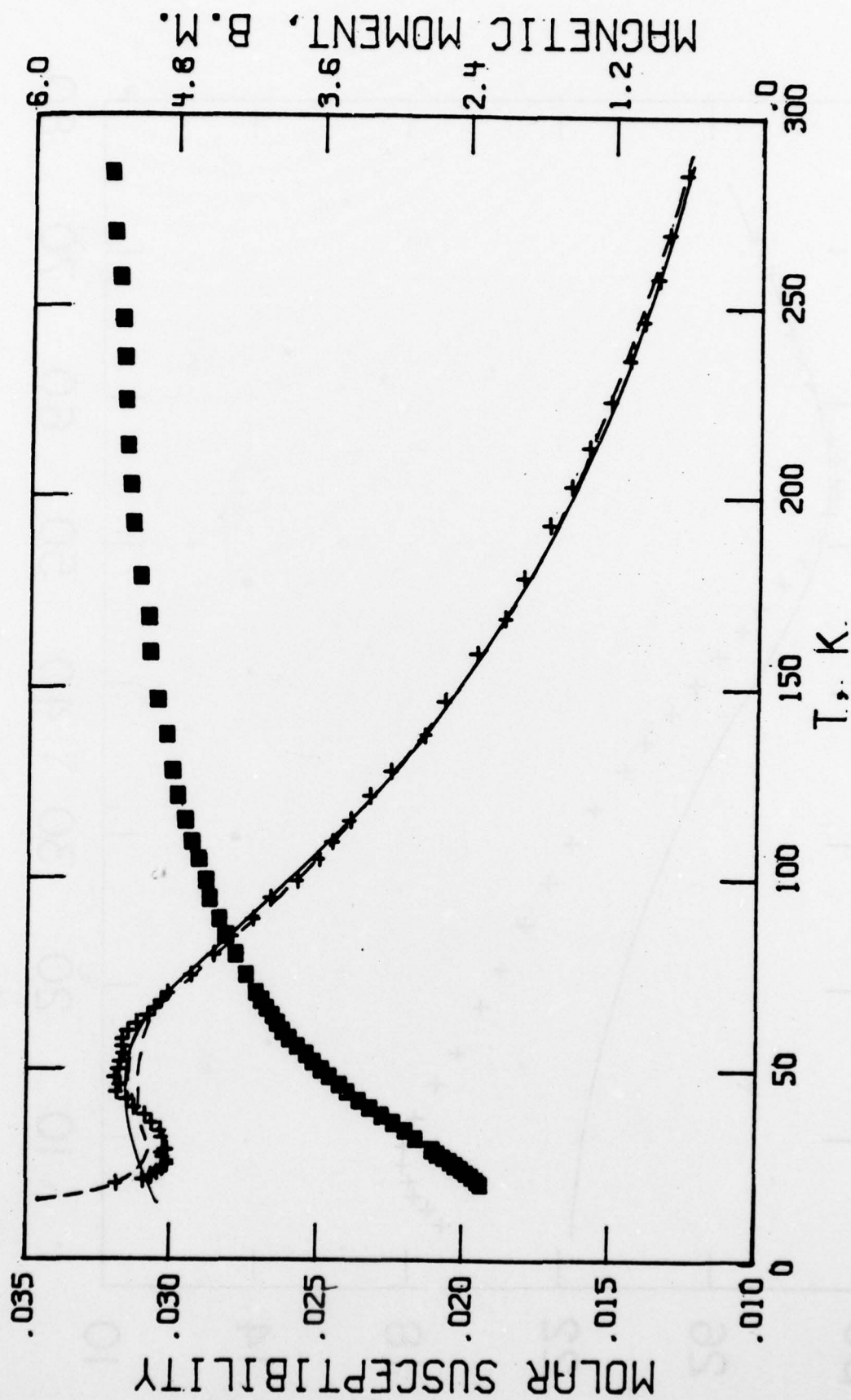
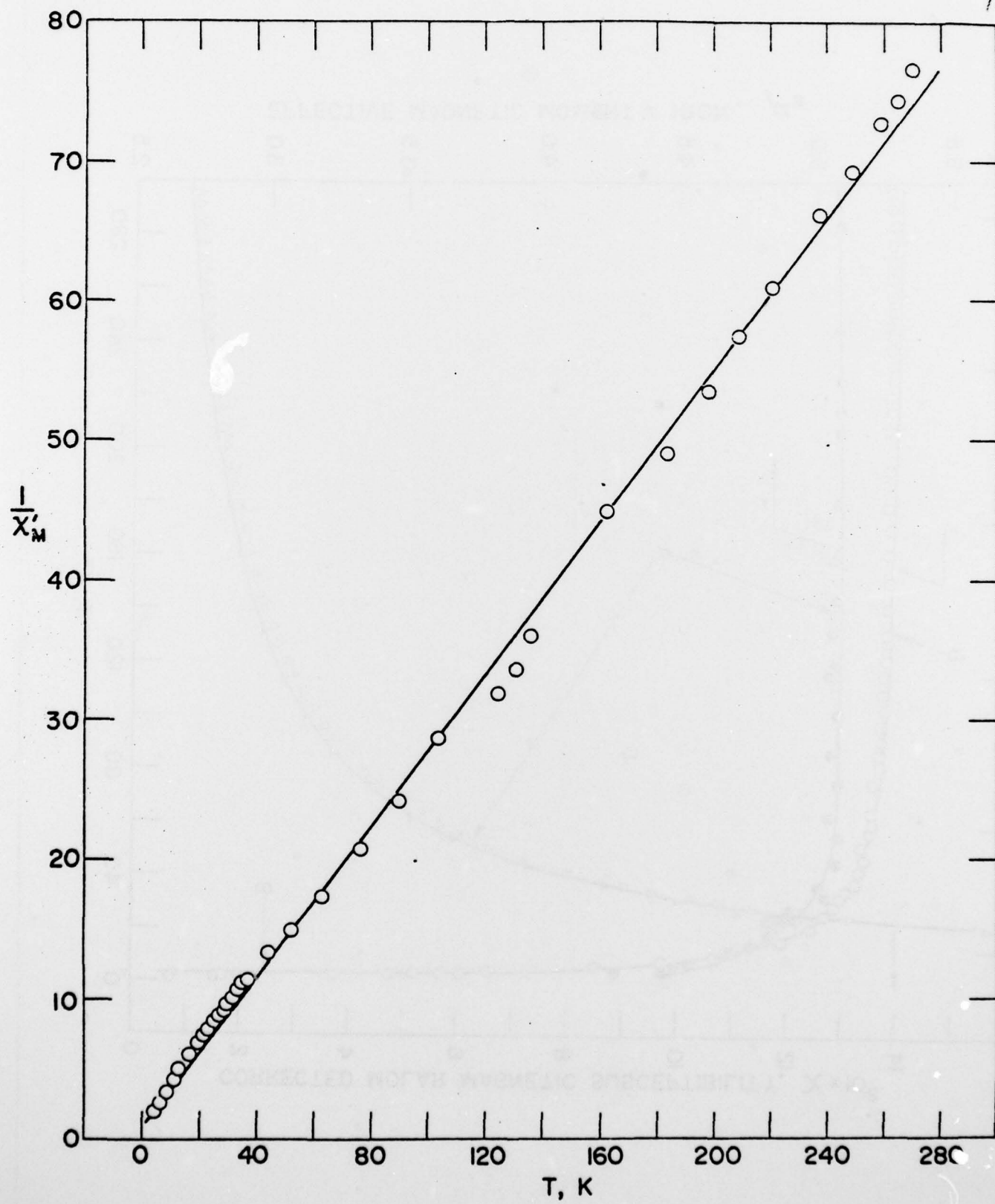
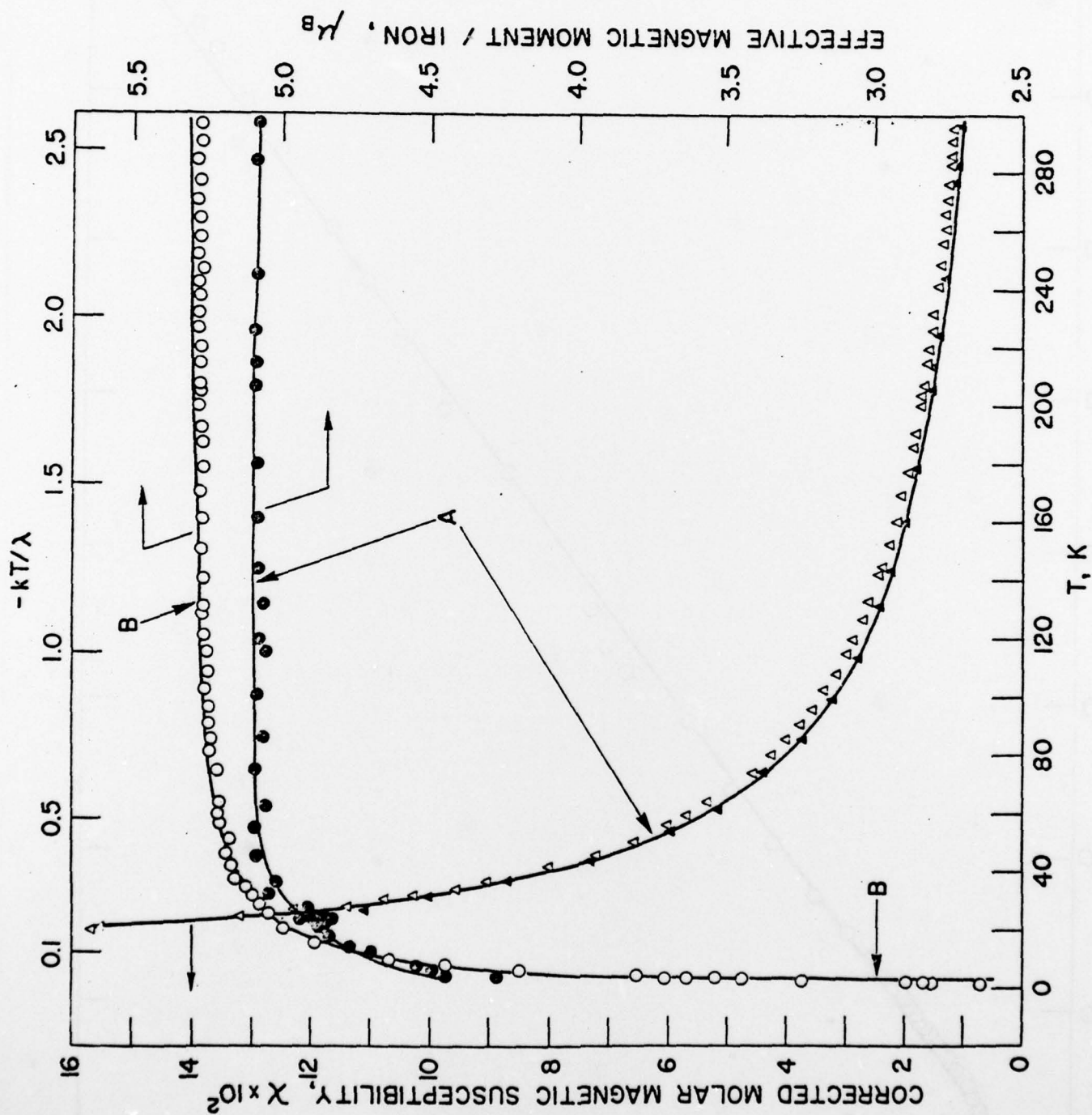
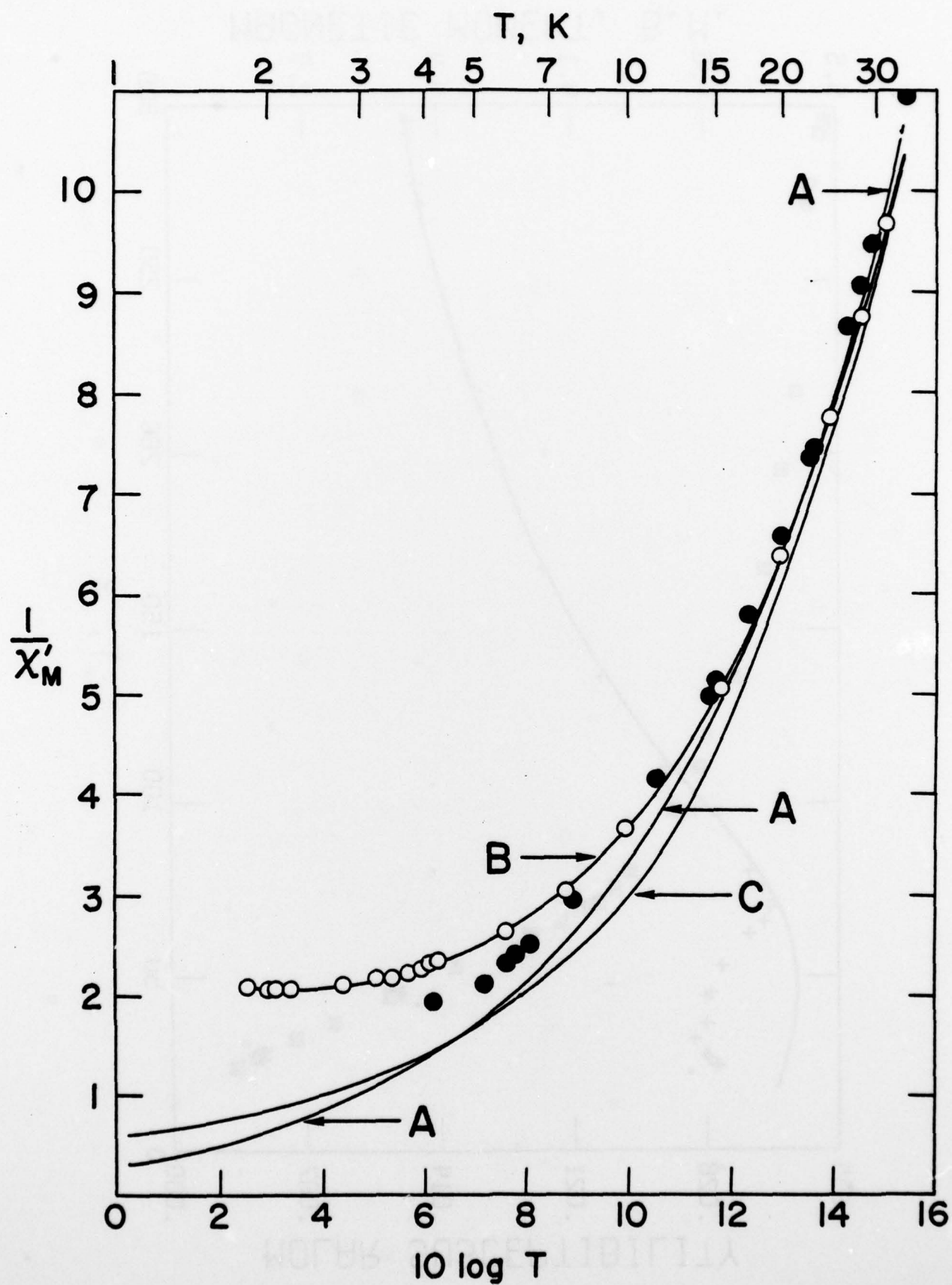
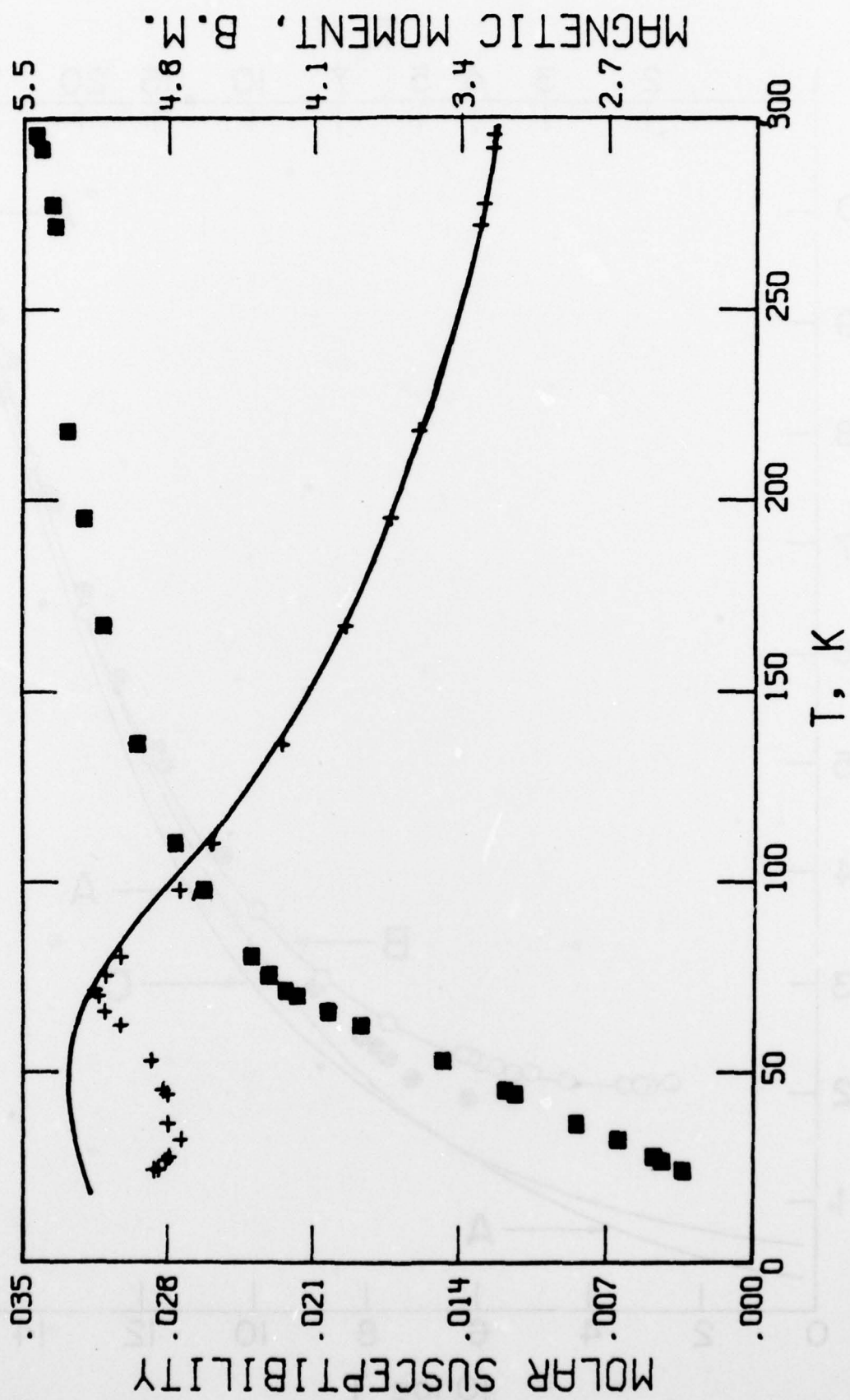


Fig 12









TECHNICAL REPORT DISTRIBUTION LIST, GEN

	<u>No. Copies</u>		<u>No. Copies</u>
Office of Naval Research 800 North Quincy Street Arlington, Virginia 22217 Attn: Code 472	2	Defense Documentation Center Building 5, Cameron Station Alexandria, Virginia 22314	12
ONR Branch Office 536 S. Clark Street Chicago, Illinois 60605 Attn: Dr. George Sandoz	1	U. S. Army Research Office P. O. Box 1211 Research Triangle Park, N.C. 27709 Attn: CRD-AA-IP	1
ONR Branch Office 715 Broadway New York, New York 10003 Attn: Scientific Dept.	1	Naval Ocean Systems Center San Diego, California 92152 Attn: Mr. Joe McCartney	1
ONR Branch Office 1030 East Green Street Pasadena, California 91106 Attn: Dr. R. J. Marcus	1	Naval Weapons Center China Lake, California 93555 Attn: Dr. A. B. Amster Chemistry Division	1
ONR Area Office One Hallidie Plaza, Suite 601 San Francisco, California 94102 Attn: Dr. P. A. Miller	1	Naval Civil Engineering Laboratory Port Hueneme, California 93401 Attn: Dr. R. W. Drisko	1
ONR Branch Office Building 114, Section D 666 Summer Street Boston, Massachusetts 02210 Attn: Dr. L. H. Peebles	1	Professor K. E. Woehler Department of Physics & Chemistry Naval Postgraduate School Monterey, California 93940	1
Director, Naval Research Laboratory Washington, D. C. 20390 Attn: Code 6100	1	Dr. A. L. Slafkosky Scientific Advisor Commandant of the Marine Corps (Code RD-1) Washington, D. C. 20380	1
The Assistant Secretary of the Navy (R,E&S) Department of the Navy Room 4E736, Pentagon Washington, D. C. 20350	1	Office of Naval Research 800 N. Quincy Street Arlington, Virginia 22217 Attn: Dr. Richard S. Miller	1
Commander, Naval Air Systems Command Department of the Navy Washington, D. C. 20360 Attn: Code 310C (H. Rosenwasser)	1	Naval Ship Research and Development Center Annapolis, Maryland 21401 Attn: Dr. G. Bosmajian Applied Chemistry Division	1
		Naval Ocean Systems Center San Diego, California 91232 Attn: Dr. S. Yamamoto, Marine Sciences Division	1

TECHNICAL REPORT DISTRIBUTION LIST, 053

	<u>No.</u> <u>Copies</u>		<u>No.</u> <u>Copies</u>
Dr. R. N. Grimes University of Virginia Department of Chemistry Charlottesville, Virginia 22901	1	Dr. M. H. Chisholm Department of Chemistry Indiana University Bloomington, Indiana 47401	1
Dr. M. Tsutsui Texas A&M University Department of Chemistry College Station, Texas 77843	1	Dr. B. Foxman Brandeis University Department of Chemistry Waltham, Massachusetts 02154	1
Dr. M. F. Hawthorne University of California Department of Chemistry Los Angeles, California 90024	1	Dr. T. Marks Northwestern University Department of Chemistry Evanston, Illinois 60201	1
Dr. W. B. Fox Naval Research Laboratory Chemistry Division Code 6130 Washington, D. C. 20375	1	Dr. G. Geoffrey Pennsylvania State University Department of Chemistry University Park, Pennsylvania 16802	1
Dr. J. Adcock University of Tennessee Department of Chemistry Knoxville, Tennessee 37916	1	Dr. J. Zuckerman University of Oklahoma Department of Chemistry Norman, Oklahoma 73019	1
Dr. A. Cowley University of Texas Department of Chemistry Austin, Texas 78712	1	Professor O. T. Beachley Department of Chemistry State University of New York Buffalo, New York 14214	1
Dr. W. Hatfield University of North Carolina Department of Chemistry Chapel Hill, North Carolina 27514	1	Professor P. S. Skell Department of Chemistry The Pennsylvania State University University Park, Pennsylvania 16802	1
Dr. D. Seyferth Massachusetts Institute of Technology Department of Chemistry Cambridge, Massachusetts 02139	1	Professor K. M. Nicholas Department of Chemistry Boston College Chestnut Hill, Massachusetts 02167	1